

- 872 FILE COPY

(4)

AFGL-TR-89-0036

A SPACE RADIATION TEST MODEL STUDY

AD-A208 760

R.W. Nightingale  
Y.T. Chiu  
G.T. Davidson  
W.E. Francis  
M.A. Rinaldi  
R.M. Robinson  
R.R. Vondrak

Space Sciences Laboratory, 091-20, B255  
Lockheed Palo Alto Research Laboratories  
3251 Hanover Street  
Palo Alto, CA 94304

17 February 1989

Final Report  
20 May 1985 - 17 February 1989

Approved for public release; distribution unlimited


Prepared for:

AIR FORCE GEOPHYSICS LABORATORY  
AIR FORCE SYSTEMS COMMAND  
UNITED STATES AIR FORCE  
HANSCOM AIR FORCE BASE, MASSACHUSETTS 01731-5000


SDTICD  
ELECTE  
JUN 09 1989  
H

89 6 09 063

"This technical report has been reviewed and is approved for publication."



(Signature)  
ROBERT H. REDUS, 1LT, USAF  
Space Particles Environment Branch  
Contract Manager



(Signature)  
E.G. MULLEN  
Chief, Space Environment Branch

FOR THE COMMANDER



(Signature)  
RITA C. SAGALYN  
Director, Space Physics Division

This report has been reviewed by the ESD Public Affairs Office (PA) and is releasable to the National Technical Information Service (NTIS).

If your address has changed, or if you wish to be removed from the mailing list, or if the addressee is no longer employed by your organization, please notify AFGL/DAA, Hanscom AFB, MA 01731. This will assist us in maintaining a current mailing list.

Do not return copies of this report unless contractual obligations or notices on a specific document requires that it be returned.

Qualified requestors may obtain additional copies from the Defense Technical Information Center. All others should apply to the National Technical Information Service.

Unclassified

SECURITY CLASSIFICATION OF THIS PAGE

## REPORT DOCUMENTATION PAGE

1a REPORT SECURITY CLASSIFICATION Unclassified			1b RESTRICTIVE MARKINGS	
2a SECURITY CLASSIFICATION AUTHORITY			3 DISTRIBUTION/AVAILABILITY OF REPORT approved for public release; distribution unlimited	
2b DECLASSIFICATION/DOWNGRADING SCHEDULE				
4 PERFORMING ORGANIZATION REPORT NUMBER(S) 1MSC/F297919			5 MONITORING ORGANIZATION REPORT NUMBER(S) AFGL-TR-89-0036	
6a NAME OF PERFORMING ORGANIZATION Lockheed Palo Alto Research		6b OFFICE SYMBOL (If applicable) LPARL	7a. NAME OF MONITORING ORGANIZATION Air Force Geophysics Laboratory (PHP)	
6c ADDRESS (City, State, and ZIP Code) 3251 Hanover Street Palo Alto, CA 94304			7b. ADDRESS (City, State, and ZIP Code) Hanscom Air Force Base Massachusetts 01731-5000	
8a NAME OF FUNDING SPONSORING ORGANIZATION		8b OFFICE SYMBOL (If applicable)	9 PROCUREMENT INSTRUMENT IDENTIFICATION NUMBER Contract F19628-85-C-0073	
8c ADDRESS (City, State, and ZIP Code)			10 SOURCE OF FUNDING NUMBERS	
			PROGRAM ELEMENT NO 62101F	PROJECT NO 7601
			TASK NO 20	WORK UNIT ACCESSION NO AA
11 TITLE (include Security Classification) A Space Radiation Test Model Study				
12 PERSONAL AUTHOR(S) Nightingale, R.W., Chiu, Y.T., Davidson, G.T., Francis, W.E., Rinaldi, M.A., /(cont'd.)				
13a TYPE OF REPORT Scientific Final		13b TIME COVERED FROM 5/20/85 TO 2/17/89		14 DATE OF REPORT (Year, Month, Day) 1989 February 17
15 PAGE COUNT 92				
16 SUPPLEMENTARY NOTATION				
17 COSAT CODES			18 SUBJECT TERMS (Continue on reverse if necessary and identify by block number)	
FIELD	GROUP	SUB-GROUP		
20	08		Space radiation Radiation belt Adiabatic invariants	
20	09		Energetic particles Radial diffusion SCATHA	
			Electrons Pitch-angle diffusion	
19 ABSTRACT (Continue on reverse if necessary and identify by block number)				
<p>The tools for dynamic modeling of the energetic populations in the outer radiation belts are being developed to better understand the extreme variations of particle flux in response to magnetospheric and solar activity. The study utilizes the SCATHA SC3 high-energy electron data for energies from 200 keV to 2 MeV, with fine pitch-angle measurements (<del>30°</del> field of view) over the L-shell range of 5.3 to 7 for quiet and moderate geomagnetic periods in April 1979 and June 1980. A solution of the simultaneous bimodal (radial and pitch-angle) diffusion equation for the radiation belts has been developed with special regard for the requirements of satellite radiation belt data analysis. The solution has been used to test the bimodal theory of outer-electron-belt diffusion by confronting it with satellite data. The tests demonstrate that the general solution can /(cont'd.)</p>				
20 DISTRIBUTION/AVAILABILITY OF ABSTRACT <input checked="" type="checkbox"/> UNCLASSIFIED/UNLIMITED <input type="checkbox"/> SAME AS RPT <input type="checkbox"/> DTIC USERS			21 ABSTRACT SECURITY CLASSIFICATION Unclassified	
22a NAME OF RESPONSIBLE INDIVIDUAL 1Lt. Robert H. Redus			22b TELEPHONE (include Area Code) (617) 861-3213	22c OFFICE SYMBOL PHP

Block 12 (cont'd.):

Robinson, R. M. and Vondrak, R.R.

Block 19 (cont'd.):

represent the SCATHA data to a high degree of accuracy for periods up to 10 hours. The data representation requires and provides diffusion parameters that are in agreement with all previous experimental and theoretical determinations of such diffusion coefficients. Such a representation satisfies the basic requirements towards the dynamic modeling of the outer electron radiation belt for  $L < 7$  at quiet and moderate geomagnetic conditions. The representation has also been shown to be unique when projected off of the satellite trajectory in  $(L, t)$ -space. For  $L \sim 7$  the representation has difficulties with "butterfly" distributions that may signify energetic electron encounters with the magnetopause. It has been demonstrated by computer simulation of electron encounters with the magnetopause that the effects of the encounter may be highly anisotropic in configuration or in invariant space. The test modeling developed in this study for the physical interpretation of the space radiation environment is a prototype dynamic model for characterizing the full radiation-belt data from the forthcoming CRRES mission.

# CONTENTS

Section	Page
I. INTRODUCTION .....	1
II. A GENERAL SOLUTION OF BIMODAL DIFFUSION .....	5
III. FIRST RESULTS FROM SIMULTANEOUS BIMODAL DIFFUSION .....	7
IV. HIGH-ENERGY OUTER RADIATION BELT DYNAMIC MODELING .....	11
V. A NONLINEAR MODEL OF WAVE-PARTICLE INTERACTIONS IN THE TRAPPED RADIATION BELTS .....	14
VI. TOWARDS DYNAMIC MODELING OF THE OUTER ELECTRON RADIATION BELT .....	15
VII. RESULTS AND CONCLUSIONS .....	27
VIII. RECOMMENDATIONS .....	28
REFERENCES .....	29
APPENDICES .....	32



Accession For	
NTIS GRA&I	<input checked="" type="checkbox"/>
DTIC TAB	<input type="checkbox"/>
Unannounced	<input type="checkbox"/>
Justification	
By _____	
Distribution/	
Availability Codes	
Dist	Avail and/or Special
A-1	

## ILLUSTRATIONS

Figure	Page
1. Pitch-angle diffusion coefficient as function of energy .....	8
2. Radial diffusion coefficient as function of energy at $L = 5.30$ . ....	10
3. Illustration of the nonlinear nature of fitting the solution representation to data	12
4. Values of the right hand side and left hand side of the separation Equation (8) are plotted as functions of order $n$ for the initial iteration and the final iteration. ....	17
5. Three-dimensional presentation of the phase space density of the data base and its reconstitutions for the 288.5 keV channel of Day 165, 1980 in pitch angle and $L$ . ....	19
6. Three-dimensional presentation of the phase space density of the data base and its reconstitutions for the 448 keV channel of Day 110, 1979 in pitch angle and $L$ . ....	20
7. The distribution of fit percentage errors in the reconstitution of all the data points in the Day 165, 1980 data base .....	21
8. The distribution of fit percentage errors in the reconstitution of all the data points in the Day 110, 1979 data base .....	22
9. Comparison of the radial diffusion coefficients determined in Paper IV for the energy range 0.2-2.0 keV with Paper I and with the compilation of West et al. ....	23
10. Demonstration of the path independence in projecting the electron distributions from on-trajectory to off-trajectory points. ....	24

## 1. INTRODUCTION

The performance of earth-orbiting satellites is profoundly affected by the high-energy particle environment. At high altitudes, spacecraft charging by keV particles can produce electrical discharges on surfaces and insulating materials that couple to satellite electronics. Impact of high-energy particles can degrade electronic components, cause single event upsets and produce internal charging. The high-energy particle environment has been studied for many years and static models have been constructed that specify the time-averaged conditions in the radiation belts. These models have aided spacecraft designers in minimizing the deleterious effects of high-energy charged particles. However, the radiation belts are very dynamic, undergoing extreme variations in response to magnetospheric and solar activity. With the coming of Air Force programs involving manned-presence in space, with the placement of spacecraft in dynamic regions of the outer radiation belt, as well as with the development of advanced systems that may be sensitive to the radiation environment, the understanding and possible early warning of this dynamic activity is critical to successful missions. Identifying the sources and sinks of high-energy electrons, and understanding their relationship to the observed variations, are the ultimate goals for developing a dynamic model of the radiation belts.

This final report covers a 45-month research effort, undertaken to investigate the dynamics of radiation-belt particle populations using an existing data base provided by the Lockheed High Energy Particle Spectrometer (SC3) on the Space Charging AT High Altitude (SCATHA) satellite. This instrument has been measuring the high-energy electron population from 47 keV to 5 MeV in the near-geosynchronous region. Because of the high angular resolution ( $3^\circ$  field of view) of the instrument and the radial movement of the spacecraft over the L-shell range of 5.3 to 8.7, the measurements constitute a unique data base that allows the interpretation of pitch-angle diffusion effects in the presence of radial transport.

The main objective of this data analysis/interpretation effort is to set up a prototype of the data effort that will be required in order to interpret and expand the single-point radiation-belt measurements to be acquired by the Chemical Release and Radiation Effects Satellite (CRRES) into dynamic models of the radiation belts as a whole. The long term goal of the CRRES program is to develop useful models of the entire radiation-belt environment. While a static phenomenological model can be constructed without much attention being paid to characterizing the physical basis of the model, such phenomenological models suffer from the major drawback of not being able to characterize the dynamic changes of the radiation-belt environment that result from natural geomagnetic activity or from high-altitude nuclear explosions. Therefore, if the CRRES data are to be used for predictive purposes, there is no alternative but to interpret the data first in terms of physical phenomena and subsequently to use them as the basis for a predictive dynamical model of the radiation-belt environment.

Such a program for CRRES is simple and effective in concept, but its implementation is a different matter since the completeness and precision of the expected CRRES data have not been matched by any other previous measurements except SCATHA. Thus, the SCATHA energetic electron data set is a natural testing ground for the CRRES data analysis/interpretation efforts. Further, since the development of such efforts requires some lead time, the present SCATHA data analysis is the perfect choice as a prototype for CRRES data analysis in 1990 and beyond.

The basic physical requirement for implementing such a prototypical program is a fundamental understanding of how radiation-belt particles are transported in space and time, how their motion is constrained by the Earth's magnetic field, and how their energy is partitioned in the complex magnetospheric plasma environment. In short, we need to "keep book" on the radiation-belt particles with as much detail as we can afford, in order to understand their dynamical interactions. The formulation of such "bookkeeping" in terms of the behavior of statistical aggregates has been developed in the late 1960's as radiation-belt diffusion theory [e.g., Reference 1]. In the statistical picture, energetic particles are transported into or out of any imaginary volume of space within the radiation belts by the cumulative effects of interactions with fluctuating electromagnetic fields. Such transport can be from one L-shell volume into another and/or along the magnetic field into the atmosphere. The diffusion formalism seeks to describe these transport phenomena by parametrizing the rates of transport, in its various modes, in terms of diffusion coefficients. Thus, in the diffusion theoretic formulation of radiation-belt dynamics, the primary task is to determine the diffusion coefficients from data, rather than construct a global predictive model based on first physical principles. A finite set of diffusion coefficients comprise the key parameters in the diffusion equation which specifies the dynamical state of the radiation belt. The chief goal of our data analysis/interpretation effort is, therefore, the characterization of the diffusion coefficients for the SCATHA data set on outer-radiation-belt electrons. This has been accomplished and discussed in detail in our papers, included in the appendices of this report, resulting from this study.

The adoption of a diffusion point of view implies that the particle distribution be specified with respect to a set of phase-space coordinates or parameters; any of which may vary during the physical interactions which lead to diffusion. The ideal coordinate frame for the description of charged-particle motion and diffusion in the radiation belts is the space of three adiabatic invariants. Each invariant corresponds to one form of cyclic motion in a static electromagnetic field. The deviations from purely cyclic motion in the presence of time varying fields lead to particle diffusion with respect to one or more of the adiabatic invariants. In the inner radiation belts the adiabatic-invariant formalism is especially valuable because there is a simple mapping of the adiabatic-invariant space onto the configuration space defined by the L shells: the mix of particles on any given L-shell is invariant with respect to longitude under static conditions.

For the outer radiation belt, and for geomagnetically active times, however, the mat-



ter is not so simple. The primary problem is that the definition of an "L-shell" is not very meaningful under such circumstances because the mapping of adiabatic-invariant space onto the configuration space (i.e., radial distance, longitude, and latitude) is not invariant with respect to longitude. The mapping also changes whenever the geomagnetic field varies with time on a scale that cannot be described as "fluctuation". Consequently, L is not a good coordinate with which to characterize radial diffusion "across L-shells". The concept of adiabatic invariants, however, is still well-defined. The breakdown of the mapping between invariant and configuration spaces can lead to coupling between the modes of diffusion; a phenomenon which can be treated correctly only with adiabatic-invariant coordinates. Therefore, the generalized description of diffusion in adiabatic-invariant space is the proper choice to address radiation-belt diffusion in the outer regions at geomagnetically active times. A prerequisite to our goal of data interpretation is the capability of transforming between the two sets of coordinates for realistic geomagnetic fields relevant to various active conditions. The difficulty of generating an efficient transformation from configuration space to a fully adiabatic-invariant coordinate frame is the primary reason why there has been, until this time, no method for routinely characterizing diffusion in the analysis of outer-radiation-belt data for geomagnetically active times.

The diffusion analysis has been attacked on several fronts. Our efforts for the first nine months of this study were mostly directed at a diffusion description in the static geomagnetic field. At the same time we proceeded to develop basic tools to cope with changes in the magnetic field during active times. A first step toward a fully dynamic diffusion model was the acquisition for this study of a divergence-less realistic geomagnetic field valid for high  $K_p$  values. That requirement seems to be fully met in the form of the *Tsyganenko-Usmanov* model [References 2 and 3] as modified by Dr. David Stern of NASA Goddard Space Flight Center [private communication]. The second step was to acquire the capability to compute adiabatic invariants in this model. Only efficient computation of the third invariant was needed since the computation for the first and second invariants is routine. The third adiabatic invariant, which is proportional to the area vector integral of the magnetic flux enclosed by the particle drift orbit around the Earth, is rather cumbersome and time-consuming to compute on a routine basis. We are not aware of previous attempts to do so on a routine basis. An important development of the present effort was that we have been able to develop an accurate transformation to reduce the two-dimensional integration for the third invariant into a simple one-dimensional integration, thus opening the way to analysis of outer-belt diffusion at active times, as well as for other applications, such as for the proton belts.

Detailed descriptions of these achievements are described in our interim report for the first nine months [Reference 4]. These include a brief survey and description of the SCATHA SC3 electron data along with characterization of some active periods of interest; modeling of the temporal variations by mapping the phase-space distribution functions in terms of observable parameters at fixed first and second adiabatic invariants; a com-

putationally efficient procedure for calculating the third adiabatic invariant and the drift motion of the particles; and the first phase of fitting a period of SC3 electron data with an eigenfunction formulation, combining both radial and pitch-angle diffusion.

Following this initial phase of our study, a general solution of the bimodal (radial and pitch-angle) diffusion equation for the radiation belts was developed with special regard to the requirements of satellite radiation belt data analysis. Utilizing a period of SCATHA SC3 electron data, the radial and pitch-angle diffusion coefficients were determined and compared to previous results as a first test of our solution. This was presented in our first paper [Reference 5], which can be found in Appendix A and will be hereafter referred to as Paper I. These results were expanded on in our second paper [Reference 6], which also included a discussion of issues concerning dynamic modeling. This work will be referred to as Paper II and can be found in Appendix B. The development of a nonlinear response model of radiation belt particles to wave growth and particle precipitation [Reference 7] was partially sponsored by this study, can be found in Appendix C and will be referred to as Paper III. As we have progressed in this study towards a computationally efficient dynamic model of the outer electron belt, we have refined our earlier work on the solution of the bimodal diffusion equation and its uniqueness into our fourth paper (Paper IV) [Reference 8]. This work can be found in Appendix D. In Section II of this final report, the bimodal diffusion equation and our general solution is presented, as developed in Papers I, II and IV. This general solution can serve as the basis of a new approach to dynamic modeling of the radiation belts, having the capability to include temporal variations, diffusion and trapping. The next four sections summarize the results of each of our papers from this study. Our results and conclusions from this Space Radiation Test Model Study are presented in Section VII. Recommendations for implementation of dynamic modeling in the CRRES time frame are given in Section VIII.

## II. A GENERAL SOLUTION OF BIMODAL DIFFUSION

In order to organize the discussion in this report, we briefly summarize the salient features of simultaneous bimodal diffusion theory [References 1, 9 and 10] and its specific form developed for efficient data representation in Paper I.

By introducing an approximate invariant valid over a sufficiently thin slice of  $L$ -space, Walt [Reference 9] showed that the bimodal diffusion equation can be formulated in configuration and pitch-angle coordinates  $(L, x, t)$  where  $x \equiv \cos \alpha$ . Such a formulation is particularly convenient for data applications because the coordinates are simple, although it needs to be emphasized that its validity is restricted to slices in  $L$ -space, over which energy gained or lost from radial diffusion does not impact Walt's invariant. As discussed in Paper I the simultaneous multi-mode diffusion equation for the electron distribution function  $f$  can be written

$$\frac{\partial f}{\partial t} = D_{xx} \left[ \frac{\partial^2 f}{\partial x^2} + \frac{1}{x} \frac{\partial f}{\partial x} \right] + \xi L^{-2-\frac{1}{2}\nu} \frac{\partial}{\partial L} \left[ L^{\mu+2-\frac{1}{2}\nu} \frac{\partial f}{\partial L} \right] \quad (1)$$

where  $\mu$  and  $\nu$  are considered to be constant parameters. In Paper I, we showed that if the pitch-angle and radial diffusion coefficients,  $D_{xx}$  and  $D_{LL}$ , respectively, take on certain generic forms

$$\begin{aligned} D_{xx} &\equiv D_{xx}(E) \\ D_{LL} &\equiv \xi(E)L^\mu \end{aligned} \quad (2)$$

then the general solution to the bimodal diffusion equation can be expanded in terms of eigenfunctions of various Bessel forms. This convenient property forms our basic principle to characterize the state of the outer electron belt in a piecewise-continuous fashion in terms of a data base measured along a satellite trajectory  $L(t)$ .

The general solution consists of the linear sum of three modal expansions: (1) single-mode pitch-angle diffusion, (2) single-mode radial diffusion and (3) simultaneous bi-modal diffusion. Using the device of the Kronecker delta  $\delta_{n0}$ , the three modal expansions can be written in terms of a single eigenfunction expansion

$$f = \sum_{n=0}^{\infty} \left[ \delta_{n0} - (1 - \delta_{n0}) \frac{\sqrt{2}}{x_c} \cdot \frac{J_0(k_n x/x_c)}{J_1(k_n)} \right] \left( c_n(1 - \delta_{n0}) e^{t/\tau_n} + e^{t/t_n} [a_n Y_n(L) + b_n Z_n(L)] \right) \quad (3)$$

where  $k_n$  is the  $n^{\text{th}}$  zero of the Bessel function  $J_0$  and  $x_c = \cos \alpha_c$ . The parameters and functions are defined as follows:

$$\begin{aligned} \epsilon &\equiv 3(1 - \frac{\nu}{2})/(\mu - 2) \\ \sigma &\equiv -\frac{\mu}{2} - \frac{1}{2} + \frac{3}{4}\nu \end{aligned} \quad (4)$$

$$\lambda \equiv \frac{\mu}{2} - 1$$

$$Y_n(L) = L^\sigma \cdot [J_{1+\epsilon}(|\beta_n|/L^\lambda)]_> \cdot [I_{1+\epsilon}(|\beta_n|/L^\lambda)]_< \quad (5)$$

$$Z_n(L) = L^\sigma \cdot [N_{1+\epsilon}(|\beta_n|/L^\lambda)]_> \cdot [K_{1+\epsilon}(|\beta_n|/L^\lambda)]_< \quad (6)$$

$J$  is the regular Bessel function,  $I$  and  $K$  are the modified Bessel functions, and  $N$  is the Neumann function. The usual notation  $[g]_>$  is defined in this case by

$$[g]_> = g \quad \text{if} \quad t_n > 0 \quad (7)$$

$$[g]_> = 1 \quad \text{if} \quad t_n < 0$$

and analogously for  $[g]_<$ . The separation constants  $(t_n, \beta_n)$  and parameters of the solution are related by the algebraic relations

$$t_n^{-1} = (1 - \delta_{n0})\tau_n^{-1} - \xi\beta_n^2\lambda^2 \quad (8)$$

$$\tau_n^{-1} \equiv -D_{xx}k_n^2/x_c^2 \quad (9)$$

The parameter value  $\lambda = 4$  (i.e.,  $\mu = 10$ ) is chosen to conform with the consensual  $L$ -dependence of the radial diffusion coefficient [Reference 11]. From Paper I the parameter  $\nu$  is set to 2 (i.e.,  $\epsilon = 0$ ) for ease of computing the Bessel functions. Other values of  $\nu$  are easily accommodated at the expense of computational speed. Our work so far has demonstrated the economy of using  $\nu = 2$ , but further refinements can be readily accommodated in our procedure. Equation (8) will be referred to as the separation equation because the entire separable diffusion differential equation is reduced by the eigenfunction expansion into this constraint on the diffusion parameters. It is seen from (9) that the single pitch-angle mode time constants are negative as expected, since single-mode pitch-angle diffusion always leads to decay. For radial diffusion, however, the time constants  $t_n$  can be either positive or negative over a finite time interval. This is due to the fact that the phase space density in the finite  $L$  domain can rise or fall in time in response to particle transport into and out of the adjacent volumes. With the sign of each  $t_n$  not predetermined, the separation constant  $\beta_n^2$  can be positive or negative. This is the origin of the  $(J, I)$  and  $(N, K)$  options of (5) and (6). This general solution to the simultaneous bimodal diffusion equation and the data representation were introduced and utilized in three of the four papers to be discussed below as part of our test model study.

### III. FIRST RESULTS FROM SIMULTANEOUS BIMODEL DIFFUSION

The general solution of the simultaneous bimodal (radial and pitch-angle) diffusion equation for the outer electron radiation belts developed in the previous section was first put forth in Paper I [Reference 5] and is included in this report as Appendix A. The solution was developed with special regard for the requirements of satellite radiation belt data analysis and is used to test the bimodal theory of outer electron belt diffusion by confronting it with satellite data. Satellite observations, usually over finite volumes of  $(L, t)$  space, are seldom sufficient in space-time duration to cover the relaxation to equilibrium of the entire radiation belt. Since time scales of continuous data coverage are often comparable to that of radiation belt disturbances, it is, therefore, inappropriate to apply impulsive semi-infinite time response solutions of diffusion theory to interpret data from a finite window of  $(L, t)$  space. Observational limitations indicate that appropriate solutions for the interpretation of satellite data are general solutions for a finite-volume boundary value problem in bi-modal diffusion. In the paper we tested such a solution as the prime candidate for comprehensive radiation-belt dynamic modeling by applying the solution and developing a method of analysis to radiation belt electron data obtained by the SCATHA satellite at moderate geomagnetic activity. The success of our first results and the generality of our solution indicate its promise as a new approach to dynamic modeling of the radiation belts. Such an approach should be based on our bimodal diffusion solution and on satellite data taken on a routine global basis.

Our test data base from the SCATHA SC3 experiment was discussed in Paper I, followed by an in-depth introduction to bimodal diffusion in the outer-belt region. When a period of data from day 165, June 13, 1980, was fit to the general solution expansion (Equations 3 through 9), exclusive of the separation equation (8), the electron distribution function was characterized by the set of parameters  $(a_n, b_n, c_n, t_n, \tau_n, \beta_n)$ . The phase space volume for this fit covered the region  $(5.3 \leq L \leq 6.7; \Delta t = 5 \text{ hrs.}; 200 \text{ keV} \leq E \leq 2000 \text{ keV}; \alpha_c \leq \alpha \leq 90^\circ)$ , where  $\alpha$  is the pitch-angle,  $\alpha_c$  is the edge of the loss cone and  $E$  is the energy. It was found that five orders of eigenfunctions ( $n=0-4$ ) per energy channel, i.e., 30 parameters per energy channel, were sufficient to characterize the full data base of 5040 data points. Note that  $\tau_n$  and  $\beta_n$  were independently derived from the fit and (8) was not imposed. No iterations were made and a value of  $\xi$  was determined for each order from (8), i.e. a set of  $\xi_n$ . From Equation (9) the pitch-angle coefficient  $D_{zz}$  can be derived from the data set for each energy channel. Figure 1 shows the derived  $D_{zz}$  together with the fit errors as functions of  $\text{el. rgy.}$  In the solution,  $D_{zz}$  was assumed independent of  $L$  in order to achieve separability. From the figure, it is seen that  $D_{zz}$  is constant with energy, except for the 448 keV channel. No iterations were made in this early work. In Paper I these values of  $D_{zz}$  were found to agree with other determinations giving a pitch-angle diffusion lifetime of about 5 days.

The derivation of the radial diffusion coefficient serves two roles of providing for phys-

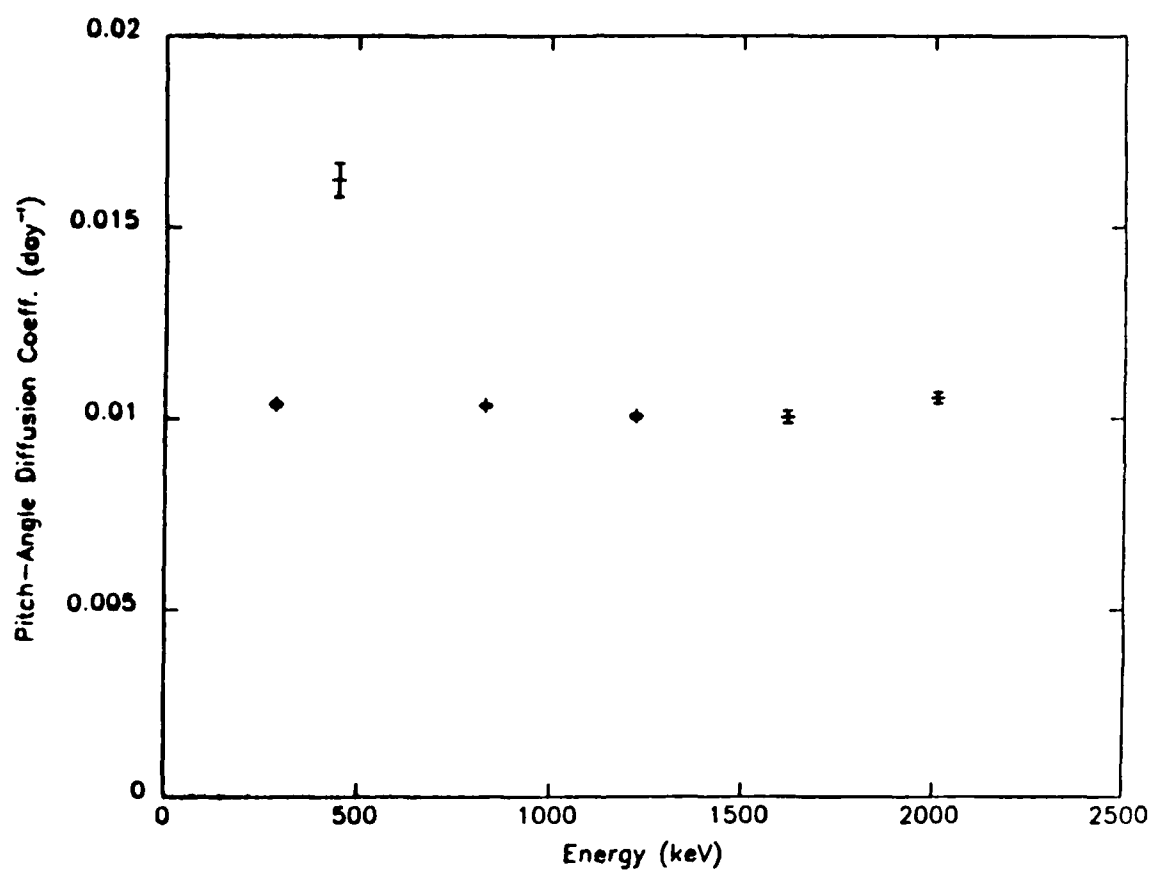


Figure 1. Pitch-angle diffusion coefficient as function of energy.

ical data in the outer belt, which can be compared with other determinations from direct particle observations, and of testing independently the adequacy of our representation to the data. Figure 2 shows a scatterplot of  $D_{LL}$  versus energy for  $L = 5.3$ . As mentioned above the scatter values of  $D_{LL}$  result from our deliberately not enforcing (8) in an iterative manner. A worst case variance of the fit is obtained from the set of  $\xi_n$  at each order. It was found that these order-dependent values of  $\xi$  clustered closely around those determined by other workers, an indication that the representation is reasonable. The results of Paper I were encouraging in that solutions of simultaneous bimodal (pitch-angle and radial) diffusion theory were shown to have the potential to provide an efficient description of a SCATHA outer-belt electron data set. The description was achieved in essentially the initial pass without a systematic fitting procedure. These initial results established plausibility for the approach.

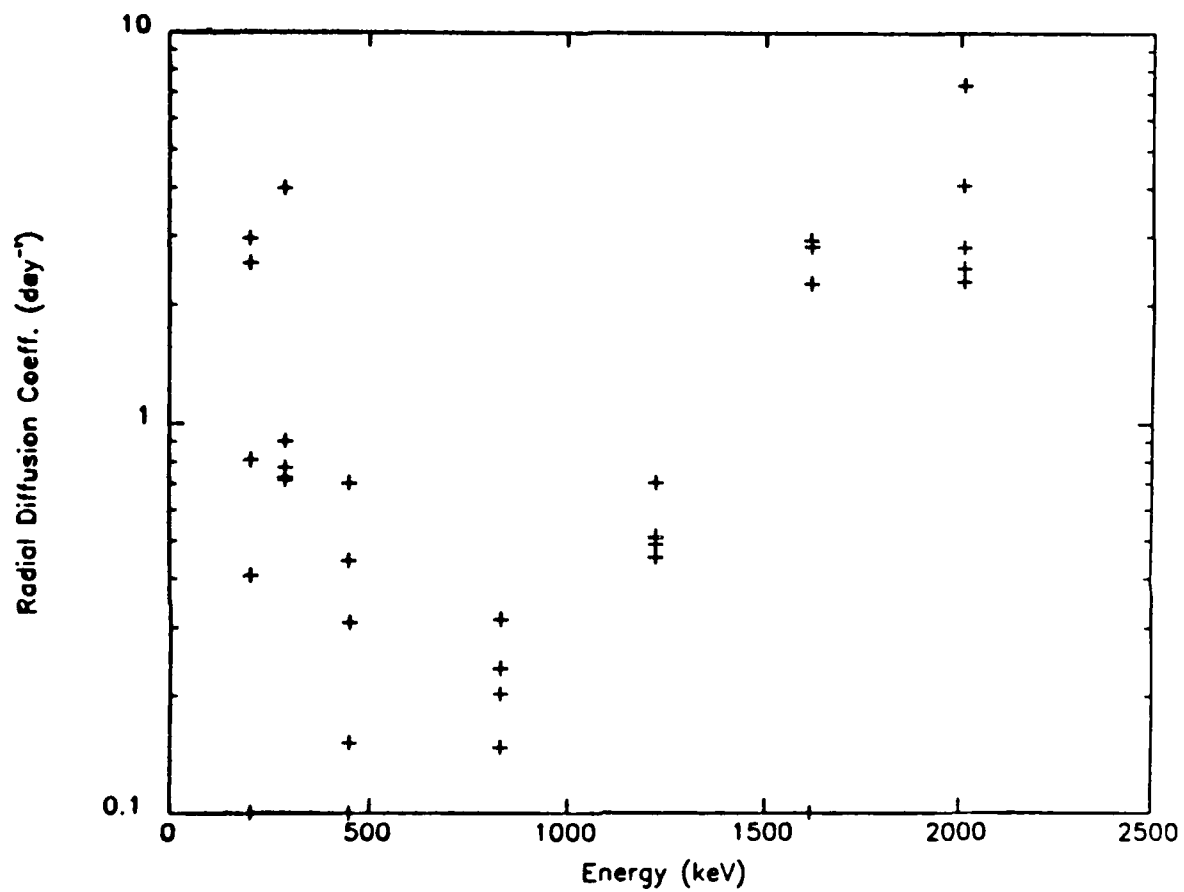


Figure 2. Radial diffusion coefficient as function of energy at  $L = 5.30$ . The spread of values for each energy is a measure of the worse-case variance in its determination.



#### IV. HIGH-ENERGY OUTER RADIATION BELT DYNAMIC MODELING

Paper II [Reference 6], which can be found in Appendix B, originated from two papers we presented at the Conference on High Energy Radiation Background in Space in anticipation of the dynamic modeling objective of the upcoming CRRES program. We described the good results of our initial attempt at constructing the dynamics of the outer electron radiation belt by combining diffusion theory with data as found in Paper I and summarized in the previous section, as well as discussed issues concerning dynamic modeling in general. The latter was pertinent to the conference because dynamic modeling should provide a means to map the particle phase-space distributions away from the satellite track. However, the uniqueness of such an off-trajectory projection needs to be determined in light of the fitting errors involved in the data representation. These issues were brought up here and analyzed in more detail in Paper IV, summarized in Section VI below.

The formulation of the simultaneous bimodal diffusion problem and our approach is introduced in a different way from that of Paper I. This may provide a better, or at least different, perspective of our solution representation. Further, we introduced the fact that the radial portion of the solution is explicitly a function of  $t$  by expressing  $L$  as a function of  $t$ . We may rewrite the radial portion of Equation (3) as

$$h(L(t), t) = e^{t/t_n} [a_n Y_n(L(t)) + b_n Z_n(L(t))] \quad (10)$$

Utilizing  $L(t)$  minimizes the mixing of space-time in our fitting. For the near-geosynchronous SCATHA satellite covering only a small range of  $L$ , the effect of space-time mixing is minimal. This allowed us to complete the first test case shown in Paper I. However, for the more comprehensive situation of highly-elliptic orbits such as that for CRRES, which attempts to specify the radiation belts over a wide range of  $L$ , the trajectory  $L(t)$  is a nonlinear function of  $t$ , requiring a nonlinear fit for the determination of the diffusion parameters. This is illustrated in Figure 3, which shows plots of  $h(L)$  for three situations: (a)  $L$  and  $t$  independent, (b) SCATHA orbit on which  $L$  is nearly independent of  $t$ , and (c) CRRES-like orbit on which  $L$  is strongly dependent on  $t$ . The strong distortions on panel (c) for  $h(L(t), t)$  relative to the same function  $h(L, t)$  on panel (a) signifies that dynamic modeling in conjunction with a satellite data base involves much more than obtaining solutions to diffusion theory. Using  $L(t)$  results in a better fitting scheme and supports unique off-trajectory mappings. Paper II also briefly touched on the problem of magnetic and electric  $L$ -shell-splitting, which needs to be studied further so that it can be taken into account in the dynamic models.

The discussion in Paper II showed that dynamic modeling differs fundamentally from radiation belt analysis in that a theoretical representation of the on-trajectory data set is required to predict fluxes outside of the satellite orbit. The faithfulness of the projection depends on whether the representation is a good description of the physical diffusive processes seen in the on-trajectory data. Our test case study yielded results

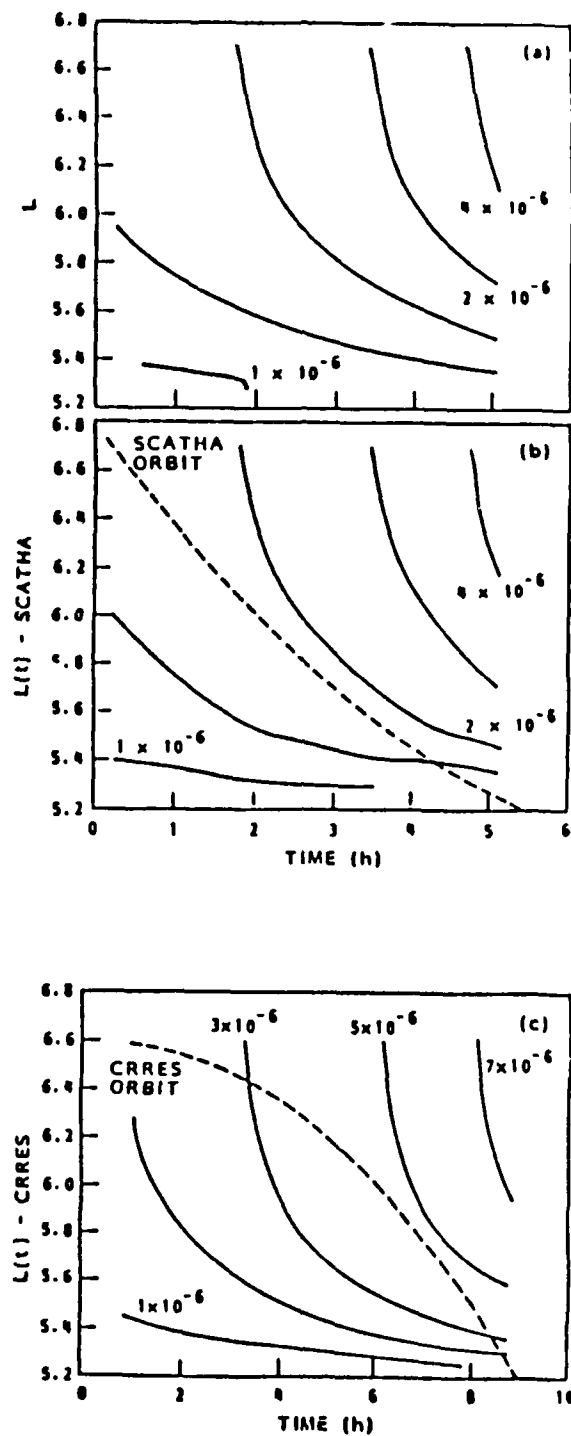


Figure 3. Illustration of the nonlinear nature of fitting the radial representation to data. In all panels, the function  $h(L, t)$  is plotted with the same set of arbitrarily chosen constant parameters. The solid lines are contours of  $h(L, t)$  and the dashed lines are  $L(t)$ . Panel (a) is for an independent  $(L, t)$  grid. Panel (b) is for  $L(t)$  specified by SCATHA orbit and panel (c) is for the CRRES orbit. Note the drastic change of time scale required in order for the CRRES case to have similar contours for the  $h(L, t)$  function as the nearly identical panels (a) and (b).

consistent with basically all other measurements in the moderately active outer electron radiation belt. The resolution of a number of important issues brought by examination of the test case awaits further work before operational dynamic models can be constructed.

## V. A NONLINEAR MODEL OF WAVE-PARTICLE INTERACTIONS IN THE TRAPPED RADIATION BELTS

The interactions of waves and trapped electrons are described in Paper III [Reference 7], which is attached in Appendix C, by a closed system of three nonlinear coupled equations. The model has applications to many aspects of wave-particle interactions in the magnetosphere. Nonlinear numerical solutions pertinent to auroral pulsations have been computed for realistic ranges of physical parameters. The results confirm that precipitating pulsations can be initiated by either an injection of energetic trapped particles or an increase in the plasma ionization density. Relaxation of the system results in cyclic phase trajectories about a (quasi equilibrium) point that is not located at the initial equilibrium point. That observation may explain the tendency of auroral pulsations to appear superimposed upon an increase in the general rate of electron precipitation. The results also imply that precipitation pulsations are most readily initiated by an encounter of drifting energetic electrons with a region of enhanced cold plasma density.

The interaction between waves and trapped particles in the magnetosphere is a key problem in magnetospheric physics [Reference 12], whose basic elements are considered to be well understood. However, the complexity of a full treatment, based on first principles, of the diffusion of particles into the loss cone and the response of waves to particle diffusion has restricted quantitative studies to a handful. Davidson et al. [Reference 13] utilize the SCATHA SC3 data base to test the theoretical trapping limit proposed by Schulz and Davidson [Reference 14]. The results of the study, under a different sponsorship than that of this report, were found to be consistent with the proposed model and the numerical results agreed with the earlier predictions of Reference 8. In this study the pitch-angle distribution was fit to determine the parameters of the shape. The representation of our bimodal diffusion solution also determines shape parameters of the pitch-angle distribution. Thus our representation can monitor the state of the radiation belt and indicate when the particle populations are approaching isotropy, i.e., approaching the trapping limit.

The modeling applications for which the solutions of Paper III can be applied are many. In fact, the physical principles and the code used in the paper are applicable with virtually no modifications to radiation belt particle response to wave-particle interactions and flux limiting. The nature of the detailed wave modes enters only in the determination of the physical parameters. This wave-particle interaction model may play a role in our dynamic modeling in the future.

## VI. TOWARDS DYNAMIC MODELING OF THE OUTER ELECTRON RADIATION BELT

We show in Paper IV [Reference 8], which is in Appendix D, that the general solution of a simple form of the simultaneous bimodal (radial and pitch-angle) diffusion equation can represent the SCATHA outer belt electron distribution to a high degree of accuracy for periods up to 10 hours. The data representation requires diffusion parameters that are in agreement with all previous experimental and theoretical determinations of such diffusion coefficients. Such a representation satisfies the basic requirements towards the dynamic modeling of the outer electron radiation belts for  $L < 7$  at quiet and moderate geomagnetic conditions. For  $L \sim 7$  the representation has difficulties with "butterfly" distributions that may signify energetic electron encounters with the magnetopause. It is demonstrated with a typical example of computer simulation of electron encounters with the magnetopause that the effects of the encounter may be highly anisotropic in configuration or in invariant space.

This paper addresses many of the issues still remaining in our test model study for developing the tools needed for dynamic modeling of the radiation belts. Because the resolution of several of these issues are new in this study, we therefore include major sections of the paper where they are relevant to our results and conclusions. At least three major issues require attention if the bimodal diffusion approach to dynamic modeling is to be pursued. First, we must establish a systematic iterative procedure to achieve a fit of the data consistent with all the constraints of the solution. This requirement involves not only specification of the accuracy of the fit in four-dimensional phase space but also satisfaction of diffusion parameter constraints imposed by bimodal theory. Second, the form of the bimodal diffusion theory used was computationally efficient but its validity was recognized to be restricted to a sufficiently thin slice of  $L$ -space [Reference 9]. Such a property is not incompatible with dynamic modeling with a satellite data base since satellite data are necessarily restricted in  $(L, t)$  space. Nevertheless, it is crucial to determine the observational extent of  $L$ -space over which the version of bimodal diffusion theory is valid. Third and most important, the degree of uniqueness of the data representation must be established since dynamic modeling implies the projection of electron fluxes from measurements on a satellite trajectory to other regions of phase space where direct measurements are not available. Note that the solution representation of the theory is necessarily unique everywhere if the on-trajectory specification is unique. However, the data fit to the solution is over a trajectory on which  $L$  and  $t$  are mixed; therefore, the on-trajectory specification is not necessarily unique insofar as the separation of  $L$  and  $t$  effects are concerned. In order to insure that our iterative procedure for untangling  $L$  and  $t$  effects does not alias the projection to other regions of space-time, we must at least demonstrate that our data representation yields flux projections independent of the projection path.

In Paper IV, we have addressed the above three issues. We have demonstrated that simultaneous bimodal diffusion theory is an efficient representation of SCATHA outer-belt

electron data in the configuration space range ( $5 \leq L \leq 7$ ;  $\Delta t < 10$  hrs.) for Day 165, 1980 and Day 110, 1979. Iterative procedures have been devised to improve the fit and to satisfy diffusion parameter constraints that were not enforced in Paper I. The result is a reduction of parameters (by  $\sim 15\%$ ) to achieve better fits over a much larger data base (by  $\sim 100\%$ ). We were also able to demonstrate that fit errors do not impact the uniqueness of off-trajectory flux projections based on the solution representation.

In Paper I it was found that five orders of eigenfunctions ( $n=0-4$ ) per energy channel, i.e., 30 parameters per energy channel, were sufficient to characterize a data base of 5040 data points. For Paper 4, we included the effects of the separation equation (8) in constraining the diffusion parameters ( $\tau_n, \beta_n, \xi$ ). Note that the diffusion parameter  $\xi$  is independent of order  $n$ , whereas the others are order dependent. In Paper I,  $\tau_n$  and  $\beta_n$  were independently derived from the fit and (8) was not imposed. No iterations were made and a value of  $\xi$  was determined for each order from (8), i.e. a set of  $\xi_n$ . It was found that these order-dependent values of  $\xi$  clustered closely around those determined by other workers, an indication that the representation is reasonable. Here we used the constraint (8) as the focus for an iterative fitting scheme in determining the best order-independent value of  $\xi$ . Since (8) was imposed, ( $\tau_n, \xi$ ) and  $\beta_n$  were no longer independent, thus the number of required parameters per energy channel was reduced by 4 in this work. The iteration also improved the fit to the data set. The process of fitting a data set to the representation begins with decomposing the electron distribution functions into pitch-angle eigenfunctions and their amplitudes. We have demonstrated in Paper I that this procedure is highly accurate. We shall focus our discussion below on the decomposition of the pitch-angle amplitudes into eigenfunction expansions in  $L$ .

We have devised a nonlinear fitting procedure keyed to the iterative determination of the order-independent radial diffusion parameter  $\xi$  in the separation equation (8). In the first pass, the procedure described in Paper I is applied and the separation equation (8) is solved for each order, resulting in a set of order-dependent parameters  $\xi_n$ . Iterations begin with the choice of an interim mean value  $\xi = \langle \xi_n \rangle$  where the averaging is weighed by the eigenfunction amplitudes ( $a_n, b_n$ ). The interim value  $\xi$  is enforced in (8) to determine new values of the parameters ( $\tau_n, \beta_n$ ) in a new fit. With the new parameters, a new set of  $\xi_n$  is determined by solving (8) exactly and another iteration cycle begins. The iterative procedure continues until the residual error in the equality between the left and right hand side of (8) can no longer be improved upon. The final value of  $\xi$  is taken to be the fit value of the diffusion parameter. This is a nonlinear iterative procedure; therefore, there is no a priori guarantee that it is convergent. In practice, it converges because the set of  $\xi_n$  in the first pass is closely clustered to begin with. Figure 4 shows an example of the degree to which the constraint (8) is obeyed by the initial and final iterations of the procedure.

The iterative scheme has been applied to  $\sim 4$  hours of SCATHA electron belt data for Day 165, 1980 and to  $\sim 9$  hours of data for Day 110, 1979. Figures 5 and 6 show three-dimensional plots of the data and the fit reconstructions for these two days, respectively. It

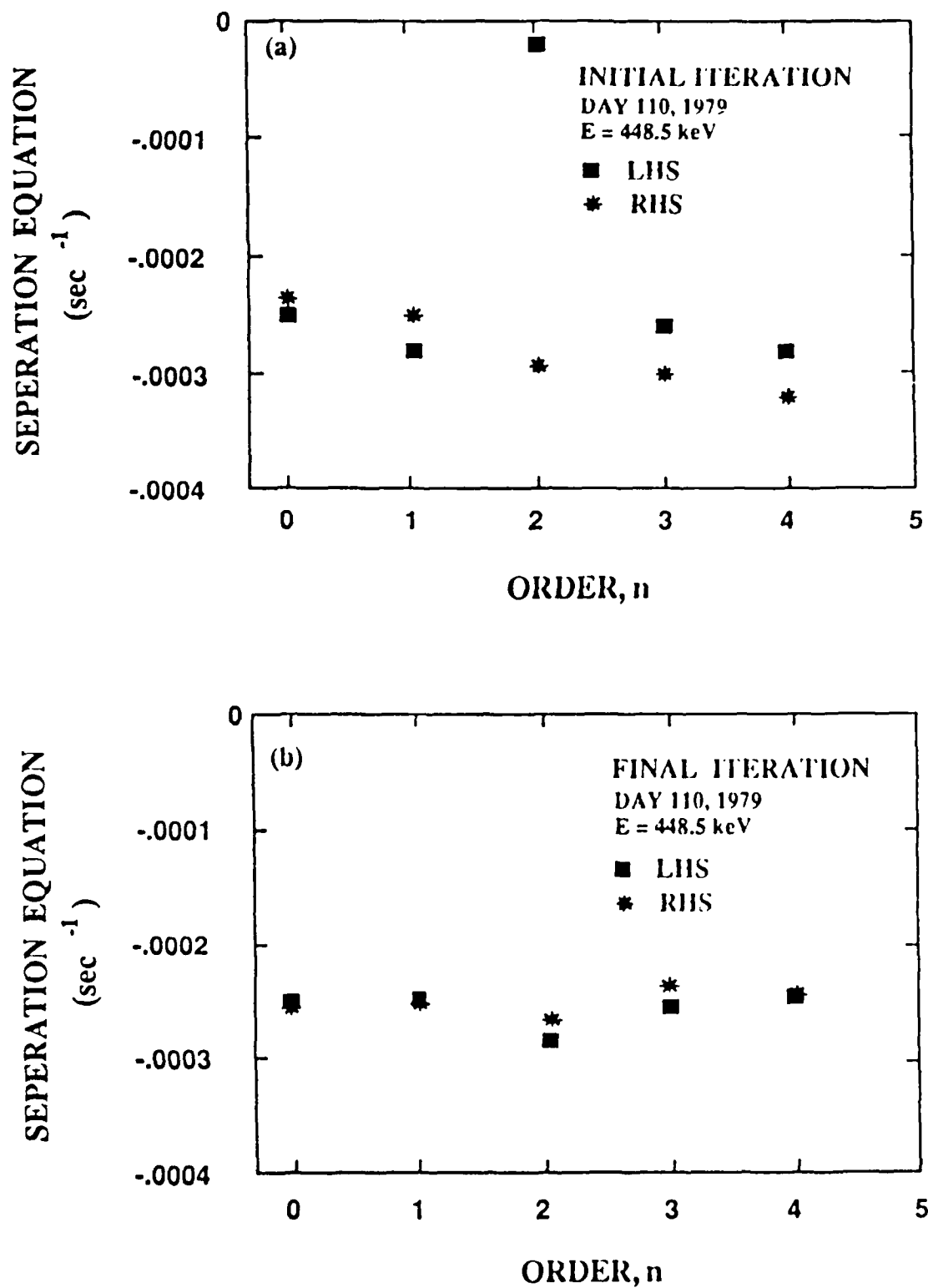


Figure 4. Values of the right hand side (RHS) and left hand side (LHS) of the separation Equation (8) are plotted as functions of order  $n$  for (a) the initial iteration and (b) the final iteration. The equality is enforced as a fit constraint in this paper. Note the large divergence at order 2 in the initial iteration.

should be noted that reconstruction errors for both days are primarily concentrated in the high- $L$  and  $\alpha \sim 90^\circ$  region. We found that this region is rich in "butterfly" distributions [References 15 and 16]. These will be discussed in more detail below. Figures 7 and 8 show the distributions of the fit errors for each data point in the initial and final passes of the iterations for the two days, respectively. The data points associated with the large-error tail of the error distributions, less than 1000 data points in each data set, are again related to "butterfly" distributions, although a substantial portion of the large fit errors are also contributed to by some noisy data in the data base. Unsmoothed raw data is used to tally the percentage error in these figures. Figure 9 shows the comparison of radial diffusion coefficients determined in this work with all other known observational and theoretical determinations [References 17 through 29]. The mottled band of  $D_{LL}$  values in the figure corresponds to this work. The spread of the band is due to energy dependence of the diffusion coefficient. The larger cross-hatched band of  $D_{LL}$  values was determined in Paper I and is due not only to the spread of energy channels but also primarily to the dependence of  $\xi$  on order. It is seen that our enforcement of (8) allows for a much more precise determination of the radial diffusion coefficient. Energy dependence is not always addressed in other work.

For a data representation scheme to qualify as a dynamic modeling scheme, it must demonstrate the ability to uniquely predict (or obtain by projection), the off-trajectory electron distributions, from a set of on-trajectory electron distributions. The use of the general solution to bimodal diffusion theory yields a naturally unique off-trajectory projection within the limitations of the assumed physics. Whether the assumed physics correctly describe the actual processes prevailing in the particular region of the outer electron belt is a separate issue to be discussed below. Within the scope of diffusion theory, if the on-trajectory representation is exact, the projection to any off-trajectory point is also independent of path because the solution is uniquely specified everywhere that it is valid. Since the on-trajectory representation is not given a priori (but given as a fit based on a data set that mixes  $L$  and  $t$ ), an important question arises: Can the fit errors due to aliasing  $L$  and  $t$  destroy the uniqueness of the projection by making it path dependent?

We have investigated this problem of projection consistency (or path dependence) for our representation by projecting to an off-trajectory point from two well-separated on-trajectory points: one having the same  $L$  and the other having the same  $t$  as the off-trajectory point. The projection paths are thus along the  $t$  and the  $L$  axes, respectively. Figure 10 shows the results of such a uniqueness test for Day 110, 1979. The projection in our representation is indeed path independent. This test clears a hurdle for using the bimodal diffusion solution for outer-belt dynamic modeling, since it demonstrates that uniqueness is not destroyed by the fit errors. It must be noted that this is only an internal consistency test, not a validity test that diffusion theory correctly describes the prevailing physics of the outer belt. A validity test requires data sets from more than one satellite.



DAY 165, 1980

$E = 288.5 \text{ keV}$

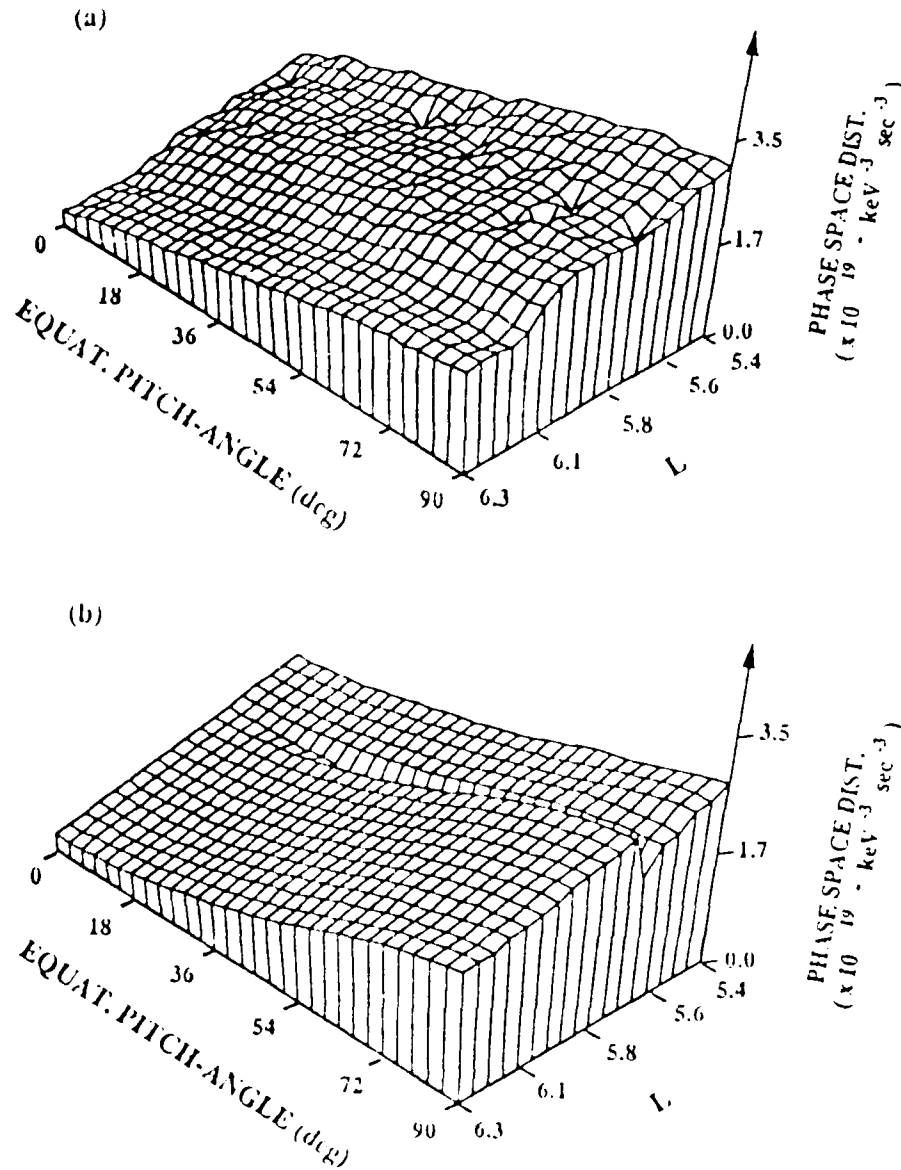


Figure 5. Three-dimensional presentation of the phase space density of (a) the data base and (b) its reconstitutions for the 288.5 keV channel of Day 165, 1980 in pitch angle and  $L$ . Large errors are found primarily in the corner of (b) pertaining to large  $L$  and large pitch angles. Noisy data near  $L \sim 5.7$  also resulted in some error.

DAY 110, 1979

$E = 448 \text{ keV}$

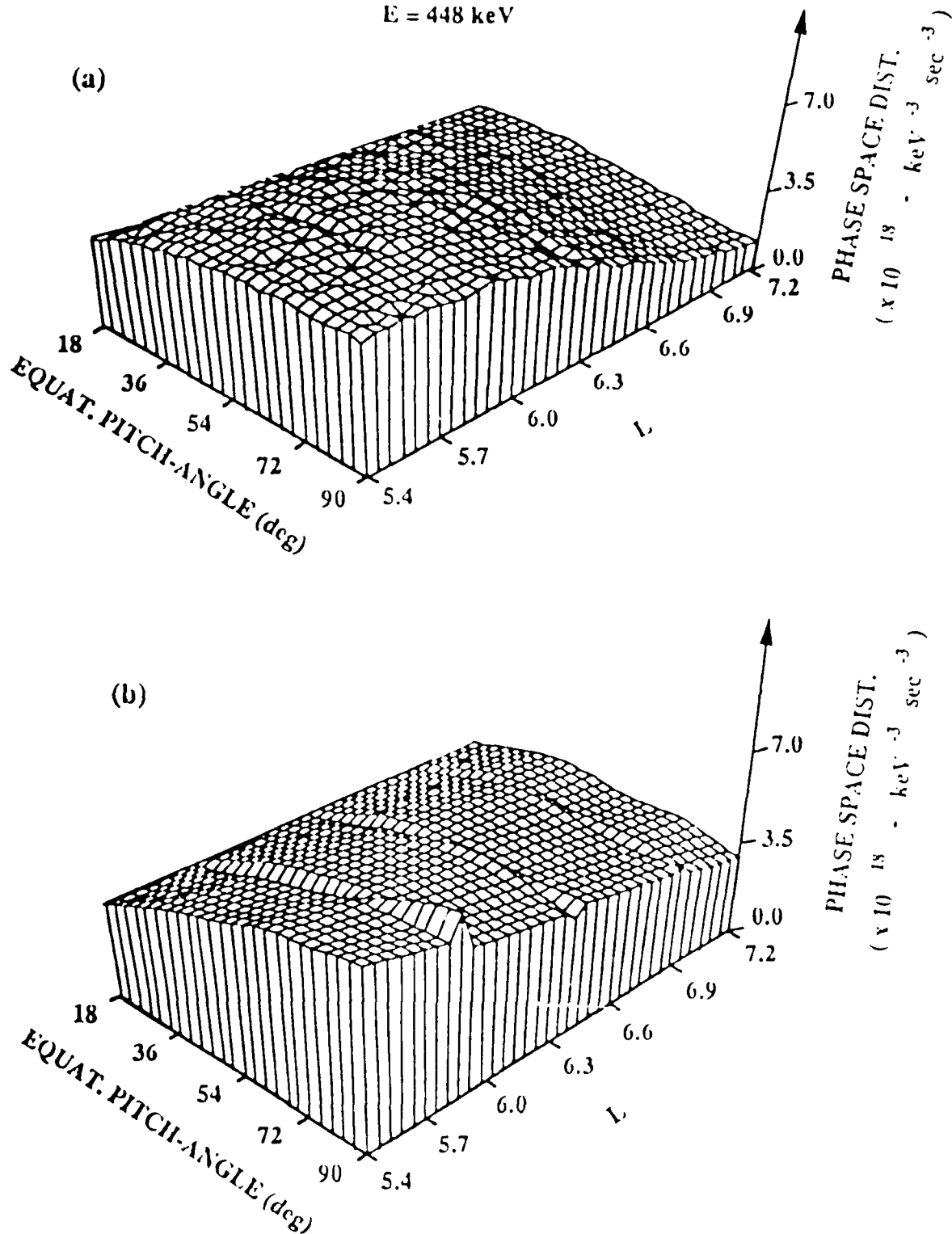


Figure 6. Three-dimensional presentation of the phase space density of (a) the data base and (b) its reconstitutions for the 448 keV channel of Day 110, 1979 in pitch angle and  $L$ . As in Figure 5, the large errors are mainly confined to the corner of (b) pertaining to large  $L$  and large pitch angles.

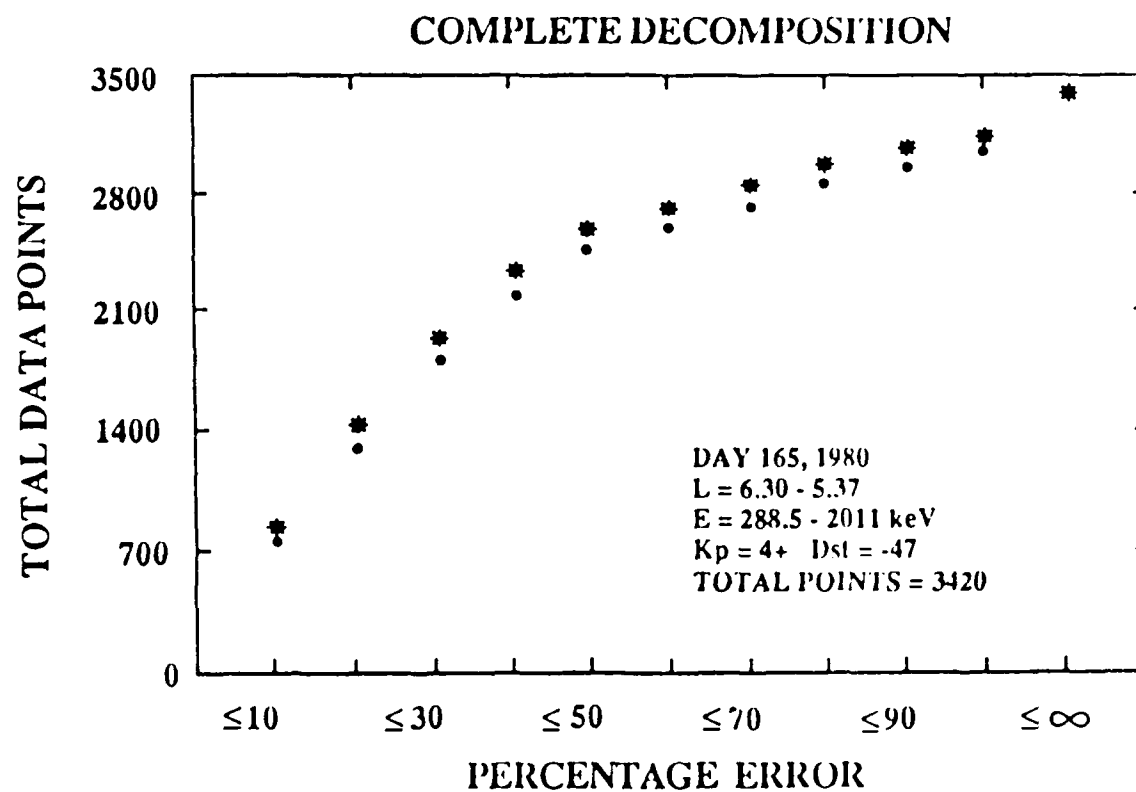


Figure 7. The distribution of fit percentage errors in the reconstitution of all the data points in the Day 165, 1980 data base. The error distributions of the initial and final iterations are shown as dots and asterisks, respectively.

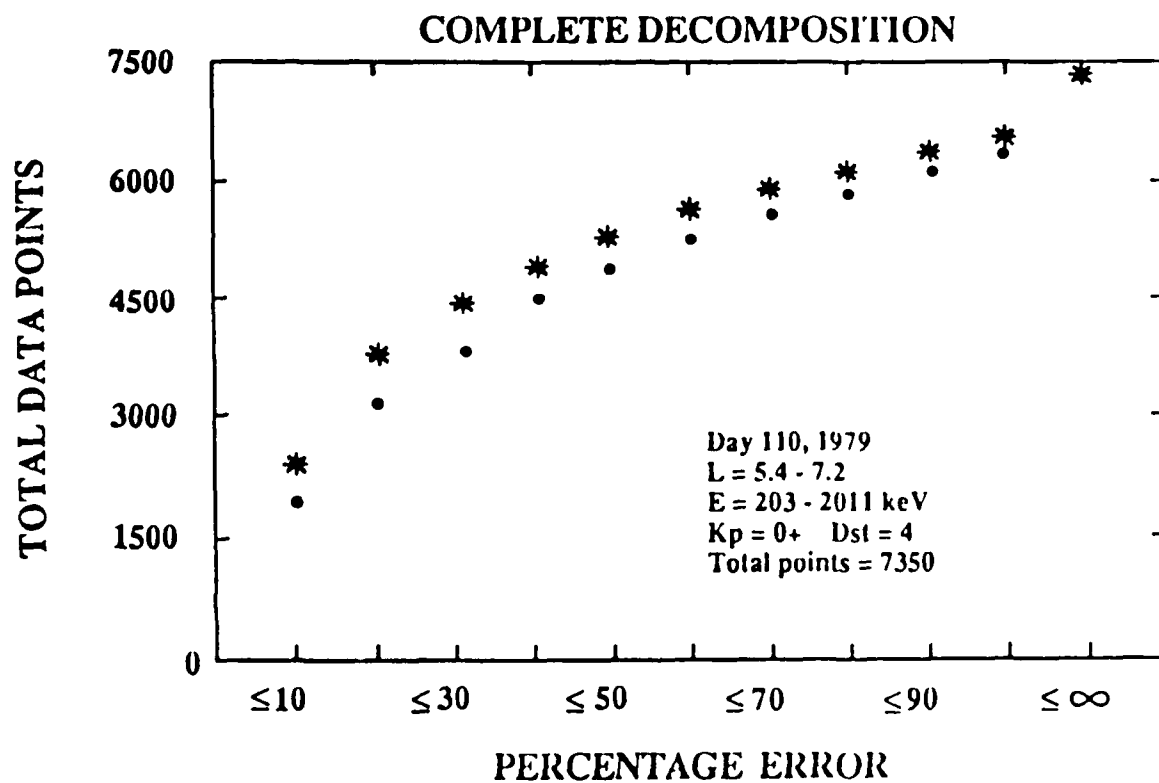


Figure 8. The distribution of fit percentage errors in the reconstitution of all the data points in the Day 110, 1979 data base. The error distributions of the initial and final iterations are shown as dots and asterisks, respectively.

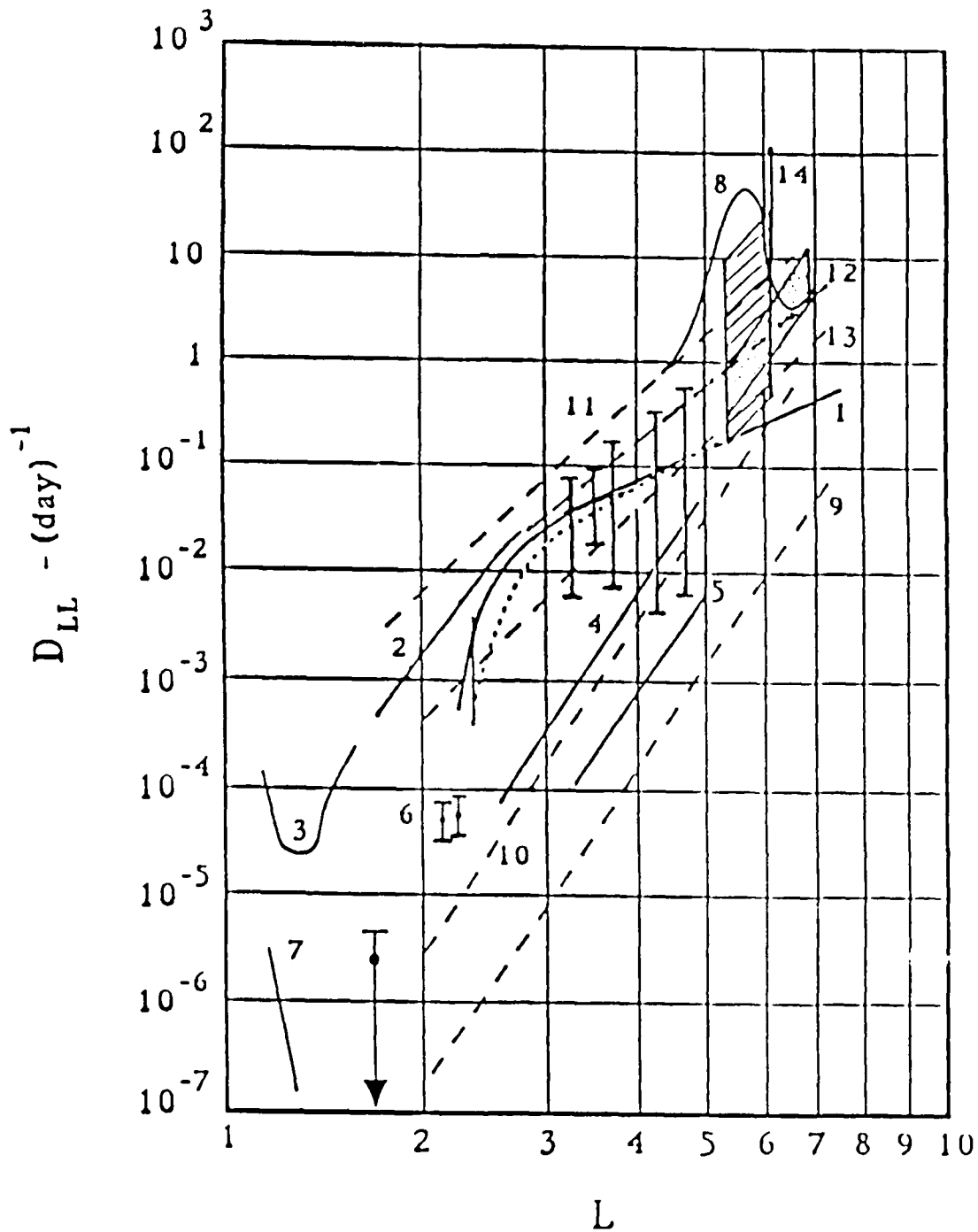


Figure 9. Comparison of the radial diffusion coefficients determined in Paper IV for the energy range 0.2-2.0 keV (mottled area) with Paper I (cross-hatched area) and with the compilation of West et al. [1981], whose individual analysis yields curve 1. Curves 2-8 are experimental: 2, Tomassian et al. [1972]; 3, Farley [1969]; 4, Newkirk and Walt [1968b]; 5, Lanzerotti et al. [1970]; 6, Newkirk and Walt [1968b], Fälthammar [1970]; 7, Newkirk and Walt [1968a]; 8, Kavanaugh [1968]. Curves 9-14 are theoretical or semi-theoretical: 9, Nakada and Mead [1965]; 10, Tverskoy [1965]; 11, Birmingham [1969]; 12, 13, Cornwall [1968]; 14, Holzworth and Mozer [1979]; [References 17 through 29, respectively].

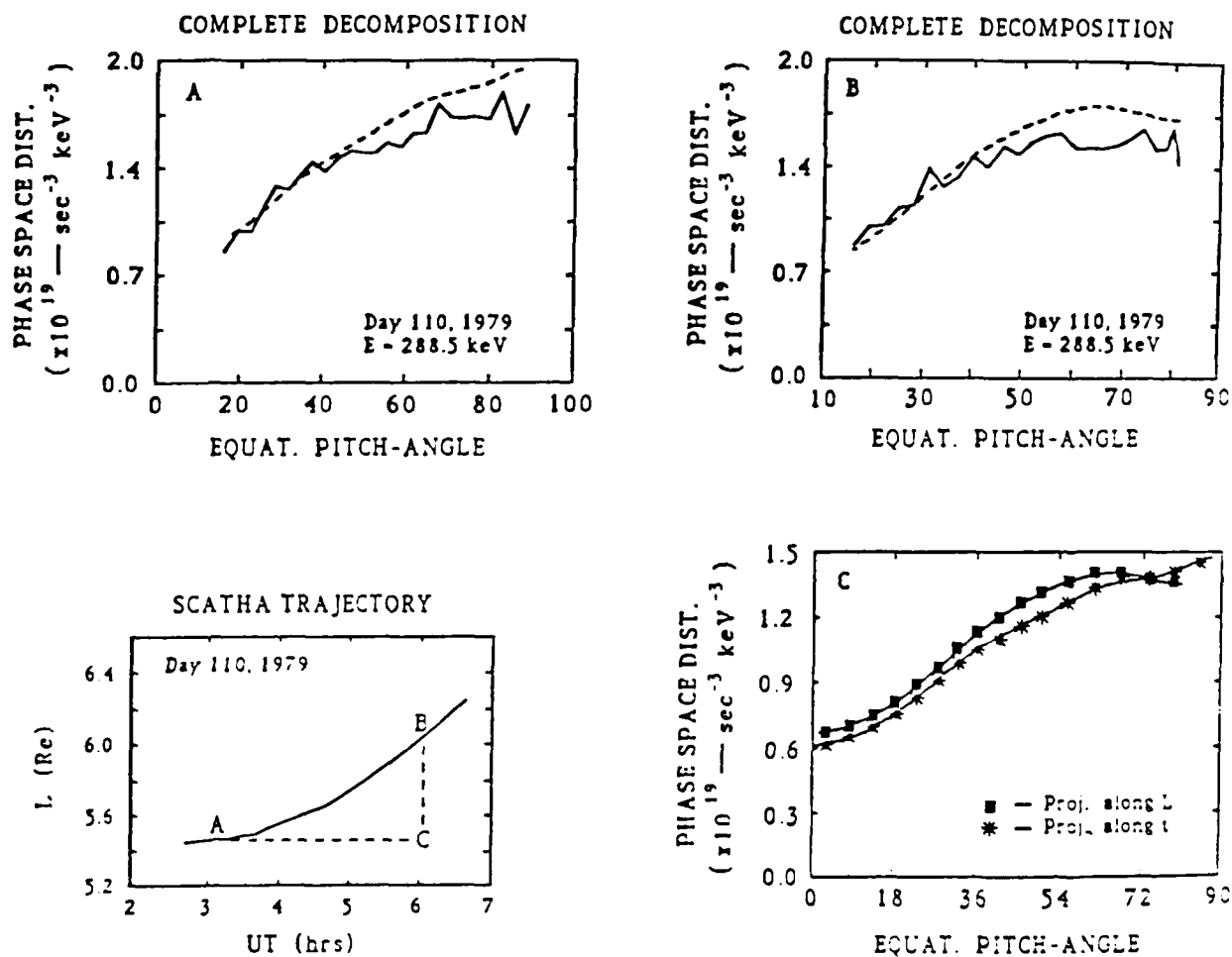


Figure 10. Demonstration of path independence in projecting the electron distributions from on-trajectory to off-trajectory points. Panels A and B are measured and fitted phase space distributions at the trajectory locations shown on the SCATHA trajectory panel. Using the eigenfunction representation, the distributions are projected along the  $t$  and  $L$  axes respectively to the off-trajectory point C. The comparison of the two projected distributions is shown on Panel C.

A valid dynamic model should be able to "predict" one satellite data set from the solution fit to the other satellite's data set, and vice versa.

We have repeatedly stated from the outset that the validity of the form of simultaneous bimodal diffusion theory chosen for this study is very severely limited, particularly in regions of the outer electron belt at  $L \geq 7$ . The first limitation is that Walt's invariant [Reference 9] remains so only within a limited slice of  $L$ . This property of piecewise invariance is exploited as much as possible in our application in the region  $5 \leq L < 7$ , but there must be constraints to the exploitation. In the stable regions of the outer belt at  $L < 5$ , we do not see any reason why the application of the representation will be different from that shown here, although it is necessary to test it with another satellite data set because SCATHA does not cover that region. For  $L > 6$ , we sometimes encounter difficulties with "butterfly" pitch-angle distributions. We recognized at the outset that an important factor limiting the validity of the representation is the effects of third invariant violations that may or may not be describable in terms of diffusion. Such effects can be due to severe magnetic or electric shell splitting or to encounters with the magnetopause. In such encounters, the electron distribution on a given  $L$ -shell can be changed catastrophically. Since such third-invariant violating effects are deemed to be most effective at the equatorial region, it is usually assumed that their signature is a loss to the drift shell of equatorially mirroring particles (those with  $\sim 90^\circ$  pitch angle) leading to the so-called "butterfly" distributions [References 15 and 16]. Such an expectation seems reasonable as far as the pitch-angle distribution is concerned; however, the transport in the configuration part of phase space is a matter that has not been investigated beyond the expectation that the third invariant is drastically violated.

Since our representation is not expected to be valid for describing such drastic violations of the third invariant, the inclusion of such distribution functions in our data base incurs large errors in the representation. These constitute a part of the large-error tail of the error distributions shown in Figures 7 and 8. The successful treatment of the "butterfly" events constitutes the remaining hurdle towards dynamic outer electron belt modeling. The solution to this important problem is beyond the scope of this brief report but we shall address some salient points here. An initial reaction to the failure of the simple form of radial diffusion used is to assume that another form of radial diffusion, perhaps in third invariant coordinates, may be a better description of the physics involved in "butterflies". Such may indeed be the case, but a more primitive question needs to be considered first: Are encounters involving drastic violations of the third invariant necessarily diffusive in the configuration part of phase space?

In order to answer this and related questions, we have initiated computer simulations of 10 MeV electrons encountering a realistic, non-turbulent paraboloidal magnetopause [Reference 30] in the configuration of a Tsyganenko [Reference 3] field model. The magnetic field magnitude drops by 30 nT across the magnetopause at the sub-solar point. The field configuration outside merges smoothly into a uniform southward interplanetary

configuration. The important feature of the magnetopause encounter is that the electron executes trapped bounce motion occasionally on inward field lines and, in between bounces, it skips along the equatorial regions sometimes inward and sometimes outward of the magnetopause boundary with differing amounts of residence time, dependent on pitch angle and gyration phases; i.e., there is little evidence of scatter perpendicular to the boundary. Such anisotropic scatterings in encounters with the magnetopause can hardly be described in simple terms of isotropic diffusion, in invariant coordinates or otherwise. The encounter effects are somewhat more isotropic in configuration space if the magnetopause is not smooth, but the anisotropy will remain since the average magnetic field is non-zero both inside and outside. Clearly the equatorial skippings are likely to lead to enhanced pitch-angle diffusion; however, pitch-angle diffusion cannot produce a "butterfly" population. On the other hand, skippings along the equatorial magnetopause, which cuts through many  $L$ -shells, clearly constitute transport in  $L$  and, consequently, violation of the third invariant, as expected. The loss to a given  $L$ -shell of electrons, which skip to a different  $L$ -shell along the equatorial magnetopause, will clearly produce a "butterfly" distribution. The surprising feature of the simulation is that this transport in  $L$  is anisotropic in configuration space and can hardly be considered diffusive. Based on computer simulations of magnetopause encounters, the "butterfly" distribution is but a superficial signature peculiar to the process in which violations of invariants occur with drastic anisotropy in configuration space. Further, the channeling of electron motion provided by the sharp magnetic field gradient at the magnetopause boundary surface indicates that it acts macroscopically as a scattering boundary to outer-belt electrons, having simultaneously the properties of a sink to electrons approaching the boundary on given initial  $L$ -shells intercepting the magnetopause and of a highly anisotropic source of electrons to  $L$ -shells intercepting the magnetopause inward of the initial  $L$ -shell. In the non-turbulent magnetopause case, virtually no electrons were lost to interplanetary space. It appears that diffusion in invariant space is not the panacea that cursory considerations make it out to be.

By testing against a SCATHA electron data base, we have found a computationally practicable representation for the outer-belt electron distribution from the general solution of a simple version of the simultaneous bimodal diffusion theory that satisfies the basic requirements for outer-belt dynamic modeling inwards of  $L \sim 7$ . The representation fails to characterize the small portion of outer-belt electron populations known as "butterfly" distributions. The nature of outer-radiation-belt electron encounters with the magnetopause needs to be investigated beyond the superficial formation of "butterfly" pitch-angle distributions. In particular, the distribution of "butterflies" in configuration space can shed light on the scattering processes in encounters with the magnetopause.



## VII. RESULTS AND CONCLUSIONS

Early in this Space Radiation Test Model Study we developed the necessary tools for handling the SCATHA SC3 electron data in both configuration and invariant coordinates. We mapped the phase-space distribution functions in terms of observable parameters at fixed first and second adiabatic invariants. We have subsequently developed the inverse algorithms for mapping the distribution in terms of the invariants at constant energy and pitch angle, the observable parameters. A computationally efficient procedure for calculating the third adiabatic invariant and the drift motion of particles was also demonstrated. Using these tools the SCATHA environmental data base was surveyed for periods of interest to this study. We then proceeded in an iterative fashion to solve the bimodal diffusion equation and test it with the data base. The following results and conclusions can be drawn from this study:

1. A computationally efficient representation was obtained based on a solution of the simultaneous bimodal (radial and pitch-angle) diffusion equation in the configuration and pitch-angle coordinates  $(L, x, t)$ .
2. The solution representation was tested against the SCATHA SC3 data base and was found to be good for  $L < 7$ .
3. The Bessel function expansion in the pitch-angle coordinate provides a means for identifying the pitch-angle distribution, e.g., for a normal, "butterfly" or isotropic distribution, and thus for monitoring the state of the radiation belt over time.
4. Data obtained on-trajectory as a function of  $L(t)$  and  $t$  do not necessarily lead to a unique off-trajectory projection. However, we have explicitly tested our representation and procedure, finding that they provide a unique projection away from the spacecraft orbit.
5. Based on the off-trajectory uniqueness, our representation will provide dynamic modeling for  $L \leq 7$ , if there are no "butterfly" pitch-angle distributions present in the data base.
6. "Butterfly" distributions lead to large errors when they are included in the data set to which the simultaneous bimodal diffusion solution is applied.
7. The nature of "butterfly" distributions has been elucidated with a particle simulation code. They are characterized by third invariant violation, as well as anisotropic transport, in configuration space. This effect has not been discovered until now.

## VIII. RECOMMENDATIONS

From the results and conclusions in the previous section of the report, the following recommendations are suggested for implementation in the near future in order to perform dynamic modeling of the radiation belts in the CRRES time frame.

1. In order to implement dynamic modeling of the outer radiation belt, our representation of the electron data should be used for  $L \leq 6$ .
2. The "butterfly" distributions should be investigated further with computer simulation and the findings should be incorporated into the diffusion theory.
3. Shell-splitting effects on lower-energy particles due to steady electric fields and magnetic fields should be investigated.
4. A procedure should be developed to couple all of these effects into the diffusion theory and our data representation, leading to the capability for dynamic modeling of the radiation belt.
5. The dynamic model should be tested with SCATHA SC3 data for the outer belt region.
6. The dynamic model should be tested with CRRES high-energy electron data over the whole radiation belt.

## REFERENCES

1. Fälthammar, C. G. and M. Walt, "Radial motion resulting from pitch-angle scattering of trapped electrons in the distorted geomagnetic field," *J. Geophys. Res.*, 74, p. 4184, 1969.
2. Tsyganenko, N. A. and A. V. Usmanov, "Determination of the magnetospheric current system parameters and development of experimental geomagnetic field models based on data from IMP and HEOS satellites," *Planet. Space Sci.*, 30, p. 985, 1982.
3. Tsyganenko, N. A., "Global quantitative models of the geomagnetic field in the cislunar magnetosphere for different disturbance levels," *Planet. Space Sci.*, 35, 1347, 1987.
4. Nightingale, R. W., Y. T. Chiu, G. T. Davidson, W. E. Francis, M. A. Rinaldi, R. M. Robinson, and R. R. Vondrak, "A space radiation test model study." Report AFGL-TR-86-0064, (ADA169412), Air Force Geophysics Laboratory, Hanscom Air Force Base, MA 01731, March 1986.
5. Chiu, Y. T., R. W. Nightingale and M. A. Rinaldi, "Simultaneous radial and pitch angle diffusion in the outer electron radiation belt," *J. Geophys. Res.*, 93, 2619, 1988.
6. Chiu, Y. T., R. W. Nightingale and M. A. Rinaldi, "High-energy outer radiation belt dynamic modeling," *AIP Conference Proceedings* for the Conference on High Energy Radiation Background in Space, held at Sanibel Island, Florida, Nov. 3-5, 1987, (to be published in) 1989.
7. Davidson, G. T., and Y. T. Chiu, "A nonlinear model of wave-particle interactions in the trapped radiation belts: Auroral pulsation solutions," *Geophys. Res. Lett.*, 14, 1166, 1987.
8. Chiu, Y. T., M. A. Rinaldi, W. E. Francis, and R. W. Nightingale, "Towards dynamic modeling of the outer electron radiation belt," (to be submitted for publication), 1989.
9. Walt, M., "Radial diffusion of trapped particles," in *Particles and Fields in the Magnetosphere*, ed. by B. M. McCormac, D. Reidel, Hingham, MA, p. 410, 1970.
10. Roederer, J. G., and M. Schulz, "Effect of shell splitting on radial diffusion in the magnetosphere," *J. Geophys. Res.*, 74, 4117, 1969.
11. Schulz, M. and L. J. Lanzerotti, *Particle Diffusion in the Radiation Belts*, Springer-Verlag, Berlin, Germany, 1974.

12. Kennel, C. F., and H. E. Petschek, "Limit on stably trapped particle fluxes," *J. Geophys. Res.* 71, 1, 1966.
13. Davidson, G. T., P. C. Filbert, R. Nightingale, W. L. Imhof, J. B. Reagan, and E. C. Whipple, "Observations of intense trapped electron fluxes at synchronous altitudes," *J. Geophys. Res.* 93, 77, 1988.
14. Schulz, M., and G. T. Davidson, "Limiting energy spectrum of a saturated radiation belt," *J. Geophys. Res.* 93, 59, 1988.
15. West, H. I., Jr., "The signature of the various regions of the outer magnetosphere in the pitch angle distributions of energetic particles," in *Quantitative Modeling of Magnetospheric Processes*, ed. by W. P. Olson, American Geophysical Union, Washington D. C., p. 121, 1979.
16. Sibeck, D. G., R. W. McEntire, A. T. Y. Lui and R. E. Lopez, "Magnetic drift-shell splitting: Cause of unusual dayside particle pitch angle distributions during storms and substorms," *J. Geophys. Res.*, 92, 13,485, 1987.
17. West, H. I., Jr., R. M. Buck, and G. T. Davidson, "The dynamics of energetic electrons in the earth's outer radiation belt during 1968 as observed by the Lawrence Livermore National Laboratory's spectrometer on Ogo 5," *J. Geophys. Res.*, 86, p. 2111, 1981.
18. Tomassian, A. D., T. A. Farley, and A. L. Vampola, "Inner-zone energetic electron repopulation by radial diffusion," *J. Geophys. Res.*, 77, 3441, 1972.
19. Farley, T. A., "Radial diffusion of starfish electrons," *J. Geophys. Res.*, 74, 3591, 1969.
20. Newkirk, L. L., and M. Walt, "Radial diffusion coefficients for electrons at  $1.76 < L < 5$ ," *J. Geophys. Res.*, 73, 7231, 1968b.
21. Lanzerotti, L. J., C. G. MacLennan, and M. Schulz, "Radial diffusion of outer zone electrons: An empirical approach to third invariant violation," *J. Geophys. Res.*, 75, 5351, 1970.
22. Fälthammar, C. G., "Introductory survey of radiation belt diffusion," in *Particles and Fields in the Magnetosphere*, ed. by B. M. McCormac, D. Reidel, Hingham, MA, p. 387, 1970.
23. Newkirk, L. L., and M. Walt, "Radial diffusion coefficients for electrons at low  $L$  values," *J. Geophys. Res.*, 73, 1013, 1968a.
24. Kavanaugh, L. D., Jr., "An empirical evaluation of the radial diffusion coefficients for electrons of 50-100 keV from  $L = 4$  to  $L = 7$ ," *J. Geophys. Res.*, 73, 2959, 1968.

25. Nakada, M. P., and G. D. Mead, "Diffusion of protons in the outer radiation belt." *J. Geophys. Res.*, 70, 4777, 1965.
26. Tverskoy, B. A., "Transport and acceleration of charged particles in the earth's magnetosphere," *Geomagn. Aeron. Engl. Transl.*, 5, 617, 1965.
27. Birmingham, T. J., "Convection electric fields and the diffusion of trapped magnetospheric radiation," *J. Geophys. Res.*, 77, 2169, 1969.
28. Cornwall, J. M., "Diffusion processes influenced by conjugate point wave phenomena." *Radio Sci.*, 3, 740, 1968.
29. Holzworth, R. H., and F. S. Mozer, "Direct evaluation of the radial diffusion coefficient near  $L = 6$  due to electric field fluctuations," *J. Geophys. Res.*, 84, 2559, 1979.
30. Stern, D. P., "Parabolic harmonics in magnetospheric modeling: The main dipole and the ring current," *J. Geophys. Res.*, 90, 10851, 1985.

## APPENDICES

Appendix	Page
A Paper I Simultaneous Radial and Pitch Angle Diffusion in the Outer Electron Radiation Belt .....	A-1
B Paper II High-Energy Outer Radiation Belt Dynamic Modeling .....	B-1
C Paper III A Nonlinear Model of Wave-Particle Interactions in the Trapped Radiation Belts: Auroral Pulsation Solutions .....	C-1
D Paper IV Towards Dynamic Modeling of the Outer Electron Radiation Belt ...	D-1

# Simultaneous Radial and Pitch Angle Diffusion in the Outer Electron Radiation Belt

Y. T. CHIU, R. W. NIGHTINGALE, AND M. A. RINALDI

*Lockheed Palo Alto Research Laboratory, California*

A solution of the bimodal (radial and pitch angle) diffusion equation for the radiation belts is developed with special regard for the requirements of satellite radiation belt data analysis. In this paper, we use this solution to test the bimodal theory of outer electron belt diffusion by confronting it with satellite data. Satellite observations, usually over finite volumes of  $(L, t)$  space, are seldom sufficient in space-time duration to cover the relaxation to equilibrium of the entire radiation belt. Since time scales of continuous data coverage are often comparable to that of radiation belt disturbances, it is therefore inappropriate to apply impulsive semi-infinite time response solutions of diffusion theory to interpret data from a finite window of  $(L, t)$  space. Observational limitations indicate that appropriate solutions for the interpretation of satellite data are general solutions for a finite-volume boundary value problem in bimodal diffusion. Here we test such a solution as the prime candidate for comprehensive radiation belt dynamic modeling by applying the solution and developing a method of analysis to radiation belt electron data obtained by the SCATHA satellite at moderate geomagnetic activity. The results and the generality of our solution indicate its promise as a new approach to dynamic modeling of the radiation belts.

## 1. INTRODUCTION

In the three decades since the discovery of the radiation belts, the physics of geomagnetically trapped radiation has evolved from the position of being the motivating force of space plasma physics into the current state of relative quiescence. This is not necessarily due to a matured understanding of radiation belt dynamics; rather, it is due to a relative lack of opportunities to place into suitable orbit advanced instruments that can cover the large dynamic range of radiation belt particle variations in space, time, energy and pitch angle (phase space). New discoveries in auroral phenomena in the late 1970s and early 1980s have also attracted research interest away from the radiation belts toward the low-energy high-latitude plasma. Indeed, aside from geo-synchronous-orbit instruments which are especially suitable for studies of sources [e.g., Baker *et al.*, 1978], there exist few electron radiation belt data sets since OGO-5 in 1968 [e.g., West *et al.*, 1981, and references therein] that can provide the appropriate dynamic range in phase space coverage suitable for specifying the dynamics of the outer electron radiation belt. Among these, the data from the Lockheed SC-3 instrument on board the SCATHA (P78-2) spacecraft launched in 1979 is unique in that it has excellent pitch-angle resolution covering the very narrow loss cone at the quasi-equatorial orbit of the spacecraft [Reagan *et al.*, 1981]. Further, since the spacecraft is not exactly geosynchronous, the  $L$  shell coverage of 5.3 to 8.7 in the data provides a testing ground for further specifications of the dynamics of the outer radiation belt.

Relative inactivity in the scientific aspects of radiation belt physics in the last decade does not imply, however, a decrease of applicational demand for radiation environment specification. Indeed, as a result of increasingly complex and sensitive space instrumentation and activities, demands for improved radiation environment specification have become the

driving force for a revisit and a further effort at solving the important problems of radiation belt dynamics left unsolved in the early 1970s. The upcoming Air Force NASA Combined Release and Radiation Effects Satellite (CRRES) crystallizes these research trends, for the goal of its main complement of instruments is to develop a data base for comprehensive specification of the particle populations in the space radiation environment.

The collection of data by a single satellite mission, however, comprehensive, is not sufficient to specify the worldwide radiation environment in space and time. This can only be achieved by the theoretical explication of the dynamics with a priori physical laws so that predictive models, based upon and verified by data, can be constructed for applicational needs. Such an objective is the eventual goal for which the present work is intended as a first step.

In this paper, we focus on deriving a practicable solution of the diffusion physics for outer radiation belt electrons. The solution must be appropriate for the finite space-time coverage of the data so as to limit theoretical assumptions that are not directly relevant to the data. We shall demonstrate that these goals can be achieved, at least for the region of space covered by the SCATHA spacecraft in a moderately active outer radiation belt, by application of a general eigenfunction expansion solution to the simultaneous radial and pitch angle diffusion equation. Although our solutions are admittedly approximations to the complex bimodal diffusion physics, our work here represents, insofar as we can determine, a first comprehensive attempt to confront simultaneous bimodal diffusion theory with data. As such, at the current primitive stage of simultaneous bimodal diffusion theory, we found it necessary to make a number of simplifying assumptions in order to achieve a complete solution, which, insofar as we can determine, has not been written down before. We impose strict discipline in fitting the data to the solution, however. The result is a fit to the entire data in energy spectrum,  $L$  shell, pitch angle and time. The diffusion parameters yielded by the fit compare well with other determinations from single-mode diffusion theory. It is important to note, however, that the results of the present work are not meant to be applicable to

Copyright 1988 by the American Geophysical Union

Paper number 7A9122  
0148-0227/88/007A-9122\$05.00

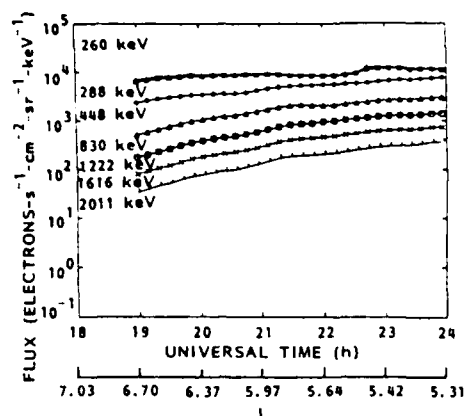


Fig. 1. Ten-minute averaged electron fluxes integrated over all pitch angles for seven energy channels measured by the Lockheed SC3 instrument on board SCATHA during day 165, 1978. This is the data set to be analyzed in this paper.

outer belt electrons under very active geomagnetic conditions when shell splitting and magnetopause transit effects become dominant.

In section 2, the unique characteristics of the Lockheed SCATHA data base are discussed in terms of their applicability to explicating dynamics of the outer radiation belt. In section 3, a brief review of the theoretical development in radiation belt diffusion physics is followed by the derivation of a general bimodal simultaneous diffusion solution suitable for situations encountered in satellite sampling of radiation belt dynamics. The most important point is that satellite observations in a finite segment of space-time are not amenable to interpretations in terms of a relaxation to equilibrium. The application of theory upon the chosen data set is presented in section 4. In section 5, the physical implication of the data representation and its applications to comprehensive dynamic modeling of the outer radiation belt will be discussed.

## 2. DATA BASE CHARACTERISTICS

The USAF/NASA P78-2 spacecraft studying satellite charging at high altitudes (SCATHA) was launched on January 30, 1979. In its final orbit the satellite nominally spins at  $\sim 1$  rpm and traverses an altitude range between  $\sim 27,500$  km at perigee and  $\sim 45,200$  km at apogee twice a day within a latitude range of  $\pm 15^\circ$ . This coverage corresponds to an  $L$  shell range of about 5.3 to 8.7 in the near-geosynchronous region. Regardless of the orientation of the orbit with respect to the Earth-Sun line, SCATHA spends  $\sim 83\%$  of the time beyond  $L = 6$ .

The Lockheed high-energy particle spectrometer, SC3, is a solid-state particle telescope, employing a series of surface barrier silicon detectors, that primarily measures energetic electron fluxes as a function of energy and pitch angle. The instrument normally operates in two energy modes with the lower mode covering the electron energy range between 47 to 299 keV in 12 channels, each about 21 keV wide. The higher energy mode extends over the electron energy range from 256 to 4970 keV in 12 channels each 393 keV wide. SC3 has excellent pitch angle resolution and pointing alignment, sufficient to look into the loss cone, thereby allowing precise fitting of the pitch angle distributions. The field of view of the detector is  $3^\circ$ , providing an effective angular width for the

detector response of  $\sim 4^\circ$ , which includes the  $3^\circ$  sweep of the detector for each 0.5-s accumulation period. This detector response should be compared with the expected loss-cone width of  $4^\circ$  to  $6^\circ$  in the near-synchronous region. The spectrometer is aligned perpendicular to the spin axis of the satellite, sweeping through almost all pitch angles (from  $0^\circ$  to  $90^\circ$ ) four times per minute. The SC3 instrument has been acquiring data and operating normally since launch. A more complete description of the instrument can be found in Reagan *et al.* [1981].

The Lockheed SCATHA SC3 data base consists of  $\sim 950$  days of digitized data on magnetic tape from launch in 1979 to the present in several intervals. The pitch angle for each accumulation period is determined using data from the on-board vector magnetometer (SC11). From the data tapes a condensed data base of 10-min averaged, pitch angle binned electron fluxes for the 24 energy channels over the full energy range of 47 to 4970 keV, has been generated for on-line storage on a VAX 11/780. For each 10-min time interval the data are grouped by pitch angle values into  $3^\circ$  bins from  $0^\circ$  to  $90^\circ$ , making 30 pitch angle bins for each energy channel in the interval. Every 10-min interval also includes the universal time (UT), local time (LT), latitude, longitude,  $Kp$ ,  $Dst$ , magnetic latitude,  $B/B_0$  value, and the  $L$  shell value for the SCATHA spacecraft. The quiet time Olson-Pfitzer [Olson *et al.*, 1979] magnetic field model together with the formulations of McIlwain [1961] for  $L$  shell were used to calculate the last three ephemerides. This multiparameter data base facilitates the generation of energetic electron distribution functions in adiabatic-invariant coordinate space.

The SCATHA orbit has a daily perigee of  $L \sim 5.3$  and an apogee that often carries it beyond  $L = 8.6$ . The orbit precesses eastward at  $\sim 5.3^\circ$  of longitude per day; so the line of apsides gradually rotates eastward with respect to the noon-midnight meridian at  $\sim 4.3^\circ$  per day. An especially important region is near  $7 R_E$ , where trapped-particle drift orbits can cross the magnetopause boundary, the latter depending on the activity level and located somewhat beyond  $L = 7$  on the day-side. Electrons with large pitch angles that encounter the magnetopause boundary are presumed to be scattered and effectively removed from the drift shell on which they had started. As a result of losses at the magnetopause, the electron distributions on the evening side are often depleted at large pitch angles; this depletion is very pronounced when the magnetic field is distorted in the development of a substorm (or storm), and is an important indicator of geomagnetic activity. Sibeck *et al.* [1987] discussed such a case of anomalous shell splitting but our distributions in the selected data base do not show such features.

The SCATHA SC3 temporal data set was from the latter portion of day 165, June 13, 1980, a moderately active period with  $Kp = +4$  and  $Dst = -50$ . Two days earlier a geomagnetic storm had occurred, but the magnetosphere had since relaxed enough that the observed electron fluxes on day 165 were smoothly varying with no pitch angle signatures of particle loss in the magnetopause. Figure 1 shows the 10-min averaged data integrated over all pitch angles for seven channels of electron flux. During this period the spacecraft was drifting inward from  $L = 7.2$  to  $L = 5.3$ . The  $L$  shell range included in the analysis has been restricted to  $L < 6.48$  to eliminate the large variability of the electron fluxes beyond the geosynchronous region [West *et al.*, 1981] and the low count rates due to the approximately exponential fall off with increasing  $L$  shell [Reagan *et al.*, 1981]. In addition we have



selected for the formal analysis only those data channels above 256 keV so as to eliminate channels which are most likely to be affected by convective forces or resulting from consequences of the major storm preceding the data period. Data with electron energies above 2208 keV have low statistics and are also excluded from the data set. Data from energy channels outside of these limits are also analyzed to show the extraneous factors in data analysis that a theoretical diffusion picture must contend with. Figure 2 illustrates typical pitch angle distributions during this time for the selected energies. Although the period was moderately active, the magnetic field was smoothly varying, with a field direction that remained perpendicular to the spacecraft spin vector. This allowed SC3 to look into the loss cone for the whole period, providing data over the full pitch angle range. In addition, the pitch angle distributions were smoothly varying and without signatures that indicate loss at the magnetopause.

Finally, it must be reiterated that the above test data set was preselected on the bases of moderate geomagnetic activity, nonexistence of magnetopause boundary crossing signatures, avoidance of convective effects and statistical sufficiency alone. Once the data set was chosen, no other data sets were analyzed until the tests presented below were completed. In the course of the work, no other criterion was applied to the data and no search for another data set was conducted.

### 3. BIMODAL DIFFUSION IN THE OUTER BELT

The framework of radiation belt diffusion theory has been based on the well-developed Jacobi-Hamilton formulation for motion of magnetically trapped particles and the Boltzmann equation for an ensemble of such particles in space [cf. Schulz and Lanzerotti, 1974]. In the ideal case, because of the existence of cyclic co-ordinates corresponding to the gyration, bounce and drift periodic motions, the state of the radiation belt is given by the solution to the collisionless Boltzmann's equation for the distribution function

$$f(M, J, \Phi) = \text{const} \quad (1)$$

where  $(M, J, \Phi)$  are, respectively, the first, second and third adiabatic invariants ( $I_1, I_2, I_3$ ) to the motion. To the extent that scatterings of the trapped particles (by plasma waves in the magnetosphere and by interactions with the collisional atmosphere at the mirrors) violate the invariants, the distribution  $f$  undergoes redistribution in  $(M, J, \Phi)$  space, or equivalently, in phase space. This redistribution of  $f$  is most rigorously treated in kinetic space plasma physics as solutions to Boltzmann's equation with collision integrals. However, a traditional Fokker-Planck development of microscopic kinetic theory leads to a formulation of the familiar diffusion picture for which the effects of the above scatterings in random-phase aggregate are assumed to be described by the diffusion equation,

$$\frac{\partial f}{\partial t} = \sum_i \frac{\partial}{\partial I_i} D_{ii} \frac{\partial f}{\partial I_i} \quad (2)$$

where we have adopted the convention that repeated indices are summed over the canonical invariant variables. In (2), the energies of the particle population are assumed sufficiently high that the physics of the scatterings is contained in the components of the diffusion matrix  $D_{ii}$ . The scatterings that violate the adiabatic invariants can, in general, violate any combination of them at the same time and the existence of

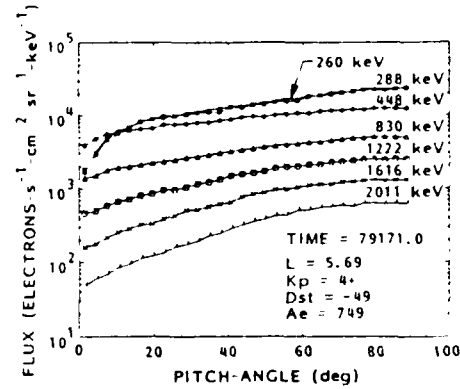


Fig. 2 Typical pitch distributions for the seven energy channels of the data set referred to in Figure 1

many plasma wave modes imply that the nine terms on the right-hand side of (2) may in general be hopelessly tangled. As a result, it can almost be said that radiation belt diffusion theory consists of attempts to consider approximations in isolating the dominant contributions to the right-hand side of (2). Included in such efforts are attempts to discover coordinates other than invariants in which only one or two dominant diffusion terms and diagonal diffusion matrices can be obtained. Unfortunately, only one-dimensional considerations, in radial or in pitch angle diffusion, have previously been attempted.

The intractability of (2) in any form more complex than that of a single mode has given rise to the traditional treatment of single-mode radiation belt diffusion in some single variable, say  $y$ , in the form

$$\frac{\partial f}{\partial t} = -\frac{1}{K} \frac{\partial}{\partial y} K D_y \frac{\partial f}{\partial y} - \frac{f}{\tau} + S \quad (3)$$

where  $K$  is a Jacobian appropriate for the transformation from particular canonical terms in (2),  $f/\tau$  is a loss term and  $S$  is a source term. Both loss and source terms are ad hoc representations under which the effects of other untreated diffusion terms are swept. Elaborate solutions of initial value problems for impulse responses in the semi-infinite time domain for single-mode radial diffusion in the ad hoc form of (3), in which  $y = L$ , have been evolved [e.g., Schulz, 1986; Schulz and Newman, 1987]. Single-mode pitch angle diffusion has also been treated in detail (e.g., see references in Schulz and Lanzerotti [1974, chap. 2]). Such elaborate solutions to an ad hoc one-dimensional approximation are clearly of value in delineating the theoretical behavior of radiation belt diffusion in the single chosen variable  $y$  in the semi-infinite time domain, but progress in developing the multimode area of radiation belt diffusion theory is also called for. Let us now consider the role of data in the next step in complexity, i.e., in multimode diffusion in finite space-time. It is crucial to note that this new step calls for two new elements that will require special consideration: (1) multimode diffusion, and (2) finite space-time span. Since our general solution is developed to address these two issues, a discussion of each is necessary at the outset.

Bimodal diffusion (simultaneous in radial and pitch angle) formulations were discussed early in the development of radiation belt physics [Hacrendel, 1968; Theodoridis, 1968; Frankenthal et al., 1968; Falthammar and Walt, 1969; Walt, 1970].

Here the chief difficulty was in developing a scheme to unconditionally diagonalize the diffusion operator so that solutions by the separation of independent variables could be used for the diffusion equation. Walt [1970] introduced a variable

$$\zeta \equiv MB_m/B_e \quad (4)$$

which is shown to be approximately conserved by both radial and pitch angle diffusion. In (4), the magnetic field ( $B$ ) subscripts,  $m$  and  $e$ , refer to the mirror and the equator, respectively. Under the approximate invariance of  $\zeta$ , the variables  $x$  and  $L$  act as approximate canonical coordinates so that the diffusion equation can approximately be written in diagonal form [Falthammer and Walt, 1969; Roederer and Schulz, 1969]

$$\frac{\partial f}{\partial t} = \frac{1}{xT(x)} \frac{\partial}{\partial x} \left[ xT(x)D_{xx} \frac{\partial f}{\partial x} \right] + L^{2+(3/2)v} \frac{\partial}{\partial L} \left[ D_{LL}L^{-(3/2)v} \frac{\partial f}{\partial L} \right] \quad (5)$$

where  $x = \cos \alpha$  and  $T(x)$  is the quarter-bounce integral, which can be conveniently approximated by expansion in several slightly different forms [e.g., Schulz and Lanzerotti, 1974, p. 19; Davidson, 1976]. Here we use Davidson's formula

$$T(x) \approx 1.3802 - 0.6397(1 - x^2)^{3/8} \quad (6)$$

In (5), a source term  $S(x, L)$  (or a loss term) is not needed to represent effects of other modes of diffusion, as is customary in single-mode diffusion treatments, unless a real source (such as neutron decay) exists in the volume under consideration. Indeed, if pitch angle ( $x$ ) and radial ( $L$  shell) diffusions represent all the particle transport in the solution volume, the boundary conditions for  $f$  specified by satellite observations in a given finite space-time volume are the "sources" of (5). This point will be discussed more thoroughly below. Because  $\zeta$  in (4) is not an exact invariant corresponding to which the  $x$  and  $L$  terms of (5) are exactly separable, the index  $v$  in (5) has a vestigial dependence on  $x$ . For example,  $v = 3$  at  $x = 0$  for which (5) is exact and  $v = 2$  at  $x = 1$ . In the region  $0 < x < 0.94$ ,  $v \approx 3$  is a very good approximation. In the region  $0.94 < x \leq 1$ , there are cross-diffusion, i.e.,  $D_{xL}$ , terms in (5) proportional to  $(v - 3)^2(1 - x^2)^2$ . These are small and will be ignored.

Aside from the above approximations arising from representational and kinematical considerations in the reduction of the full multimode diffusion equation, the bimodal equation (5), similar to the ad hoc single-mode equation (3), is also beset with the same physical uncertainties in the proper forms for the diffusion coefficients. Without simultaneous and global measurements of wave modes and their amplitudes, there is virtually no information on the nature of  $D_{xx}$  and  $D_{LL}$  for a given radiation belt data set. This major lack of supporting information for all known data sets implies that one of the "zeroth order" tasks in radiation belt diffusion theory is to determine the approximate properties of the coefficients. In ad hoc single-mode diffusion theory, it is often assumed that a diffusion parameter can be derived simply by spatial quadrature of the diffusion equation [e.g., Schulz and Lanzerotti, 1974, chap. 5], provided that the data is sufficiently comprehensive to allow for accurate determination of derivatives of distribution functions and that only a single mode of diffusion is operative on the data set. However, both of these are very restrictive assumptions. Quadrature techniques are based on the assumption that satellite observations provide  $f(L, t)$  in

such a way that derivatives in space and time can be performed independently. Except by ad hoc assumption and perhaps for geosynchronous satellites under certain geomagnetic conditions, no satellite data can satisfy such a condition. As for the assumption that only single-mode diffusion is operative, it is easy and tempting to argue that the time scales of radial and pitch angle diffusion are widely separated so that, for example, magnetic impulses can cause violation of the third invariant without disturbing the gyration and bounce of the particles. Such arguments are well and good in theory, but the fact of nature is that electric and magnetic fluctuations of all time scales have a tendency to occur together. A time span in which magnetic impulses occur is also a likely period for increased plasma wave activity; therefore it is perhaps futile (or somewhat vexing) to force what occurs naturally (simultaneous multimode diffusion) into too simple a mechanism even though simplicity allows for a higher degree of theoretical sophistication in the method of analysis. These are the reasons that we choose to investigate multi-mode diffusion, which is of course also beset by its own problems.

For multimode diffusion, the quadrature technique simply involves too many partial differentiations of data to be of any value. Thus to obtain diffusion parameters in multimode diffusion, the only available technique is to fit the data to solutions of (5) under various models of the diffusion coefficients. This, in turn, implies that a measure of uncertainty associated with the variations of diffusion coefficients of (5) is necessarily mixed with small residual variations associated with the definition of separable variables discussed above. These variations and uncertainties can only be handled in the manner of "learning curves," i.e., by sequential improvements built upon a "zeroth-order" analysis. The main purpose of this paper is to develop this "zeroth-order" analysis for multimode diffusion. As such, we shall make simplifying assumptions on (5) that are approximate when considered in the applied mathematics viewpoint but will clearly demonstrate the physical character of the solution. Further, a comprehensive solution technique and its application will be developed to test the reasonableness of the multimode diffusion paradigm.

The guiding principle of the following development is, therefore, to obtain an exact solution to a simplified version of (5) that is easily applied to analyze data without changing the physical character of the diffusion equation. Note that the emphasis is to obtain an exact solution to an approximate equation rather than an approximate solution to an exact equation because we have demonstrated above that (5), as in the case of single-mode diffusion (3), is by no means an exact equation. Therefore, to the extent that (5) is approximate anyway, further simplifying assumptions are acceptable as long as they do not change the character of the equation. We have attempted many optional simplifications of (5), but settled on the following for both mathematical and physical reasons. (1) We assume  $T(x)$  is constant for mathematical convenience because the theory of analytic continuation over a nonsingular domain can be applied to show that the solution character is not changed if  $T(x)$  is in the neighborhood of unity and nonconstant. No singularity of the diffusion equation is encountered when  $T(x)$  is varying from a constant in the vicinity of unity. The impact of this assumption on the pitch angle eigenfunctions is very small as a comparison between the exact eigenfunction of the pitch angle diffusion operator in (5) with variable  $T(x)$  and Bessel functions, which are the eigenfunctions for our approximation, has been given by

Schulz and Lanzerotti [1974, p. 166]. Further, the Bessel functions form a conveniently available complete set which can span the domain  $1 > x \geq 0$  aside from being eigenfunctions of the approximate pitch angle diffusion operator. (2) The pitch angle diffusion coefficient  $D_{\perp\perp}$  is assumed to be independent of  $L$  since the range of  $L$  covered in the data set is fairly small. The energy dependence of  $D_{\perp\perp}$  is to be determined by the data analysis. (3) The diffusion equation cannot be solved unless a form is specified for the radial diffusion coefficient. This is true in single-mode radial diffusion also. The radial diffusion coefficient  $D_{LL}$  is assumed to be of the general form [e.g., Schulz and Lanzerotti, 1974, p. 89; Theodoridis, 1968]

$$D_{LL} = \xi L^\mu \quad (7)$$

where  $\xi$  and  $\mu$  are parameters to be determined by the data analysis. In general,  $\xi$  can be an arbitrary analytic function of  $x$  and energy. The energy dependence is determined by applying the solution to each energy channel. If  $\xi$  depends on  $x$ , (5) is still separable but a set of parameters corresponding to matrix elements of  $\xi$  in the eigenfunctions of the pitch angle diffusion operator must be determined in addition; a special case of which is considered by Walt [1970]. These matrix elements cross-couple pitch angle modes [Fälthammar and Walt, 1969]. Inclusion of cross-mode coupling is a complication but is not included in this initial analysis; therefore, for this analysis, we assume  $\xi$  to be independent of  $x$  to simplify expressions. It should be noted that, although there is no cross-mode coupling, there is simultaneous bimodal diffusion. There exists scarce theoretical guidance on the magnitudes of  $D_{\perp\perp}$  and  $\xi$  in the outer belt, but there are theoretical reasons to expect that  $\mu \sim 6 - 10$  [e.g., Schulz and Lanzerotti, 1974, chap. 3; West et al., 1981]. We assume  $\mu = 10$  in this work. Under these simplifying assumptions, the diffusion equation can be written

$$\frac{\partial f}{\partial t} = D_{\perp\perp} \left[ \frac{\partial^2 f}{\partial x^2} + \frac{1}{x} \frac{\partial f}{\partial x} \right] + \xi L^{\mu+2-(3/2)\nu} \frac{\partial}{\partial L} \left[ L^{\mu+2-(3/2)\nu} \frac{\partial f}{\partial L} \right] \quad (8)$$

where  $D_{\perp\perp}$ ,  $\xi$ ,  $\mu$  and  $\nu$  are considered to be constant parameters.

This simplified equation is to be solved in a small finite domain  $L_i \leq L \leq L_o$  expected to be in the outer belt and in the pitch angle domain  $0 \leq x \leq x_c$ , where  $x_c$  is cosine of the loss cone angle. The effect of pitch angle diffusion is to define pitch angle behavior of  $f$  inside and outside of the loss cone boundary  $x = x_c(L)$ . The dependence of  $x_c$  on  $L$  is yet again another factor which mixes the  $x$  and  $L$  operators in (8); however, for the outer zone region, where  $(L_o - L_i) \leq 2$ ,  $x_c$  is very nearly constant and unity. We assume that  $x_c$  is constant in the data span so that separable solutions can be obtained for (8) with the present test case. This is an important point when we deal with data from a large domain of  $L$  (such as that from CRRES) which involves large variations of the loss cone both from the large variations in  $L$  and in distances to the mirrors. For our SCATHA data set the loss cone dependence on  $L$  is entirely negligible.

In general many different kinds of solutions to (8) can be developed. From the purely theoretical standpoint, a favorite solution is to consider an initial value problem for an impulsive source defined over a semi-infinite time domain and valid for the space of the entire radiation belt. Such a solution is easily written formally in terms of an eigenfunction expansion of the Green's function for the equation [e.g., Chiu and Hilton,

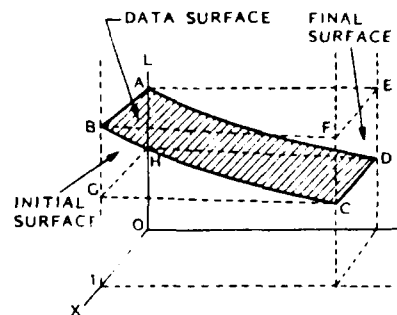


Fig. 3. Schematic illustration of the boundary volume in  $(x, L, t)$  space in which the general bimodal diffusion solution is developed. Satellite data to be matched to the solution span lie on the data surface.

1977]. However, we can think of several factors that vitiate the meaning of such a solution and its relevance to data application. First, radiation belt diffusion processes are currently not well known enough to permit single forms and values of the diffusion coefficients to be specified for the entire belt, after all the purpose of data application is to determine the ensemble of coefficients. Second, the source time scale is not well defined for radiation belt particles. What seems to be impulsive in one phenomenon need not be so when beheld with the vantage point of another. An important factor which determines the appropriate solution to (8) is the space-time span of the data set. Here two features must be recognized with the help of Figure 3. This figure illustrates the satellite data span and its relation to the appropriate solution volume in  $(x, L, t)$  space. The fundamental nature of nonsynchronous satellite data spans is that they lie on a data surface ( $ABCD$  on the figure) defined by the satellite trajectory  $L(t)$ . Further, the time span defines the  $(L, x)$  boundary surfaces of the solution volume labelled by the Roman letters  $A$  to  $H$  on the figure. In such a source-free volume, particles are transported into and out of the surfaces  $ABGH$  and  $CDEF$  by radial diffusion, in other words, these boundary surfaces are also source surfaces. Particles are lost through the surface  $BGCF$  which should rigorously lie on  $x_c$  as discussed above. If the data time span is less than or comparable to the injection and loss times in the volume, as is the case in most satellite observations such as SCATHA, the appropriate solution to be developed is the general source-free complete-set expansion solution in a finite space-time interval, and not an initial value solution in the semi-infinite time domain corresponding to response to a transient (i.e., delta function) source. In the finite space-time domain, the entire spectrum of time constants (rising as well as falling) must be included in the general complete-set expansion because unknown sources (and sinks) outside of the volume are diffusing particles into (and out of) the finite volume causing the phase space density or distribution function to increase (decrease) with time scales that can be comparable to the data time span; whereas, in the semi-infinite time domain for the Green's function, only the falling time response function is appropriate. To be sure, the Green's function can be applied to obtain the finite space-time solution by applying Green's theorem onto the boundary surfaces, which involve integration of Green's function over the surface boundary fluxes or their derivative whenever appropriate. This crucial integration imparts the source time scales onto the solution. The important point is that this integration convolves the rising and

falling time constants of the surface sources with the natural falling time constants of diffusion to result in a spectrum of both rising and falling time constants for the spatial eigenfunctions. As a result of this time convolution, the final solution for finite volume need not look anything like the Green's function that would be developed for the initial value problem over semi-infinite time. To be sure, all excited states eventually decay by diffusion to equilibrium, but the satellite, with its finite space-time data span, does not know whether it has caught the rising or falling phase of a modal disturbance of unknown time scale.

These esoteric characteristics of solutions to partial differential equations are familiar enough to the theorist; however, it may be relevant here to relate the situation to a more intuitive and mundane example. Consider the case of heat conduction in a bar of metal occupying the volume *ABCDEFGH* above. The heat diffusion equation is similar in structure to (8) and a transient response to a heat pulse (Green's function) is composed of a spectrum of sinusoids all exponentially decreasing in time with the appropriate rates. However, in order to obtain the solution for the case of an impressed temperature field on the surface *ABGH* that is rising in time, say exponentially, the spectrum of sinusoidal modes of heat conduction will rise or fall in time each according to their ability to conduct the heat to the volume and to the boundary surfaces. Intuitively, it is easy to imagine that if the impressed temperature is sufficiently high it may cause the temperature field of portions of the volume to rise exponentially for a finite time, although rising time constants are definitely not in any mode of the Green's function response. This case of transient heat conduction, and the relation between the diffusion Green's function and boundary conditions, are given by *Morse and Feshbach* [1953, equation 12.1.5, p. 1587]. The reader can easily carry out the Green's function convolution specified there to obtain the time response to an impressed temperature at the boundary surface and demonstrate that over finite time some modes may be rising while others are falling.

The consequence of the esoteric points discussed above is that it would be wrong to force satellite data obtained over a finite space-time volume to fit an impulsive transient response solution such as the Green's function. For purposes of satellite data analysis in a finite space-time interval, the appropriate solution to (8) is the solution corresponding to a general boundary value problem, and not corresponding to a global response to an impulsive source. Since a general solution can be obtained by eigenfunction expansion of (8) with unrestricted separation constants, which will be constrained by data, this convenient property forms the basic principle of data characterization analysis in this paper. It will be shown later, based on the success of our data analysis, that this principle can be used to characterize the state of the entire radiation belt in a piecewise-continuous fashion.

Under the precautions discussed above, a general solution to (8) in finite space-time can be developed [cf. *Morse and Feshbach*, 1953] in terms of complete-set eigenfunction expansions. In general, there are three modal expansions: (1) single-mode pitch angle diffusion, (2) single-mode radial diffusion and (3) simultaneous bimodal diffusion. Using the device of the Kronecker delta  $\delta_{n0}$ , the three modal expansions can be written in terms of a single eigenfunction expansion

$$f = \sum_n \left[ \delta_{n0} + (1 - \delta_{n0}) \frac{\chi^2}{\chi_c^2} \frac{J_0(k_n \chi)}{J_1(k_n \chi)} \right] \{ a_n (1 - \delta_{n0}) e^{t/\tau_n} + e^{t/\tau_n} [a_n J_n(L) + b_n Z_n(L)] \} \quad (9)$$

where  $k_n$  is the  $n$ th zero of the Bessel function  $J_0$ . The parameters and new functions are defined as follows:

$$\varepsilon \equiv 3 \left( 1 - \frac{\chi}{2} \right) / (\mu - 2)$$

$$\sigma \equiv -\frac{\mu}{2} - \frac{1}{2} + \frac{3}{4} \chi \quad (10)$$

$$\lambda \equiv \frac{\mu}{2} - 1$$

$$Y_n(L) = L^\sigma \cdot [J_{1+\varepsilon}(\beta_n/L^\lambda)]_> \cdot [I_{1+\varepsilon}(\beta_n/L^\lambda)]_< \quad (11)$$

$$Z_n(L) = L^\sigma \cdot [N_{1+\varepsilon}(\beta_n/L^\lambda)]_> \cdot [K_{1+\varepsilon}(\beta_n/L^\lambda)]_< \quad (12)$$

$J$  is the regular Bessel function,  $I$  and  $K$  are the modified Bessel functions, and  $N$  is the Neumann function. In the above, the separation constants are  $t_n$  and  $\beta_n$ . The usual notation  $[g]_>$  is defined in this case by

$$[g]_> = g \quad t_n > 0$$

$$[g]_> = 1 \quad t_n < 0 \quad (13)$$

and analogously for  $[g]_<$ . The separation constants and parameters of the solution are related by the algebraic relations

$$t_n^{-1} = (1 - \delta_{n0}) \tau_n^{-1} - \xi \beta_n^2 \lambda^2 \quad (14)$$

$$\tau_n^{-1} \equiv -D_{xx} k_n^2 / \chi_c^2 \quad (15)$$

which will be referred to as separation equations. It is seen that the single pitch angle mode time constants are negative as expected, since single-mode pitch angle diffusion always leads to decay. For bimodal and radial diffusion, however, the time constants  $t_n$  can be either positive or negative over a finite time interval. This is due to the fact that the phase space density in the finite  $L$  domain can rise or fall in time in response to particle transport into and out of the adjacent volumes, as discussed above. With the sign of each  $t_n$  not predetermined, the separation constant  $\beta_n^2$  can be positive or negative. This is the origin of the ( $J$ ,  $I$ ) and ( $N$ ,  $K$ ) options of (11) and (12). The solution (9) is not the most general solution, for a separate sum of pure radial modes can be added. We have not done so for two reasons: (1) we expect that episodes of radial diffusion must accompany pitch angle diffusion because of the association of magnetospheric fluctuations of all scales with each other and (2) this creates more parameters. As it presently stands, only one pure radial mode is included, i.e., for  $n = 0$ .

Finally, we return to the second feature of satellite data illustrated on Figure 3. In a data analysis effort, the fit of satellite data is on the ( $L$ ,  $t$ ) data surface *ABCD*, which samples the boundary surfaces and the volume in a way that mixes space and time. The fit to the general solution (9) is supposed to yield the parameters ( $a_n$ ,  $b_n$ ,  $c_n$ ,  $t_n$ ,  $\tau_n$ ), which would allow time constants and diffusion coefficients ( $D_{xx}$ ,  $D_{LL}$ ) to be determined. Further, the solution in the entire volume is supposed to be determined via the expansion coefficients ( $a_n$ ,  $b_n$ ,  $c_n$ ). Clearly, the solution to (9) is not specified by the data in a way that is usual to a boundary value problem. Because of the mixing between  $L$  and  $t$  on the data surface, it is difficult to devise a completely unambiguous procedure to determine all of the fit parameters. An approximate procedure that works will be outlined in section 5. The generality of (9) must not overshadow the restrictions under which (9) is derived, i.e., the assumption of separability of the  $\chi$  and  $L$  operators. Thus, the data analysis must be contemplated in terms of a piecewise

procedure, dealing with an  $(L, t)$  volume in which the quasi-invariance of  $\mathcal{E}$  is preserved. Our attempt here is to approach the specification with an appropriate piecewise method, establishing parameter sets  $(a_n, b_n, c_n, t_n, \tau_n)$  for many cases, from which, it is hoped, a "learning curve" will allow us to determine approximate specifications of the radiation belts under various classes of conditions.

The development up to this point under the simplifying assumptions is strictly theoretical and exact. From this point onward, we shall attempt to test whether bimodal theory (and its solution) is a good description of the data. This confrontation is the main objective of this paper. It may be referred to as a "fit," which is really a misnomer since our primary objective from this point onward is to see if fundamental limitations of the data in mixed space-time can be overcome in the face of purely theoretical requirements of the exact solution. No overall sophisticated "fitting" has been attempted in the radial diffusion segment of the analysis. Indeed, we deliberately avoided "fitting" in this segment in order to determine the maximal error spread of the exact bi-modal diffusion description of the data base. This maximal data spread will be illustrated in two ways: (1) as error spreads in the determination of the radial diffusion coefficient, and (2) as error in the three-dimensional reconstitution of the entire data base.

#### 4. APPLICATION TO DATA REPRESENTATION

Under the assumption that bimodal diffusion is operative, the application of the general solution (9) to satellite measurements involves yet other approximations and artifices that do not relate to the basic mathematical and physical structures of the solutions themselves. Rather, these arise chiefly from the limitations of satellite measurements.

Data limitations due to instrument and orbit coverage have been addressed in section 2. Limitations on space-time intervals of coverage have been addressed in section 3. These limitations are relatively easier to deal with than the fundamental mixing of space and time in satellite observations due to the orbiting motion of satellites. For radiation belt observations, it is somewhat unfortunate that the timescale of the order of hours is common to both physical phenomena of interest in diffusion theory and to satellite orbits. Thus additional approximations and assumptions have to be made to bring theory and data into contact with each other. The use of invariant space to examine the corresponding space-time behavior of the distribution function will help us resolve the mixing of space and time in the data. This technique of mapping between  $(L, \mathcal{E}, t)$  and invariant space is, however, the topic of another paper. For the present analysis, we shall assume a procedural chain which will be described below. We shall depend on the internal consistency of our results and agreement with analyses of other data sets to justify our procedure.

The initial steps of the procedural chain for data analysis under the guidance of diffusion theory suggest themselves in the eigenfunction expansion solution (9). After appropriate organization and processing, the set of radiation belt electron fluxes such as that shown on Figure 2 for a single 10-min interval, are converted to the distribution function  $f$  specified over the pitch-angle and energy ranges, and over the intervals of space-time in which the data are taken. The pitch angle distributions are decomposed into amplitudes  $Q_n$  of the complete set of Bessel functions, which, under our stated premises, are also the complete set of eigenfunctions of pitch angle diffusion. This decomposition of the observed distribution function

$$f = \sum_{n=0}^{\infty} Q_n(L, t, E) \left[ \delta_{n0} + (1 - \delta_{n0}) \frac{\sqrt{2}}{x_c} \frac{J_0(k_n x_c / x_i)}{J_1(k_n)} \right] \quad (16)$$

yields the pitch angle amplitudes  $Q_n$ , which are nominally functions of  $L, t$  and  $E$ . The complete-set property of the Bessel functions can be invoked for (16) even if one does not invoke the solution (9).

The set of amplitudes  $Q_n$ , separated into energy channels  $E$ , must now be resolved into separable functions of time and  $L$  value, as indicated in the second major bracket in (9). This is a somewhat ambiguous task. Several simplifying assumptions need to be made, even just to ascertain that the space variable is meaningfully represented by  $L$  in a static magnetic field model over the time span in question. The next step is to assume a procedure to disentangle the mixing of  $L$  and  $t$  by the motion of the satellite. From (9),

$$Q_n(L, t) = c_n(1 - \delta_{n0})e^{i\omega_n t} + e^{i\omega_n t}[a_n Y_n(L) + b_n Z_n(L)] \quad (17)$$

Because of the mixing due to satellite motion, spatial effects of scale  $\Delta L$  such that  $(|t_n|, |t_n|) \sim \Delta L/v_L$ , where  $v_L$  is satellite speed perpendicular to the  $L$  shell, cannot be distinguished from temporal effects. However, effects for which the two scales are distinctly different can be identified in the fit. To fit the data, an ad hoc but reasonable choice must be made to identify the time or space scales to select or to sacrifice in the procedure. For the SCATHA data, the coverage is typically  $\Delta L \sim 1 - 2$ , unlike satellites at high-latitude elliptical orbits which cover much larger  $\Delta L$ . Therefore for analysis of SCATHA data, we have chosen to emphasize the fit of long time scales and short  $L$  scales, i.e., we have chosen to ascribe slow variations along the SCATHA trajectory to temporal changes and the fast variations along the trajectory to spatial changes. Our procedure to effect this assumption is to identify the time constants to each order by first doing a nonlinear fit of each  $Q_n$  to a simplified version of (17) in which the data variations over the entire space-time span are ascribed to time only. This enables us to pick out the time scales of the data, i.e.,

$$Q_n = c_n(1 - \delta_{n0})e^{i\omega_n t} + C_n e^{i\omega_n t} \quad (18)$$

where  $\tau_n, t_n, c_n$  and  $C_n$  are constant parameters for this step. If values of  $\tau_n$  and  $t_n$  are longer than or of order of the data time span, which happens to be the case in our data set, we can proceed with our analysis hypothesized above. If not, the mixing of space and time scales must be disentangled by invariant-space mapping techniques and/or the use of proton data, both of which are outside the scope of this paper. Since this step in the fit does not involve the  $L$  dependence, the amplitudes  $C_n$  obtained are of no significance. On the other hand, since  $c_n$  is the amplitude for single-mode pitch angle diffusion it is not expected to depend on  $L$ ; therefore  $c_n$  is accepted as a fit parameter. The time constants in the above fit step are constrained not only by the data time span but also by (14) and (15). The constraint (14) on  $t_n$  is somewhat complex and will be discussed below. Equation (15), on the other hand, constrains the dependence of  $\tau_n$  on  $n$  according to the zeroes of the Bessel functions, resulting in only one parameter,  $D_{\perp}$ . This constraint is easily applied on the nonlinear fit (18).

Having obtained the fit parameters  $(D_{\perp}, t_n, c_n)$  from the above procedure, we next obtain a fit of the  $L$  dependence according to the solution (9). For this step, we construct a residue  $R_n(L)$  by

$$R_n(L) = [Q_n(L, t) - c_n(1 - \delta_{n0})e^{i\omega_n t}]e^{-i\omega_n t} \quad (19)$$

which, according to (17) and our fit hypothesis above, is solely a function of  $L$ .

The construction of this residue is algebraically straightforward, but care must be taken not to amplify the natural fluctuations in the bracketed difference. The above method of derivation forces  $|\tau_n|$  and  $|t_n|$  to be of the order of or larger than  $\Delta t$ , i.e.,

$$(|\tau_n|, |t_n|) \geq \Delta t \quad (20)$$

This constraint also assures that the natural fluctuations in the residue  $R_n(L)$  will not be amplified by the factor  $\exp(-t/t_n)$  for  $t_n < 0$ . The criterion (20) allows for a reasonable unraveling of the space-time scale mixing in single nonsynchronous satellite observations.

Hitherto in this section, we have treated the application of the general solution (9) in the form (16) to the data without making any reference to the property that the expansion is a general solution. Rather, we have been exploiting the property that it is a complete-set expansion not tied to a specific solution. In other words, the development in this section up to this point can be effected without reference to the bimodal diffusion equation, because (9) can be viewed as a general complete-set expansion when all the fit parameters are essentially considered free. However, our aim is to apply the solution (9), which is of similar form to (16), with the associated constraints of (9) to the data.

The next step of the procedure is fitting  $R_n(L)$  to the  $L$  eigenfunctions of the diffusion equation

$$R_n(L) = a_n Y_n(L) + b_n Z_n(L) \quad (21)$$

From (10), (11), (12) and (21), we note that the parameters of this fit are  $(v, \beta_n, a_n, b_n)$  which, together with  $t_n$ , are constrained by (14). Utilizing a large computer, a matrix of these fit parameters can be cycled and the best fit chosen for each energy channel of the data. Such a procedure can be devised as a matrix diagonalizing routine. For our test case, however, the priority is not to attempt such large-scale computations at the outset but to examine the key relationships of subsets of these parameters to the data and, foremost among the various issues, to demonstrate that a physically reasonable fit of the data can be represented by the general bimodal diffusion solution.

We begin the procedure by reducing the number of parameters to be determined. Previous analyses indicated that  $2 \leq v \leq 3$  [e.g., West *et al.*, 1981]. The expected value of  $v$  leads to an important simplification with respect to the order of the Bessel functions in (11) and (12). From the definition of  $\epsilon$  in the first of the triplet (10), we obtain  $-3.16 \leq \epsilon \leq 0$  which indicates that  $\epsilon$  is a small number and the corresponding order of the Bessel functions is nearly unity. From (10), the order is

$$1 + \epsilon = 1 + \frac{3(1 - v/2)}{(\mu - 2)} \approx 1 \quad (22)$$

Since the Bessel functions are analytic, slowly varying functions of the order, we choose to constrain the fit with  $\epsilon = 0$  and use Bessel functions of order 1 to approximate those of order  $1 + \epsilon$ , thus resulting in a large reduction of computation. With these simplifications the fit parameters are now  $(\beta_n, a_n, b_n)$  which are specified by energy channel  $E$  and order of pitch angle eigenmode  $n$ . Once the fit for the entire data set is obtained, the parameters are used to reconstitute the data via (9). A residue distribution is then calculated to test the goodness of fit

At this point, the analysis can be viewed on two related levels. The first level is to view (9) as a convenient data representation tool which compresses many thousands of data points into a set of about a hundred fit parameters amenable to averaging and other forms of processing. Further, the tool is separated but not divorced from the solution of the bimodal diffusion equation. As such, this data representation is also convenient for interpretation, and for construction of maps of radiation belts under various conditions. The numerical examples of this paper, to be shown below, are at this level of analysis. In this approach, the final product, aside from demonstrating the efficacy of bimodal diffusion in specifying the dynamics of the outer belt electrons, is the determination of diffusion coefficients which can be compared to theory. The second level, a natural consequence of the first, is to view (9) as the basis of modeling the dynamic behavior of the radiation belt volume appropriate to the data. The data fit to the general solution of the diffusion equation can be used to (1) extract the surface sources of the finite space-time volume corresponding to the solution domain, (2) relate the ensemble of such extracted boundary conditions to the set of diffusion coefficients from a set of satellite data spans, and (3) integrate the ensemble of such verified transport parameters for the diffusion equation into a dynamic model. We shall limit ourselves to the first, less ambitious, level of application in this paper.

The data set consists of 5040 radiation belt electron flux values derived from instrument count rates. These are distributed among the seven energy channels, the 24 ten-minute flux averages over the data time span and the 30 pitch angle bins of  $3^\circ$  each, i.e.,  $7 \times 24 \times 30 = 5040$ . The fit procedure is, of course, not to deal with the 5040 flux values as independent pieces of data, for these are organized into  $7 \times 24 = 168$  pitch angle distributions such as those shown on Figure 2. These pitch angle distributions are subjected to the Bessel function decomposition (16). We found that the truncation of the sum to  $n < 4$  yielded sufficient fit accuracy without causing undue burden on a VAX/780 computer. Next, the amplitudes  $Q_n$  are fitted nonlinearly according to (18) to extract the set of time constants  $t_n$ , the pitch angle diffusion coefficient  $D_{\perp\perp}$  (via the time constants  $t_n$  and the constraint (15)) and the set of single-mode pitch angle diffusion amplitudes  $c_n$ . The time variations of choice are thus identified in the data. In the next step, we assume the variations of the residue  $R_n$  in (19) to be in  $L$  only; thus proceeding to fit the set of residues to the  $L$  eigenfunctions, (21). This fit of the residues yields the eigenfunction parameters  $\beta_n$  and the amplitude parameters  $(a_n, b_n)$  which completes the procedure in principle. However, these parameters are not entirely free because the final constraint (14) must be satisfied. The natural procedure to satisfy this constraint, without resorting to the matrix diagonalization method discussed above, is to recycle the entire procedure by using (14) as the adjustment criterion until a set of  $(t_n, \tau_n, \beta_n, \xi)$  that minimizes the variance from (14) is reached. This can be done in principle, although it is somewhat tedious. For this test case, however, it is much more meaningful to show the convergence of our procedure by displaying the variance from (14) in the first pass of the procedure. To demonstrate the variance, let us focus on (14) as an equation for determining  $\xi$ , a constant independent of order  $n$ . In any fit to a constraint, an equation such as (14) is satisfied to a minimized variance, all of which can be ascribed to  $\xi$ . This is the worse case, for the variance is usually shared in a minimization. The unminimized variance of  $\xi$  in the first pass of the above procedure, determined from solving (14) for all the orders, will

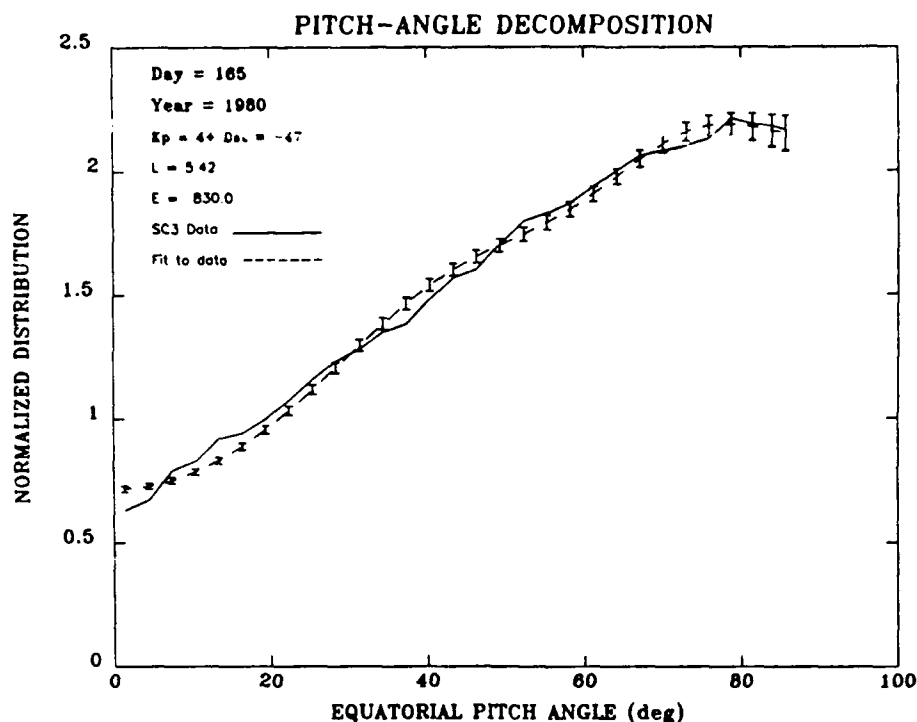


Fig. 4 Comparison between observed pitch-angle distribution for the 830 keV channel at  $L = 5.42$  (solid curve) and its reconstitution after decomposition into pitch angle eigenfunctions (dash curve). The fit propagated error bars are shown.

yield a spread of the values of  $\xi$  as function of order. This spread as a function of order is a good indicator of the degree of convergence in the first pass of the fit. Further, since  $\xi$  is directly proportional to the radial diffusion coefficient, the spread of the values determined by this first pass of the procedure can be compared with the totality of values and variances of the radial diffusion coefficients determined in the past by methods totally unrelated to this analysis. Thus the spread of  $\xi$  obtained in this way acts as an independent and worse-case indicator of the goodness of fit for our entire analysis. In this regard, it is crucial to note that  $\xi$  does not appear in our solution as a direct fit parameter, rather it is a derived quantity due to the constraint (14).

In summary, this application involves, per energy channel, 6 time constants ( $U_{0-4}$ ,  $D_{1-4}$ ), 14 amplitudes ( $a_{0-4}$ ,  $b_{0-4}$ ,  $c_{1-4}$ ) and 5 eigenfunction parameters ( $\beta_{0-4}$ ), yielding 25 fit parameters per energy channel or a total of 175 fit constants for the entire data set. These are to be compared to the total of 5040 data values organized into 168 distribution functions. It should be noted that no attempt at organizing the fit parameters into empirical functions of energy and/or pitch angle order  $n$  has been made. Further, the total number of fit parameters is exhausted by the above list; thus an enlargement of the data span will not introduce any more parameters because the above exhausts the count of parameters according to theory. Our ratio of fit constants to data values gives adequate constraints on the fit. With more data spans, such as in dynamic modeling, the energy and order dependences of the fit parameter can further be organized, resulting in a drastic reduction in the number of parameters to data values. However, as it is, the results of the fit are excellent.

In the above test procedure, special attention is paid to error propagation and goodness of fit at each intermediate stage. Each individual distribution function is reconstituted

from the fit parameters at each step of the procedure and compared to the observed distribution function. The variances between the reconstituted and observed distribution functions are calculated and minimized before going to the next step, for which the cycle is again repeated. Figures 4 and 5 illustrate this reconstitution cycle for the pitch-angle distribution of the 830-keV channel. In Figure 4 the comparison between observed data and reconstitution is performed for the pitch-angle decomposition (16) at  $L = 5.42$  to test the validity of truncation at  $n = 4$ . Figure 5 shows the same comparison after the entire decomposition and fit procedure has been completed for the same 830-keV channel but measured at  $L = 5.59$  to show the nontrivial variations in the observed data and the fit. Compared to the pitch angle distribution, the variance between observed data and fit is increased in the complete decomposition. This is expected, since it is constrained much more by the solution to diffusion theory; however, the substantial changes of the distribution are well modeled. The errors associated with the fit curves in these two figures are errors associated with the data which have been propagated onto the fit via the procedure. The original errors are statistical errors of the instrument count rates plus 3% data compression error for energy channels below 1.6 MeV. In addition, background errors are included for channels above 1.6 MeV, induced by background counts from a weak radioactive calibration source in the instrument. The data processing software does make a correction for bremsstrahlung contamination, which appears primarily at 448 keV, caused by particles of energy above 1.6 MeV partially penetrating the detector shielding. Figure 6 shows a comparison similar to Figure 5 but for the 1616-keV channel at  $L = 5.42$ . In this figure, the original errors associated with the observed data are shown for comparison with the fit propagated errors in the previous figures. Figure 7 shows a complete decomposition comparison

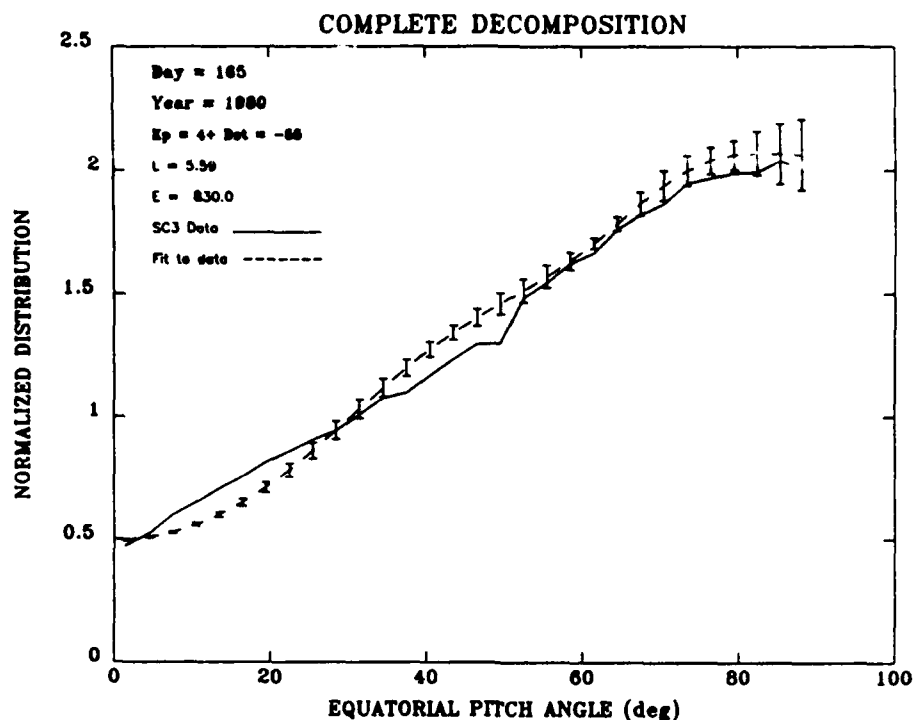


Fig. 5. Comparison between observed pitch-angle distribution for the 830-keV channel at  $L = 5.59$  (solid curve) and its reconstitution after decomposition into the complete solution expansion (dash curve). The fit propagated error bars are shown. Note the differences with Figure 4.

at  $L = 5.48$  similar to Figure 5 again but performed for the lower energy channel at 203 keV. This fit is worse than those shown in Figures 4–6. We speculate that convective signatures may be present in these lower energy channels and their dy-

namics may not be related solely to diffusion, which is why the energy channels below 256 keV are excluded from the formal analysis. Another interpretation is that storm time effects were still prevalent, although no unusual pitch angle distributions

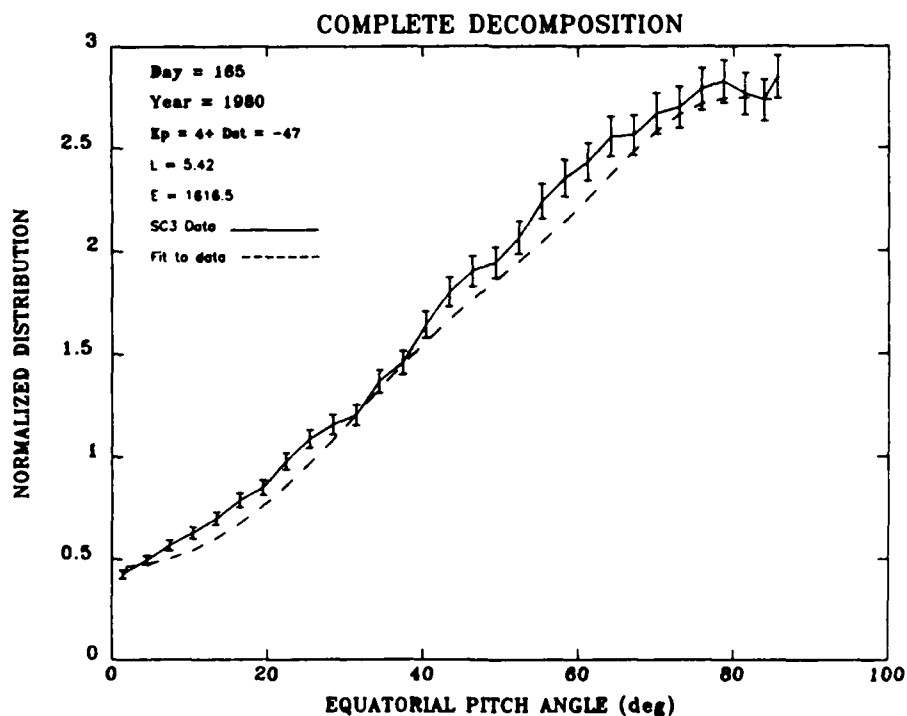


Fig. 6. Same as Figure 5 except the comparison is for the 1616-keV channel at  $L = 5.42$  and the original data error bars are shown.



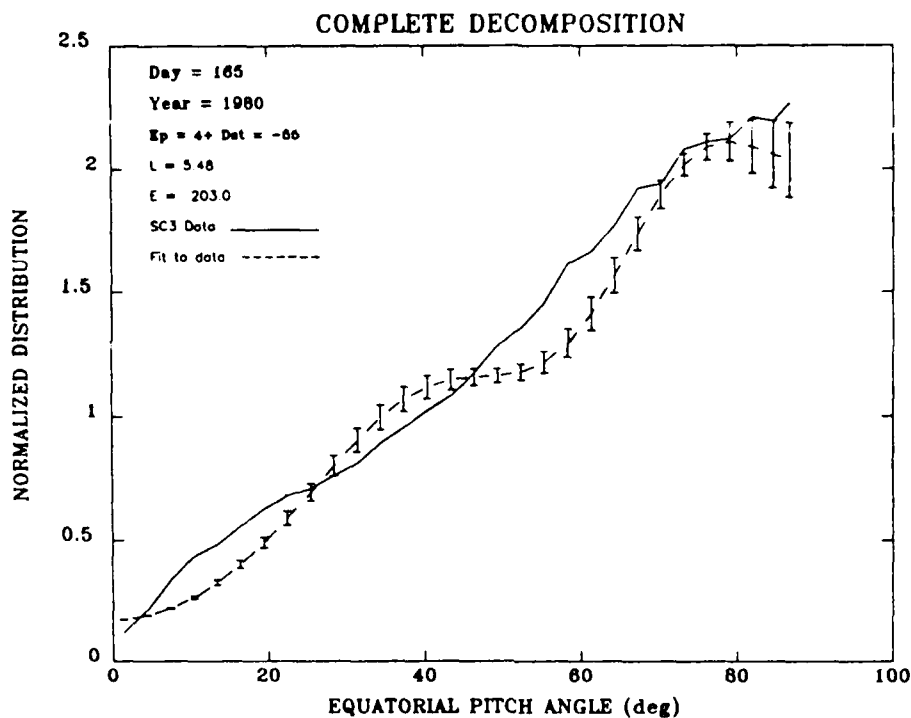


Fig. 7 Same as Figure 5 except the comparison is for the 203-keV channel at  $L = 5.48$ .

[Siheck *et al.*, 1987] were found in our data base. In Figure 8, a tally of the fit error distributions for the entire set of data points in all energy channels within  $L$  values of 5.45–5.70 is shown. The error percentage,  $100 \times |(\text{data} - \text{fit})| / \text{data}$ , for each data point is computed for each data value. It is seen that the most probable error is about 5%. We judge this to be adequate accuracy and to be a reasonable basis for dynamic modeling of the radiation belts. With the method of analysis developed above, we shall be able to distinguish real physical variations of the radiation belts from fit noise at the 5% level.

##### 5. DISCUSSION AND SUMMARY

In the foregoing, we have demonstrated that a solution of the bimodal diffusion equation appropriate to a finite space-time volume describes adequately the dynamics of outer-belt electrons in the space-time span of a selected SCATHA data set during moderate geomagnetic activity after a major sub-storm. Although simple-minded assumptions have been made

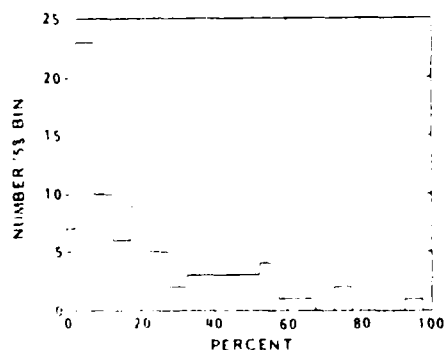


Fig. 8 Distribution of percentage fit errors for the entire set of data points in all energy channels within  $L$  values of 5.45–5.70.

on the form of the diffusion coefficients in order to reduce the computational effort and although the computation procedure is designed to test and illustrate the application rather than to achieve the best fit, we have been able to fit the entire data set to a general solution with a variance level of about 5%. Our results and fit accuracies demonstrate that this is an adequate and potent approach to dynamic modeling of the radiation belts. Obviously, many improvements and refinements can be made. Some of these will be dealt with in subsequent work.

While the principal goal of this paper is to demonstrate data interpretation using the general solution of bimodal diffusion in finite space-time volumes. An equally important goal is to derive the physical parameters, i.e., the diffusion coefficients, and to assess them in the light of other work. The pitch angle diffusion coefficient  $D_{\alpha\alpha}$  is derived by the imposed fit constraint (15) independent of the order of the pitch angle eigenfunction. Figure 9 shows the derived  $D_{\alpha\alpha}$  together with the fit errors as functions of energy. In the solution,  $D_{\alpha\alpha}$  is assumed independent of  $L$  in order to achieve separability. From Figure 9, it is seen that  $D_{\alpha\alpha}$  is remarkably constant with energy also, except for the 448-keV channel, which has large errors possibly introduced by bremsstrahlung contamination, although corrections have been made. The magnitude of  $D_{\alpha\alpha}$  leading to time scales via (15) is consonant with other determinations of the average pitch angle diffusion lifetime of about 5 days, although most of these are not eigenfunction specific [e.g., Schulz and Lanzerotti, 1974]. Williams *et al.* [1968] measured the rise times to half maxima of electron fluxes in similar  $L$  shells immediately after several magnetic storms to be 1–3 days. Magnetic conditions of their cases are quite different from ours and the definitions of time scale are also different from ours. Since both of the above two factors would tend to shorten our time scales (rise times of 1–3 days in Williams *et al.* [1968] can be comparable to our pitch angle diffusion time

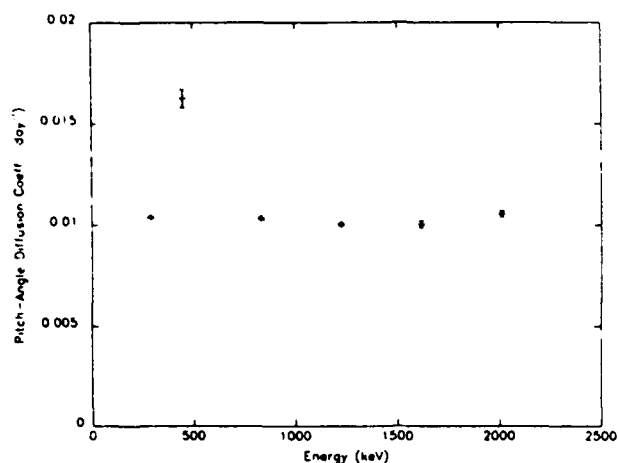
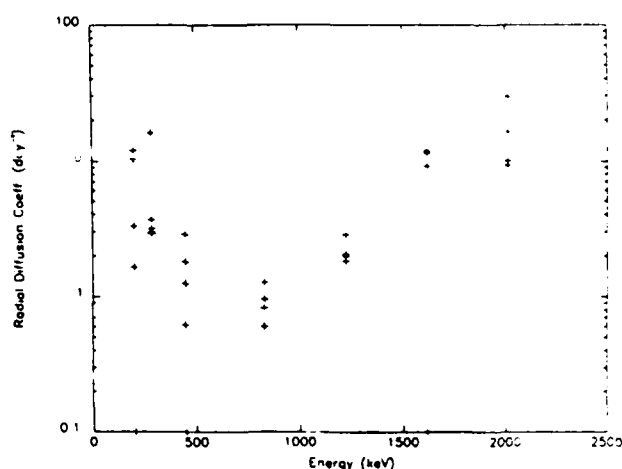


Fig. 9. Pitch angle diffusion coefficient as function of energy.

Fig. 11. Same as Figure 10 except the  $L$  value is 6.10

scales. The  $L$  dependence in their storm time data in the same  $L$  shells exhibited a variety of behavior, showing independence of  $L$  as often as not; therefore it is difficult to sort out the energy and  $L$  shell dependence of  $D_{xx}$  at present.

As we have discussed above, the derivation of the radial diffusion coefficient serves the dual role of providing for physical data in the outer belt, which can be compared with other determinations from direct particle observations [e.g., *Kavanaugh*, 1968; *Newkirk and Walt*, 1968b; *Cornwall*, 1968; *Lanzerotti et al.*, 1970; *West et al.*, 1981], and of testing independently the adequacy of our application to the data. Figures 10 and 11 show scatterplots of  $D_{LL}$  for the energy channels indicated and for  $L$  values of 5.3 and 6.1, respectively. As has been discussed above, scattered values of  $D_{LL}$  result from our deliberately not enforcing the constraint (14) in a cycled fit procedure in order to evaluate the worst case variance of the fit by solving (14) for  $\xi$  at each order. This deliberate procedure produces a  $D_{LL}$  for each order in the energy channel, accounting for the spread of values on these figures in each energy channel. The values of  $D_{LL}$  so determined have a spread of a factor of 2-5, with the largest spreads concentrated in the lower energy channels where we have noted possible convec-

tion contamination. Since these are results from the initial pass of the procedure without enforcing the constraint (14), we are confident that a reduction of the spread by a factor of at least 2 is well within the capability of the procedure without jeopardizing the goodness of fit demonstrated in the last section. Still, the spreads of  $D_{LL}$  derived in this initial pass are already considerably smaller than most previous determinations from particle data, which frequently showed spreads of 1-2 orders of magnitude for  $D_{LL}$  within the same data set. Figure 12 shows a comparison of the spread of values of  $D_{LL}$  over the high-energy range determined by this unconstrained

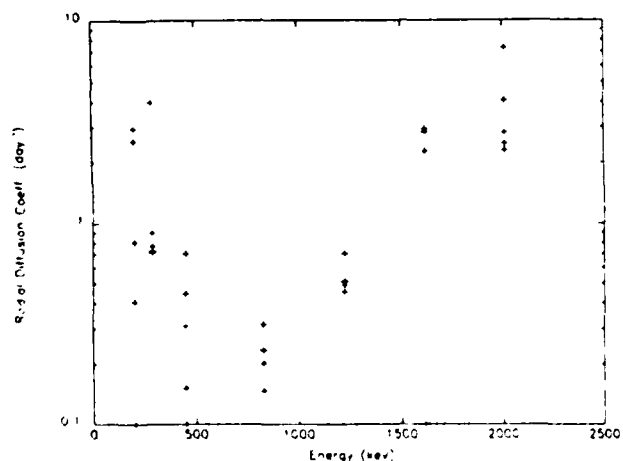


Fig. 10. Radial diffusion coefficient as function of energy at  $L = 5.30$ . The spread of values for each energy is a measure of the worst-case variance in its determination.

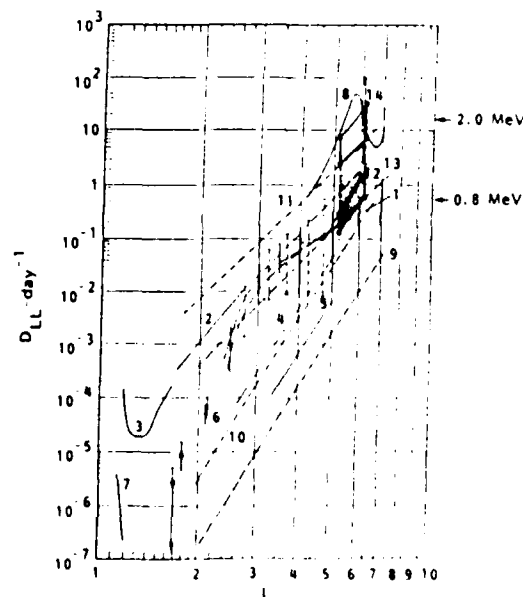


Fig. 12. Comparison of the radial diffusion coefficient determined for the energy range of 0.8-2.0 MeV (mottled area showing decreasing shading with increasing energy) with the compilation of *West et al.* [1981], whose individual analysis yields curve 1. Curves 2-8 are experimental: curve 2, *Tomassian et al.* [1972]; curve 3, *Farley* [1969]; curves 4, 6, *Newkirk and Walt* [1968b]; *Falthammar* [1970]; curve 7, *Newkirk and Walt* [1968a]; curve 8, *Kavanaugh* [1968]. Curves 9-14 are theoretical or semitheoretical: curve 9, *Nakada and Mead* [1965]; curve 10, *Trerskov* [1965]; curve 11, *Birmingham* [1969]; curves 12, 13, *Cornwall* [1968]; curve 14, *Holworth and Moez* [1979].

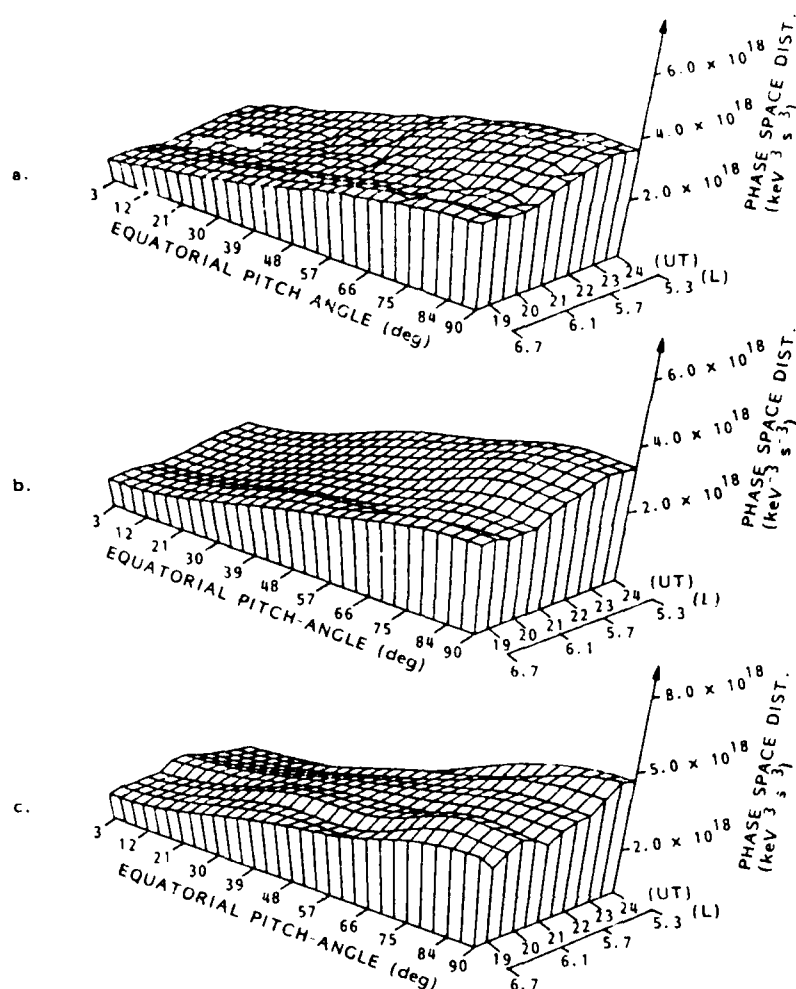


Fig. 13 Three-dimensional presentation of the phase space density of the data base and its reconstitutions for the 830-keV channel in pitch angle and space-time. Figure 13a shows the data base. Figure 13b is the reconstitution after fitting the pitch angle eigenfunction decomposition (16). Figure 13c is the reconstitution after the space-time unmixing procedure and radial diffusion analysis (17) have been applied without the benefits of a fitting procedure.

test pass plotted as function of  $L$  and compared with the up-to-date compilation of all  $D_{LL}$  determinations given by West *et al.* [1981]. Note that the determined radial diffusion coefficients agree well with the storm time data of Tomassian *et al.* [1972]. Since the data on Figure 12 are from a mixture of energies, it is difficult to test the energy dependence of the radial diffusion coefficient, which decreases with increasing shading (lower energy). Thus this independent test of the adequacy of the general solution to bimodal diffusion to represent outer belt electron data is not only satisfactory but actually indicates an improvement over previous analyses, which were restricted to single-mode diffusion.

Finally, to demonstrate the multidimensional nature of our analysis and the ability of the exact bimodal solution to represent data, we show on Figure 13 the specification of the entire data base of the 830-keV channel in pitch angle and space-time (Figure 13a), its reconstitution after fitting of the pitch angle eigenfunction expansion (Figure 13b) and its reconstitution from the complete eigenfunction expansion after the ad hoc unmixing of space and time in the radial diffusion segment of the analysis (Figure 13c). As is discussed above, a fitting procedure has not been applied to Figure 13c in order

to determine the maximal spread of the radial diffusion coefficients; therefore, the error in Figure 13c, relative to Figure 13a, reflects the error distribution in Figure 8 and manifests itself as the spread of radial diffusion coefficients shown in Figures 10 and 11. This unfitted reconstruction explicitly demonstrates the effects of the high-percentage tail of Figure 8. The basic trend of the data reconstruction reflects the effects of the most probable part (5%) of the error distribution in Figure 8. It is clear from a comparison of Figures 13a and 13c that their basic trends agree. It is also likely that the increased error in the unfitted second (radial) phase of the analysis originates from the ad hoc unmixing of space and time variables necessary in any multidimensional analysis of data from a moving satellite. Further investigations on the unmixing procedure may be necessary, if a fitting procedure does not reduce the unfitted errors.

The ultimate goal of an analysis such as in this paper is to obtain a proper theoretical foundation for dynamic modeling of the radiation belts. We have not achieved this goal by far, but we have demonstrated that our approach has vast potential to quantitatively interpret data and achieve a higher level of accuracy in determination of physical parameters. To

achieve dynamic modeling in the outer belt, an important hurdle, alluded to previously, is that the  $L$  shells are time-dependent even during moderate geomagnetic activity, resulting in not just another scale to be disentangled but also in drastic effects of drift loss through the magnetopause boundary. Loss boundaries can be accommodated naturally in the eigenfunction solution formalism; however, the choice of phase space as representation coordinates may not be as powerful as the use of invariant space in this regard. Our future efforts will be directed toward this area.

**Acknowledgments.** This work is supported by the Air Force Geophysics Laboratory under contract F19628-85-C-0073. It is a pleasure to thank S. Gussenhoven, M. Schulz, and G. Davidson for discussions on various aspects of this work. The SCATHA SC-3 payload and initial data analysis were sponsored by the Office of Naval Research under contract N00014-76-C-0444. The P78-2 SCATHA spacecraft is sponsored and operated by the USAF Space Test Program.

The Editor thanks A. L. Vampola and another referee for their assistance in evaluating this paper.

#### REFERENCES

- Baker, D. N., P. R. Higbie, E. W. Hones, Jr., and R. D. Belian, High-resolution energetic particle measurements at 6.6  $R_E$ . 3. Low-energy electron anisotropies and short-term substorm predictions, *J. Geophys. Res.*, **83**, 4863, 1978.
- Birmingham, T. J., Convection electric fields and the diffusion of trapped magnetospheric radiation, *J. Geophys. Res.*, **77**, 2169, 1969.
- Chiu, Y. T., and H. H. Hilton, Exact Green's function method of solar force-free magnetic field computations with constant  $\alpha$ , I, Theory and basic test cases, *Astrophys. J.*, **212**, 873, 1977.
- Cornwall, J. M., Diffusion processes influenced by conjugate point wave phenomena, *Radio Sci.*, **3**, 740, 1968.
- Davidson, G. T., An improved experimental description of bounce motion of trapped particles, *J. Geophys. Res.*, **81**, 4029, 1976.
- Falthammar, C. G., Introductory survey of radiation belt diffusion, in *Particles and Fields in the Magnetosphere*, edited by B. M. McCormac, p. 387, D. Reidel, Hingham, Mass., 1970.
- Falthammar, C. G., and M. Walt, Radial motion resulting from pitch-angle scattering of trapped electrons in the distorted geomagnetic field, *J. Geophys. Res.*, **74**, 4184, 1969.
- Farley, T. A., Radial diffusion of starfish electrons, *J. Geophys. Res.*, **74**, 3591, 1969.
- Frankenthal, S., F. R. Paolini, and G. C. Theodoridis, Bimodal diffusion in the earth's magnetosphere, II, On the electron belts, *Ann. Geophys.*, **24**, 1015, 1968.
- Haerendel, G., *Earth's Particles and Fields*, edited by B. M. McCormac, pp. 171-191, Reinhold, New York, 1968.
- Holzworth, R. H., and F. S. Mozer, Direct evaluation of the radial diffusion coefficient near  $L = 6$  due to electric field fluctuations, *J. Geophys. Res.*, **84**, 2559, 1979.
- Kavanaugh, L. D., Jr., An empirical evaluation of the radial diffusion coefficients for electrons of 50-100 keV from  $L = 4$  to  $L = 7$ , *J. Geophys. Res.*, **73**, 2959, 1968.
- Lanzerotti, L. J., C. G. MacLennan, and M. Schulz, Radial diffusion of outer zone electrons: An empirical approach to third invariant violation, *J. Geophys. Res.*, **75**, 5351, 1970.
- Mellwin, C. E., Coordinates for mapping the distribution of magnetically trapped particles, *J. Geophys. Res.*, **66**, 3681, 1961.
- Morse, P. M., and H. Feshbach, *Methods of Theoretical Physics*, 1978 pp., McGraw-Hill, New York, 1953.
- Nakada, M. P., and G. D. Mead, Diffusion of protons in the outer radiation belt, *J. Geophys. Res.*, **70**, 4777, 1965.
- Newkirk, L. L., and M. Walt, Radial diffusion coefficients for electrons at low  $L$  values, *J. Geophys. Res.*, **73**, 1013, 1968a.
- Newkirk, L. L., and M. Walt, Radial diffusion coefficients for electrons at  $1.76 < L < 5$ , *J. Geophys. Res.*, **73**, 7231, 1968b.
- Olson, W. P., K. A. Pfizter, and G. J. Morz, Modeling the magnetospheric magnetic field, in *Quantitative Modeling of Magnetospheric Processes*, edited by W. P. Olson, p. 77, AGU, Washington, D. C., 1979.
- Reagan, J. B., R. W. Nightingale, E. E. Gaines, W. L. Imhof, and E. G. Stassinopoulos, Outer-zone energetic electron spectral measurements, *J. Spacecr. Rockets*, **18**, 83, 1981.
- Roederer, J. G., and M. Schulz, Effect of shell splitting on radial diffusion in the magnetosphere, *J. Geophys. Res.*, **74**, 4117, 1969.
- Schulz, M., Eigenfunction methods in magnetospheric radial diffusion theory, in *Ion Acceleration in the Magnetosphere and Ionosphere*, edited by T. Chang, pp. 158-163, AGU, Washington, D. C., 1986.
- Schulz, M., and L. J. Lanzerotti, *Physics and Chemistry in Space*, vol. 7, *Particle Diffusion in the Radiation Belts*, 215 pp., Springer, New York, 1974.
- Schulz, M., and A. L. Newman, Eigenfunctions of the magnetospheric radial diffusion operator, *Phys. Scripta*, in press, 1988.
- Sibeck, D. G., R. W. McEntire, A. T. Y. Lui, R. E. Lopez, and S. M. Krimigis, Magnetic field drift shell splitting: Cause of unusual dayside particle pitch angle distributions during storms and substorms, *J. Geophys. Res.*, **92**, 13,485, 1987.
- Theodoridis, G. C., Acceleration of trapped particles through bimodal diffusion in an inhomogeneous magnetic field, *Geophys. Res. Lett.*, **21**, 1202, 1968.
- Tomassian, A. D., T. A. Farley, and A. L. Vampola, Inner-zone energetic electron repopulation by radial diffusion, *J. Geophys. Res.*, **77**, 3441, 1972.
- Tverskoy, B. A., Transport and acceleration of charged particles in the earth's magnetosphere, *Geomagn. Aeron. Engl. Transl.*, **5**, 617, 1965.
- Walt, M., Radial diffusion of trapped particles, in *Particles and Fields in the Magnetosphere*, edited by B. M. McCormac, p. 410, D. Reidel, Hingham, Mass., 1970.
- West, H. I., Jr., R. M. Buck, and G. T. Davidson, The dynamics of energetic electrons in the Earth's outer radiation belt during 1983 as observed by the Lawrence Livermore National Laboratory's spectrometer by OGO 5, *J. Geophys. Res.*, **86**, 2111, 1981.
- Williams, D. J., J. F. Arens, and L. J. Lanzerotti, Observations of trapped electrons at low and high altitudes, *J. Geophys. Res.*, **73**, 5673, 1968.
- Y. T. Chiu, R. W. Nightingale, and M. A. Rinaldi, Lockheed Palo Alto Research Laboratory, Dept. 91-20, Bldg. 255, 3251 Hanover St., Palo Alto, CA 94304.

(Received May 18, 1987;  
revised December 17, 1987;  
accepted December 22, 1987.)

## HIGH-ENERGY OUTER RADIATION BELT DYNAMIC MODELING

Y. T. Chiu, R. W. Nightingale and M. A. Rinaldi  
Lockheed Palo Alto Research Laboratory  
3251 Hanover St., Palo Alto, Ca. 94304

### ABSTRACT

Specification of the average high-energy radiation belt environment in terms of phenomenological montages of satellite measurements has been available for some time. However, for many reasons both scientific and applicational (including concerns for a better understanding of the high-energy radiation background in space), it is desirable to model the dynamic response of the high-energy radiation belts to sources, to losses, and to geomagnetic activity. Indeed, in the outer electron belt, this is the only mode of modeling that can handle the large intensity fluctuations. Anticipating the dynamic modeling objective of the upcoming Combined Release and Radiation Effects Satellite (CRRES) program, we have undertaken to initiate a study of the various essential elements in constructing a dynamic radiation belt model based on interpretation of satellite data according to simultaneous radial and pitch-angle diffusion theory. In order to prepare for the dynamic radiation belt modeling based on a large data set spanning a relatively large segment of  $L$ -values, such as required for CRRES, it is important to study a number of test cases with data of similar characteristics but more restricted in space-time coverage. In this way, models of increasing comprehensiveness can be built up from the experience of elucidating the dynamics of more restrictive data sets. The principal objectives of this paper are to discuss issues concerning dynamic modeling in general and to summarize in particular the good results of an initial attempt at constructing the dynamics of the outer electron radiation belt based on a moderately active data period from Lockheed's SC-3 instrument flown on board the SCATHA (P78-2) spacecraft. Further, we shall discuss the issues brought out and lessons learned in this test case.

### FORMULATION

Some two decades of satellite observations have shown that the electron radiation flux (including the satellite-damaging electrons of  $>500$  keV energy) in the outer belt fluctuates by orders of magnitude in response to geomagnetic activity. Some typical fluxes and spectra measured by the SCATHA SC-3 instrument<sup>1,2,3</sup> are shown in Figure 1. The practical need to characterize and predict these large radiation fluctuations for satellite survivability considerations requires an understanding of their dynamics beyond phenomenological correlations; thus, the need for dynamic modeling of the outer electron belts was initiated.

In its most comprehensive form dynamic modeling involves a theoretical accounting of the flux responses in terms of fundamental processes of electron transport and loss in the magnetosphere. Since we are dealing with energetic electrons, a Fokker-Planck description of the transport processes naturally leads to a diffusion picture in terms of several independent variables characterizing

the population.

Diffusive transport of energetic particles in the magnetosphere is an excellent theoretical approach to outer-belt dynamic modeling, but the latter involves much more. The constraint of satellite data and conditions of the magnetosphere play roles in dynamic modeling which are as important as the diffusion theory itself. In the outer belt the magnetic field is transient. Plasma and field conditions encountered by a drifting electron vary drastically and parts of the energetic particle population may even cross outside of the magnetosphere. Thus, dynamic modeling involves an accounting of fields and magnetospheric boundary configurations as much as diffusive particle transport. All of these elements are integral parts of a dynamic model of the outer electron belt.

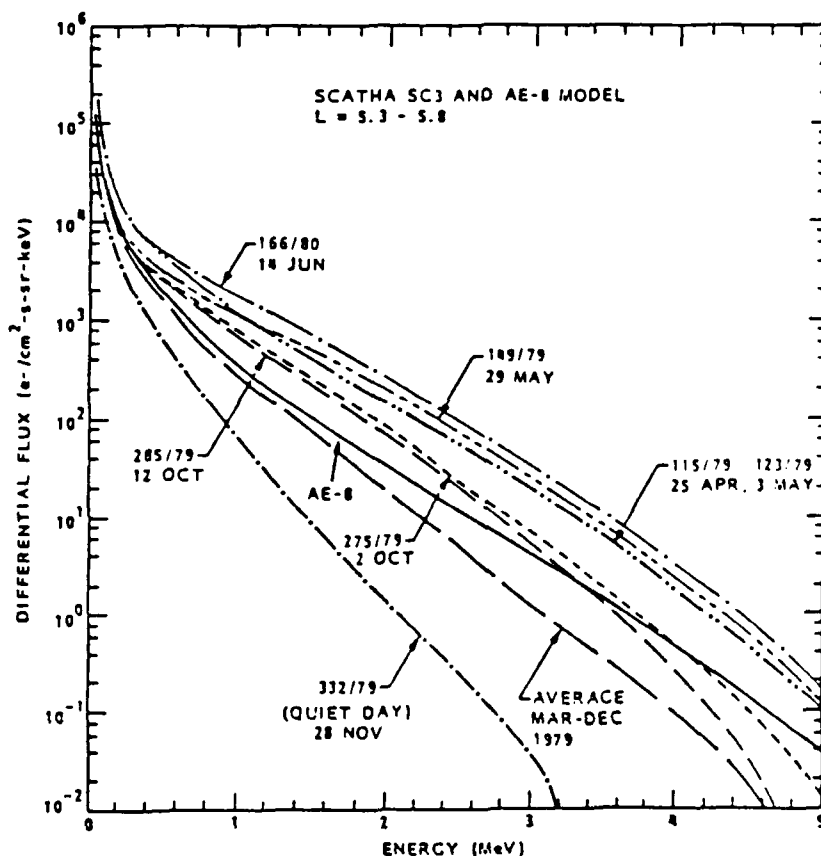


Figure 1. Sample spectra showing the variation of outer-belt electrons obtained in 1979 and 1980 by the Lockheed SC3 instrument. Phenomenological models based on 6-month averages of the data can be in error by an order of magnitude or more.

To illustrate the complexity that a dynamic model must deal with, Figure 2 shows a survey of the high-energy electron characteristics encountered by SCATHA in an active period on day 115 of 1979 in which a moderate magnetic storm occurred, with a sudden commencement just prior to the start of the day and a maximum  $Dst$  of  $-148 \gamma$ . Just before 18:00 h LT there was a brief enhancement of electron fluxes that may have been an adiabatic compression event. "Butterfly" pitch-angle distributions, indicating loss of  $90^\circ$  pitch-angle particles at the magnetopause, were seen at all energies for almost 2 hours, after which the lower-energy electron fluxes recovered to their previous levels. Shortly after

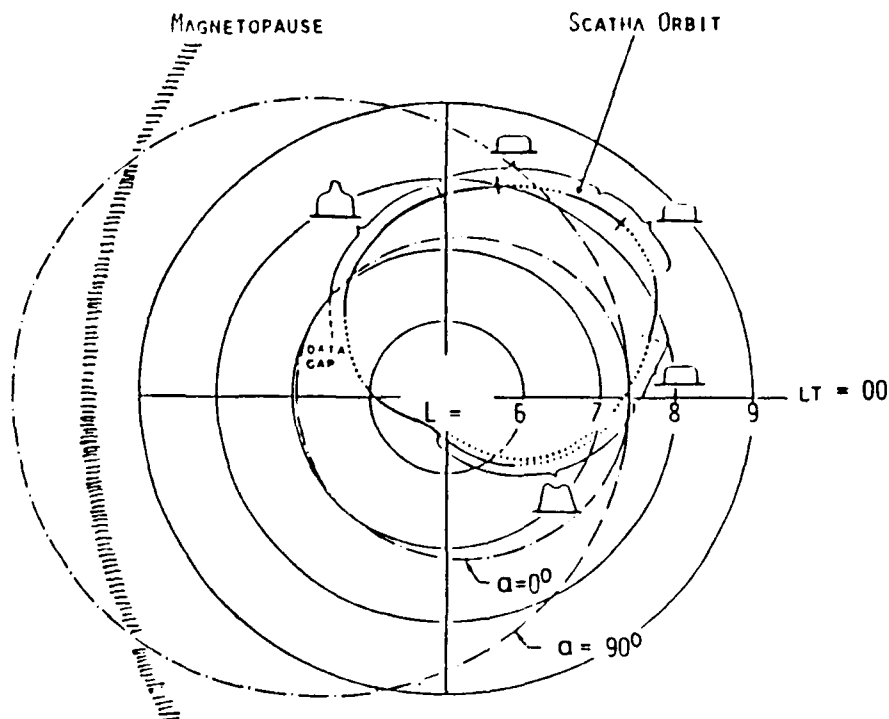


Figure 2. A montage of electron flux characteristics encountered by SCATHA on day 115 in 1979. The inset figures are schematics of pitch-angle distribution with  $90^\circ$  pitch angle placed at the center.

midnight, there began a succession of substorms, with deep flux dropouts over the portions of the orbit shown as dotted lines in Figure 2. The dropouts exhibit the expected correlation with the geomagnetic activity indices, particularly AE. These were followed by rises in the flux levels that can be interpreted as a fresh arrival of electrons on the observed flux tubes by either injection or compressional changes of the magnetic field. Such active periods are usually recognized by decreases in the total flux and the occasional appearance of nearly isotropic pitch-angle distributions as shown on the Figure. In the morning hours, typical "hat" distributions, indicating enhanced fluxes of  $90^\circ$  pitch-angle particles, are encountered.

In view of the complexity of the above data, it is sensible to separate the elements of outer-belt dynamic modeling into modules which can be individually formulated. Thus, our approach to dynamic modeling is to initially treat each of the following elements as if they are not related, but bearing in mind all the time that they are to be integrated into a whole. These elements are:

- (i) Transport, injection and loss of trapped energetic electrons in terms of diffusion in phase space;
- (ii) Description of the space-time variations of the geomagnetic field;
- (iii) Physics of transport parameters.

The principal topics of this paper deal only with issues arising out of the diffusion physics [item (i)]. The diffusion physics, which is the fundamental basis of a dynamic model, appears initially to be mostly straightforward, although mathematically cumbersome. However, it turns out that the boundary conditions corresponding to satellite data can become a major issue to be resolved irrespective of the chosen diffusion formulation. Since the boundary data issue is central to all schemes of dynamic modeling, we discuss it at the outset.

On the least ambitious level, dynamic modeling can be viewed as a means of projecting radiation belt data obtained along a satellite track by physical means to specify the radiation environment throughout some reasonable regions not on the satellite track. As such, the selected diffusion treatment is the projection mechanism and the in-track satellite data is the raw material to be processed: the "boundary" values for the diffusion physics. However, satellite measurements, obtained on a space-time trajectory, are not standard boundary conditions stated at fixed time or space coordinates to define either initial-value problems or boundary-value problems of diffusion theory. The situation for dynamic modeling is different from these simple boundary-value or initial-value cases. Figure 3 illustrates the satellite data span and its relation to the appropriate solution volume in  $(x, L, t)$  space, where  $x$  is the cosine of the pitch angle and  $L$  is the McIlwain parameter. The fundamental nature of nonsynchronous satellite data spans is that they lie on a data surface (ABCD on the figure) defined by the satellite trajectory  $L(t)$ . Further, the time span defines the  $(L, x)$  boundary surfaces of the solution volume labelled by the Roman letters A to H on the figure. In such a source-free volume, particles are transported into and out of the surfaces ABGH and CDEF by radial diffusion; in other words, these



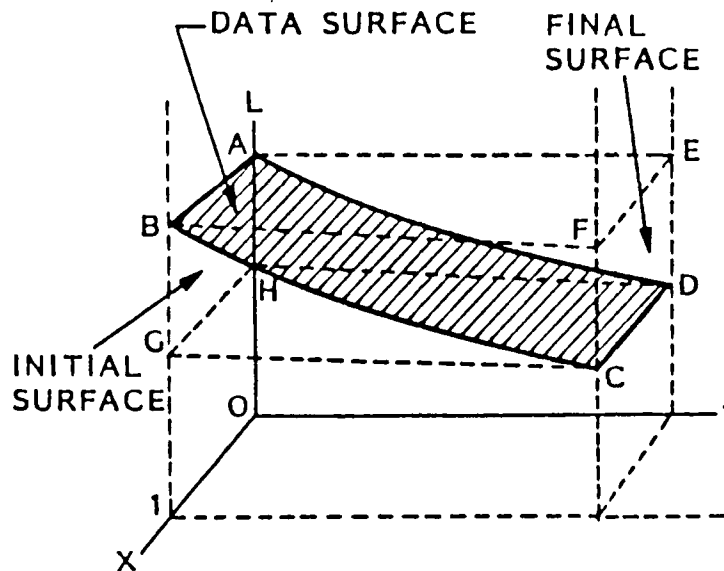


Figure 3. Schematic illustration of the boundary volume in  $(x, L, t)$  space in which the general bi-modal diffusion solution is developed. Satellite data to be matched to the solution span lie on the data surface.

boundary surfaces are also source surfaces. Particles are lost through the surface BGCF through pitch-angle diffusion into the loss cone, approximately signified by  $x = 1$  here. If the data time span is less than or comparable to the injection and loss times in the volume, as is the case in most satellite observations such as SCATHA, the appropriate solution to be developed is the general source-free solution in a finite space-time interval, and not an initial-value solution in the semi-infinite time domain corresponding to response to a transient (i.e., delta function) source. In the finite space-time domain, the entire spectrum of time constants (rising as well as falling) must be included in the general complete-set solution expansion because unknown sources (and sinks) outside of the volume are diffusing particles into (and out of) the finite volume causing the phase-space density to increase (decrease) with time scales that can be comparable to the data time span. In contrast, in the semi-infinite time domain only the falling time response function is appropriate. To be sure, this Green's function can be applied to obtain the finite space-time solution by applying Green's theorem onto the boundary surfaces<sup>4</sup>. This crucial integration imparts the source time scales onto the solution. The important point is that this integration convolves the rising and falling time constants of the surface sources with the natural falling time constants of diffusion to result in a spectrum of both rising and falling time constants for the spatial eigenfunctions. As a result of this time convolution, the final solution for finite volume need not look anything like the Green's function that would be developed for the initial-value problem over semi-infinite time. To

be sure, all excited states eventually decay by diffusion to equilibrium, but with the satellite data span, over a finite space-time interval, we do not know whether it has caught the rising or falling phase of a modal disturbance of unknown time scale. For the SCATHA orbit, space and time are relatively distinct since the range of  $L$  covered by the satellite is small. However, for highly elliptical orbits (such as for CRRES) space and time on an orbit are not linearly related. We shall see that under such circumstances the satellite data set acts as a highly nonlinear boundary for the dynamic model.

The consequence of the esoteric points discussed above is that it would be wrong to force satellite data obtained over a finite space-time volume to fit an impulsive transient response solution such as the Green's function. For purposes of satellite data analysis in a finite space-time interval, the appropriate solution to diffusion theory is the solution corresponding to a general boundary-value problem<sup>4</sup>, and not corresponding to a global response to an impulsive source. Since a general solution can be obtained by eigenfunction expansion with unrestricted separation constants, which will be constrained by data, this convenient property forms the basic principle of data characterization in dynamic modeling. It will be shown later, based on the success of our data analysis, that this principle can be used to characterize the state of the entire radiation belt in a piece-wise-continuous fashion.

Given the above general property of radiation belt dynamic modeling, let us proceed to consider our test case<sup>4</sup> for which we choose to specify the diffusion physics in a static magnetosphere in  $(x, L, t)$  space as illustrated in Figure 3. [The choice of spaces to characterize radiation belt diffusion is not arbitrary. This complex issue is treated elsewhere<sup>4</sup>.] Our choice of diffusion description is that of simultaneous multi-mode diffusion theory. The multimode diffusion equation can be simplified<sup>4,5,6</sup> under a number of reasonable assumptions. One of these is that the  $L$ -dependence of the radial diffusion coefficient  $D_{LL}$  can be parameterized as  $D_{LL} = \xi L^\mu$  where  $\xi$  and  $\mu$  are parameters to be determined by the on-trajectory satellite data. The diffusion equation for the electron distribution function  $f$  can be written

$$\frac{\partial f}{\partial t} = D_{xx} \left[ \frac{\partial^2 f}{\partial x^2} + \frac{1}{x} \frac{\partial f}{\partial x} \right] + \xi L^{-2+\frac{1}{2}\nu} \frac{\partial}{\partial L} \left[ L^{\mu+2-\frac{1}{2}\nu} \frac{\partial f}{\partial L} \right] \quad (1)$$

where  $D_{xx}$  (the pitch-angle diffusion coefficient),  $\xi$ ,  $\mu$  and  $\nu$  are considered to be constant parameters.

This simplified equation is to be solved in a small finite domain  $L_l \leq L \leq L_u$  expected to be in the outer belt and in the pitch-angle domain  $0 \leq x \leq x_c$ , where  $x_c$  is cosine of the loss-cone angle. The effect of pitch-angle diffusion is to define pitch-angle behavior of  $f$  inside and outside of the loss-cone boundary  $x = x_c(L)$ . The dependence of  $x_c$  on  $L$  is yet again another factor which mixes the  $x$  and  $L$  operators in (1); however, for the range in our test case in outer zone region, where  $(L_u - L_l) \leq 2$ ,  $x_c$  is very nearly constant and nearly unity.

We assume that  $x_c$  is constant in the data span so that separable solutions can be obtained for (1) with the present test case. This is another important point when we deal with data from a large domain of  $L$  (such as that from CRRES) which involves large variations of the loss cone both from the large variations in  $L$  and in distances to the magnetic mirror points. For the SCATHA test case the loss-cone dependence on  $L$  is entirely negligible.

Under the approximations discussed above, a general solution to (1) in finite space-time can be developed<sup>4</sup> in terms of complete-set eigenfunction expansions. In general, there are three modal expansions: (1) single-mode pitch-angle diffusion, (2) single-mode radial diffusion and (3) simultaneous bi-modal diffusion. Using the device of the Kronecker delta  $\delta_{n0}$ , the three modal expansions can be written in terms of a single eigenfunction expansion

$$f = \sum_{n=0}^{\infty} \left[ \delta_{n0} + (1 - \delta_{n0}) \frac{\sqrt{2}}{x_c} \cdot \frac{J_0(k_n x/x_c)}{J_1(k_n)} \right] \left( c_n (1 - \delta_{n0}) e^{t/\tau_n} + h(L, t) \right) \quad (2a)$$

$$h(L, t) = e^{t/\tau_n} [a_n Y_n(L) + b_n Z_n(L)] \quad (2b)$$

where  $k_n$  is the  $n^{\text{th}}$  zero of the Bessel function  $J_0$ . The parameters and new functions are defined as follows:

$$\begin{aligned} \epsilon &\equiv 3(1 - \frac{\nu}{2})/(\mu - 2) \\ \sigma &\equiv -\frac{\mu}{2} - \frac{1}{2} + \frac{3}{4}\nu \\ \lambda &\equiv \frac{\mu}{2} - 1 \end{aligned} \quad (3)$$

$$Y_n(L) = L^\sigma \cdot [J_{1+\epsilon}(|\beta_n|/L^\lambda)]_> \cdot [I_{1+\epsilon}(|\beta_n|/L^\lambda)]_< \quad (4)$$

$$Z_n(L) = L^\sigma \cdot [N_{1+\epsilon}(|\beta_n|/L^\lambda)]_> \cdot [K_{1+\epsilon}(|\beta_n|/L^\lambda)]_< \quad (5)$$

$J$  is the regular Bessel function,  $I$  and  $K$  are the modified Bessel functions, and  $N$  is the Neumann function. In the above, the separation constants are  $t_n$  and  $\beta_n$ . The usual notation  $[g]_>$  is defined in this case by

$$[g]_> = g \quad \text{if } t_n > 0 \quad (6)$$

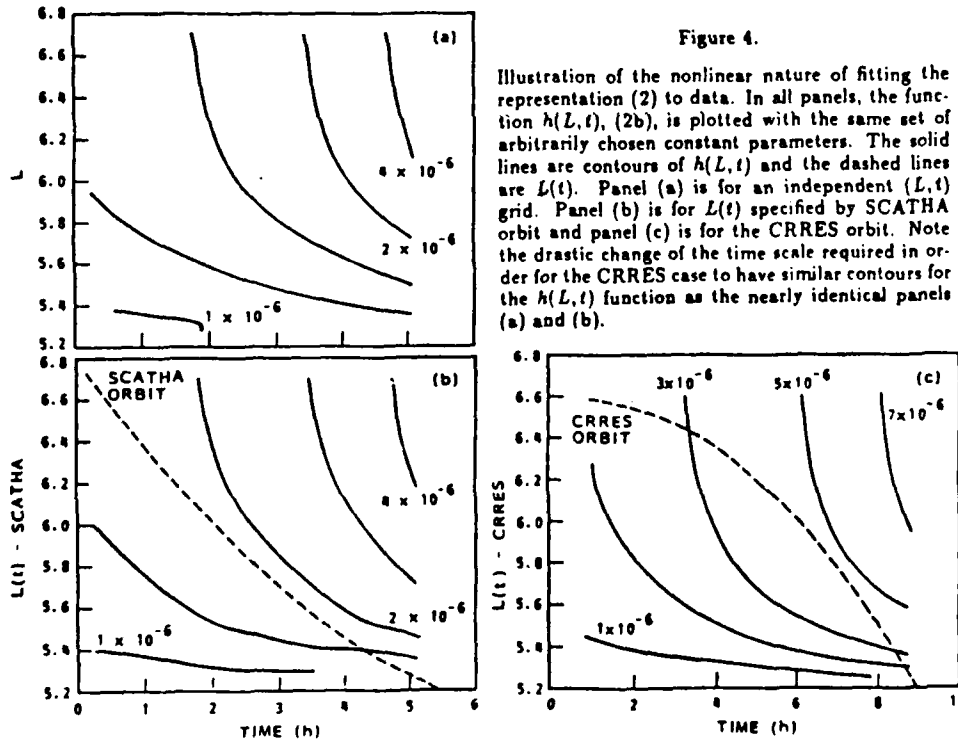
$$[g]_> = 1 \quad \text{if } t_n < 0$$

and analogously for  $[g]_<$ . The separation constants and parameters of the solution are related by the algebraic relations

$$t_n^{-1} = (1 - \delta_{n0})\tau_n^{-1} - \xi\beta_n^2\lambda^2 \quad (7)$$

$$\tau_n^{-1} \equiv -D_{xx}k_n^2/x_c^2 \quad (8)$$

which will be referred to as separation equations. It is seen that the single pitch-angle mode time constants are negative as expected, since single-mode pitch-angle diffusion always leads to decay. For bi-modal and radial diffusion, however, the time constants  $t_n$  can be either positive or negative over a finite time interval. This is due to the fact that the phase-space density in the finite  $L$  domain can rise or fall in time in response to particle transport into and out of the adjacent volumes, as discussed above. With the sign of each  $t_n$  not predetermined, the separation constant  $\beta_n^2$  can be positive or negative. This is the origin of the  $(J, I)$  and  $(N, K)$  options of (4) and (5). The solution (2) is not the most general solution, for a separate sum of pure radial modes can be added. We have not done so for two reasons: (1) we expect that episodes of radial diffusion must accompany pitch-angle diffusion because of the association of magnetospheric fluctuations of all scales with each other and (2) this separate sum creates more parameters. As it presently stands, only one pure radial mode is included, i. e. for  $n = 0$ .



Having now specified a general solution of the chosen diffusion theory, we can quantitatively illustrate how the satellite trajectory  $L(t)$  impacts the characterization of radiation fluxes away from the trajectory. The idea is of course central to dynamic modeling and is very simple: determine the parameters of the solution with on-trajectory satellite data then the solution yields fluxes at all other  $(x, L, t)$  points. But as pointed out above, the problem is that the satellite trajectory mixes  $L$  and  $t$ , i.e.,  $L(t)$ , which complicates the fit. For near-synchronous satellites such as SCATHA for which only a small range of  $L$  is covered in an orbit, the effect of space-time mixing is quite minimal. This allows us to complete the test case shown in the next section. For the more comprehensive situation of highly-elliptic orbits such as that for CRRES, which attempts to specify the radiation belts over a wide range of  $L$ , the trajectory  $L(t)$  is a non-linear function of  $t$ , requiring a non-linear fit for the determination of the diffusion parameters. This significant complication is illustrated in Figure 4 which shows plots of the function  $h(L, t)$  in (2b) for three situations: (a)  $L$  and  $t$  independent, (b) SCATHA orbit on which  $L$  is nearly independent of  $t$  and (c) CRRES-like orbit on which  $L$  is strongly dependent on  $t$ . The strong distortions on panel (c) for  $h(L(t), t)$  relative to the same function  $h(L, t)$  on panel (a) signifies that dynamic modeling in conjunction with a satellite data base involves much more than obtaining solutions to diffusion theory.

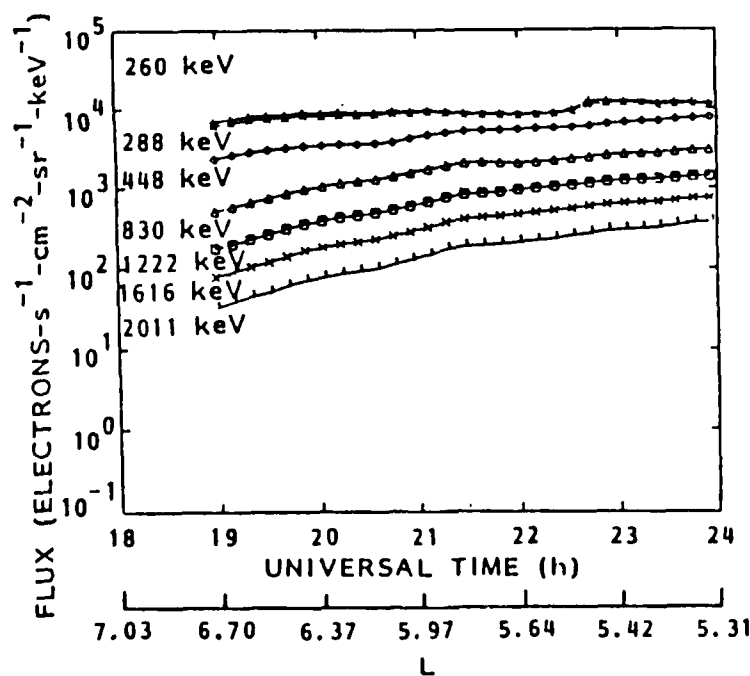


Figure 5. Ten-minute averaged electron fluxes integrated over all pitch angles for 7 energy channels measured by the Lockheed SC3 instrument on board SCATHA during day 165, 1980. This is the data set to be analyzed in this paper.

## TEST CASE VERIFICATION

Notwithstanding the difficulties of applying radiation belt diffusion theory to dynamic modeling in the comprehensive situation of the expected CRRES data base, it is of interest to test whether multi-mode diffusion theory adequately describes the simpler on-trajectory SCATHA data base. This section summarizes the results of such an investigation<sup>4</sup>.

The Lockheed SCATHA SC3 data base<sup>1,2,3</sup> consists of  $\sim 950$  days of digitized data on magnetic tape from launch in 1979 to the present in several intervals. The pitch angle for each accumulation period is determined using data from the on-board vector magnetometer (SC11). From the data tapes a condensed data base of 10-min averaged, pitch-angle binned electron fluxes for the 24 energy channels over the full energy range of 47 to 4970 keV, has been generated for on-line storage on a VAX 11/780 computer. For each 10-min time interval the data are grouped by pitch-angle values into  $3^\circ$  bins from  $0^\circ$  to  $90^\circ$ , making 30 pitch-angle bins for each energy channel in the interval.

The SCATHA SC3 temporal data set for this verification was from the latter portion of day 165, June 13, 1980, a moderately active period with  $Kp = +4$  and  $Dst = -50$ . Two days earlier a geomagnetic storm had occurred, but the magnetosphere had since relaxed enough that the observed electron fluxes on day 165 were smoothly varying with no pitch-angle signatures of particle loss in the magnetopause. Figure 5 shows the 10-min averaged data integrated over all pitch angles for 7 channels of electron flux. During this period the spacecraft

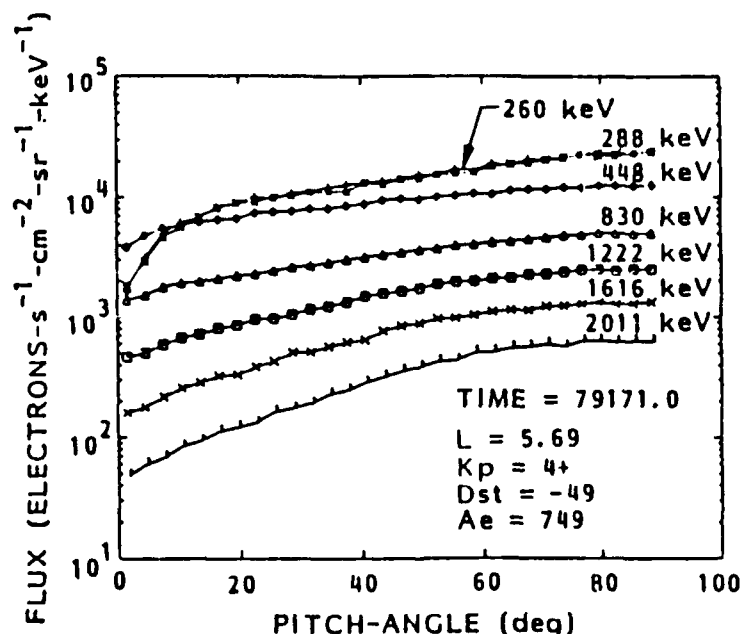


Figure 6. Typical pitch-angle distributions for the 7 energy channels of the data set referred to in Figure 5.

was drifting inward from  $L = 7.2$  to  $L = 5.3$ . The  $L$ -shell range included in the analysis has been restricted to  $L \leq 6.48$  to eliminate the large variability of the electron fluxes beyond the geosynchronous region<sup>7</sup> and the low count rates due to the approximately exponential fall off with increasing  $L$ -shell<sup>1</sup>. In addition we have selected for the formal analysis only those data channels above 256 keV so as to eliminate channels which are most likely to be affected by convective forces resulting from consequences of the major storm preceding the data period. Data with electron energies above 2208 keV have low statistics and are also excluded from the data set. Figure 6 illustrates typical pitch-angle distributions during this time for the selected energies. Although the period was moderately active, the magnetic field was smoothly varying, with a field direction that remained perpendicular to the spacecraft spin vector. This allowed SC3 to look into the loss cone for the whole period, providing data over the full pitch-angle range. In addition, the pitch-angle distributions were smoothly varying and without signatures that indicate loss at the magnetopause.

The application of the diffusion theory summarized above to the SC3 electron data for day 165 has been discussed in detail in an earlier paper<sup>4</sup>. The verification that the theory is a good description of the on-trajectory SCATHA data is indicated in Figure 7, in which the entire data set is shown in Panel(a) as a three-dimensional plot in terms of pitch angle and  $L(t)$ . Panel(b) shows the reconstructed data set after it has been decomposed into a sum of pitch-angle eigenfunctions truncated at the fourth order. Comparison of Panels (a) and (b) shows that the pitch-angle eigenfunction series is a very efficient representation of the data set. In Panel (c) we also show the reconstruction of the data set after decomposition in  $(x, L, t)$  space, using the property that  $L$  and  $t$  are approximately decoupled for the SCATHA orbit as illustrated by Panels (a) and (b) of Figure 4. In order to show the worst case scenario we show in Panel (c) of Figure 7 the reconstruction after the first iteration of the decomposition; we have not attempted to obtain the best solution at this time. As we can see by a comparison of the panels in Figure 7, we conclude that multi-mode diffusion theory in a fairly simplified form is a good representation of the electron outer belt fluxes. This implies that multi-mode diffusion theory can be used as a fundamental basis of radiation belt dynamic modeling.

Verification that multi-mode diffusion theory is a good basis for radiation belt dynamic modeling involves more than just data representation and the implied power of flux mapping throughout the entire belt, although the applicational needs are focused onto this area. From the science view point, an important part of dynamic modeling is the determination of transport parameters which are related to the microscopic physics of wave-particle interactions in the magnetospheric plasma. The above data representation exercise yields physical diffusion parameters with maximum error spread factors of 2-5 that can be compared to other determinations. The radial diffusion coefficient  $D_{LL}$  determined in our exercise and shown on Figure 8 as the shaded trapezoid region compares well with other determinations. Indeed, our determination is able to obtain the energy dependence from 0.8 MeV to 2.0 MeV. Our pitch-angle diffusion coefficients are also in good agreement with other studies<sup>8</sup>. These give confidence that our dynamic modeling exercise is not in conflict with independent expectations.

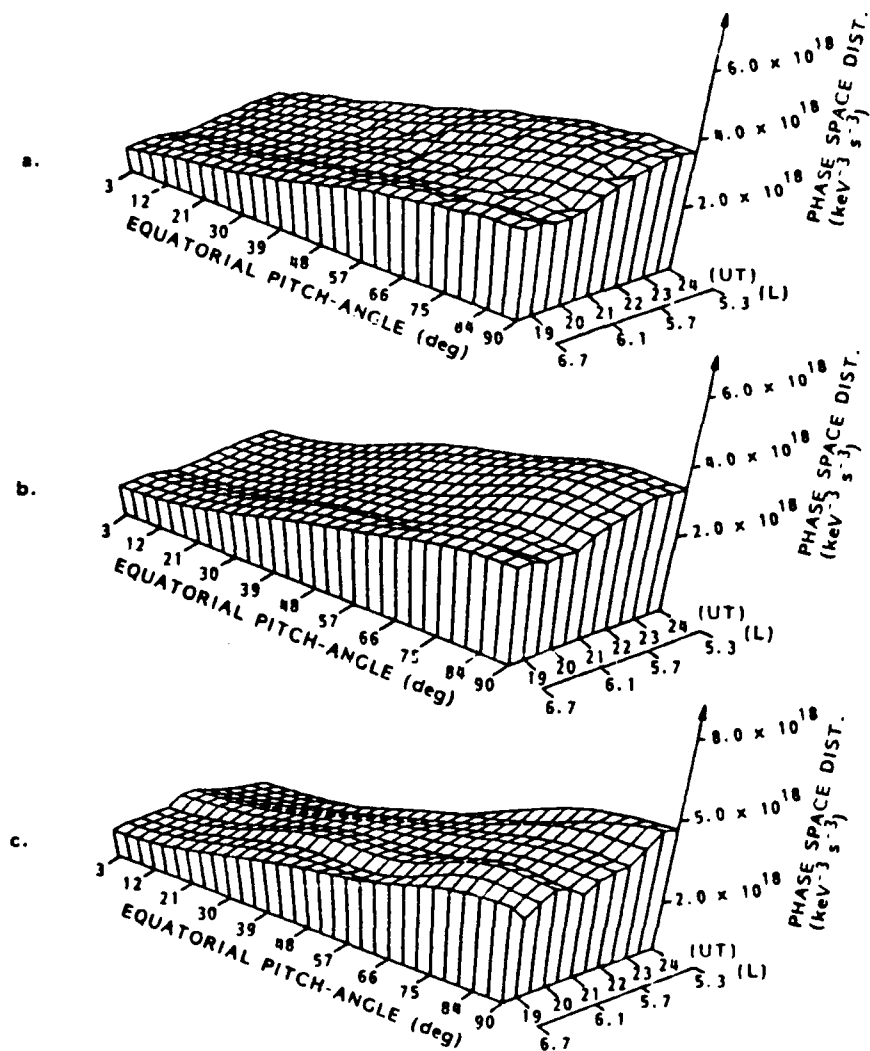


Figure 7. Three-dimensional presentation of the phase-space density of the data set and its reconstitutions for the 830 keV channel in pitch angle and space-time. Panel (a) shows the data set. Panel (b) is the reconstitution after fitting the pitch-angle eigenfunction decomposition. Panel (c) is the reconstitution with the bi-modal diffusion analysis but without the benefits of an iterative fitting procedure.



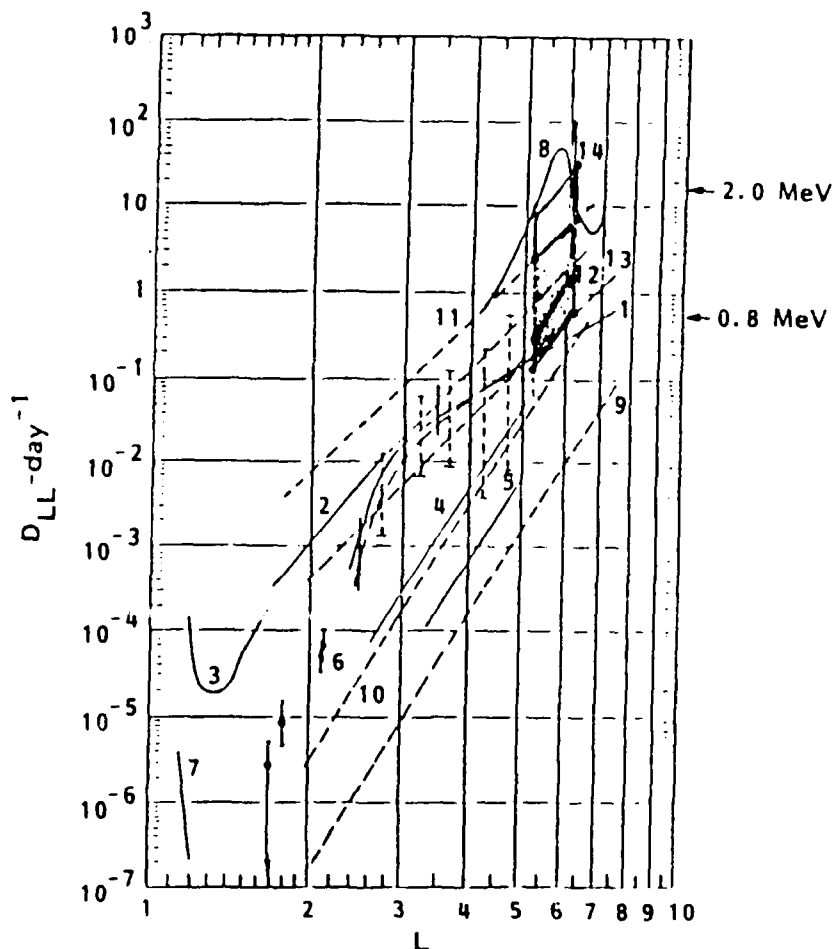


Figure 8. Comparison of the radial diffusion coefficient determined for the energy range 0.8-2.0 MeV (mottled area showing decreasing shading with increasing energy) with a previous compilation<sup>7</sup> which yields curve 1. Curves 2-8 are experimental<sup>8-14</sup>. Curves 9-14 are theoretical or semitheoretical<sup>15-19</sup>.

#### FURTHER ISSUES IN DYNAMIC MODELING

The test case exercise<sup>4</sup> summarized above may have resolved an important issue in radiation belt dynamic modeling, namely that multi-mode diffusion theory is a viable basis for dynamic modeling. However, there are several other issues that must be resolved before CRRES-like applications can be made. Here we shall discuss what we perceive to be the two most important issues.

(A) Flux mapping: The representational use of dynamic modeling must clear another hurdle before it can be made operational. The issue arises because of the multi-dimensional nature of phase space. Instead of basing the discussion on phase space mapping in the abstract, we can illustrate the issue with our familiar  $(L, t)$ -space. Armed with a diffusion theory representation tested on-trajectory, as in the exercise above, we can obtain fluxes at any given off-trajectory point by "mapping" the on-trajectory flux utilizing the representation. Without a general representation such as (2), the mapping is not unique if it is not based on a solution of the assumed diffusion physics. Figure 9 illustrates this mapping based on the assumed diffusion theory of the SCATHA test case above. The fluxes at Point 2, outside of the SCATHA trajectory, are uniquely specified by the diffusion parameters based on the fitted fluxes (dashed curves) on all points along the SCATHA trajectory between Points 1 and 3. In this regard, uniqueness is somewhat relative because it depends on the errors involved in specifying the on-trajectory diffusion parameters. A case of extreme contrast to Figure 9 is to imagine that no solution of diffusion theory was available as the basis for dynamic modeling. In such a case, Point 2 can still be mapped in  $(L, t)$

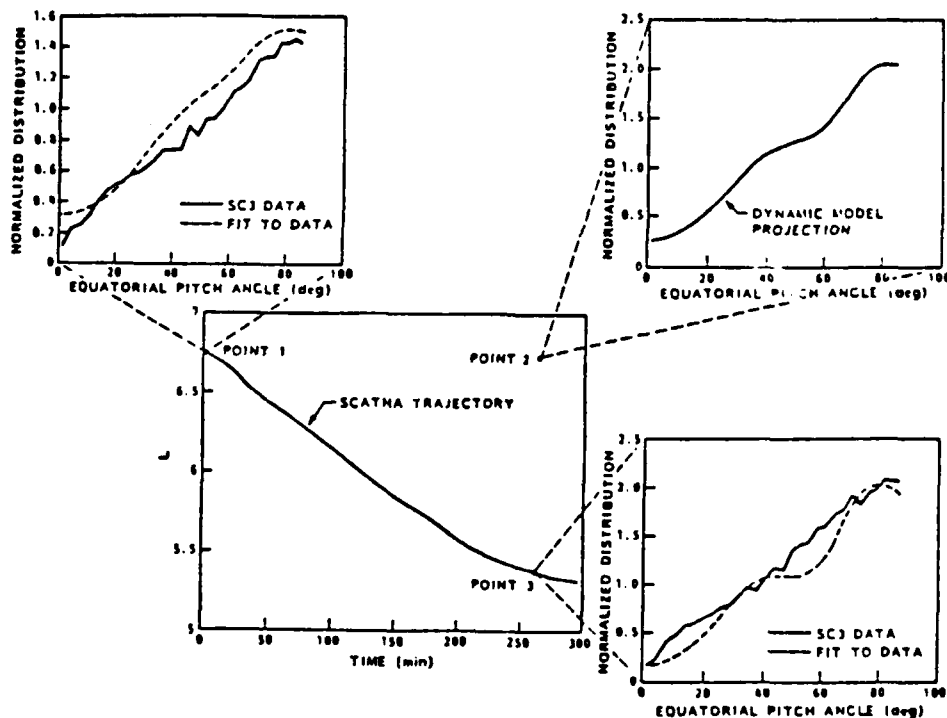


Figure 9. Illustration of flux mapping using a nominal dynamic model: our test case verified on the SCATHA trajectory. To the extent that the on-trajectories fits are good, the mapping by the diffusion representation (2) is "unique".

from Point 1 or Point 3 along  $t$  and  $L$  axes, respectively, by some phenomenological construct. Indeed, a large multitude of such mappings can be made to Point 2 from data on the trajectory. Since these individual mappings need not be consistent with each other, the uniqueness (within observational errors) of the predicted flux at Point 2 will be lost without the diffusion representation as a consistent basis for the mapping. Having a diffusion representation, however, does not free us from the fetters of non-uniqueness. Indeed, the errors incurred in finding the on-trajectory diffusion parameters operate in the same way as the inconsistent multiple mappings. Similar to these, the errors tend to vitiate the validity of a given representation for dynamical modeling. There are two necessary elements in ensuring "uniqueness" in data mapping. The first is to minimize errors in diffusion parameters for a given test diffusion representation. The second is to determine the most "unique" representation among several theoretical specifications of the diffusion physics. The first element is much easier to carry out than the second since the only way to insure that a diffusion representation is "unique" is to show that it works in practice. The theory of transport coefficients in the magnetosphere is presently not advanced enough to allow us to choose the "unique" physics on an a priori basis.

(B) Invariant Representations: An area of dynamic modeling not touched upon above is the validity of the implicit assumption in the test case that fluxes on the same  $L$ -shell are the same at the same time and energy. We know from Figure 2 that on the time scale of a day this is not true as effects of magnetic and electric shell-splitting, local injections and losses introduce a local time (azimuthal) dependence upon the data. This crucial aspect of radiation data is under current investigation on a case by case basis<sup>20</sup>; however, there is currently little work done on how these effects can be incorporated into a dynamic response model. A possible solution to this important problem may be to return to the most fundamental representation of radiation belt diffusion physics, i.e., that of diffusion in adiabatic invariant space rather than in its various reductions to configuration space<sup>4</sup>, such as in the above. The abstraction required to treat data at such a level is somewhat of a drawback; however, a test case attempt is needed to identify the detailed issues involved.

## CONCLUSIONS

Various elements required in radiation belt dynamic modeling have been discussed. It is seen that dynamic modeling differs fundamentally from radiation belt data analysis in that a theoretical representation of the on-trajectory data set is required to predict fluxes outside of the satellite orbit. The faithfulness of the projection depends on whether the representation is a good description of the physical diffusive processes seen in the on-trajectory data. We have summarized the results of a test case study<sup>4</sup> on such a tractable representation which yields results consistent with basically all other measurements in the moderately active outer electron radiation belt. The resolution of a number of important issues brought out by the examination of the test case awaits further work before operational dynamic models can be constructed.

## ACKNOWLEDGMENT

This work is supported by the Air Force Geophysics Laboratory under contract F19628-85-C-0073. It is a pleasure to thank Drs. S. Gussenhoven, M. Schulz, and G. Davidson for discussions on various aspects of this work. The SCATHA SC-3 payload and initial data analysis were sponsored by the Office of Naval Research under contract N00014-76-C-0444. The P78-2 SCATHA spacecraft is sponsored and operated by the USAF Space Test Program.

## REFERENCES

1. Reagan, J.B., R.W. Nightingale, E.E. Gaines, W.L. Imhof, and E.G. Stassinopoulos, *J. Spacecraft Rockets*, 18, 83, 1981.
2. Reagan, J.B., R.E. Meyerott, E.E. Gaines, R.W. Nightingale, P.C. Filbert, and W.L. Imhof, *IEEE Trans. Elect. Insul.*, EI-18, 354, 1983.
3. Davidson, G.T., P.C. Filbert, R.W. Nightingale, W.L. Imhof, J.B. Reagan and E.C. Whipple, *J. Geophys. Res.*, 93, Jan. 1988.
4. Chiu, Y.T., R.W. Nightingale and M.A. Rinaldi, *J. Geophys. Res.*, 93, accepted, 1988.
5. Schulz, M., and L.J. Lanzerotti, in *Physics and Chemistry in Space 7: Particle Diffusion in the Radiation Belts*, Springer, New York, 1974.
6. Walt, M., in *Particles and Fields in the Magnetosphere*, edited by B.M. McCormac, D. Reidel Hingham, Mass., 1970.
7. West, H.I., Jr., R.M. Burk, and G.T. Davidson, *J. Geophys. Res.*, 86, 2111, 1981.
8. Tomassian, A.D., T.A. Farley, and A.L. Vampola, *J. Geophys. Res.*, 77, 3441, 1972.
9. Farley, T.A., *J. Geophys. Res.*, 74, 1969.
10. Newkirk, L.L., and M. Walt, *J. Geophys. Res.*, 73, 1013, 1968a.
11. Fälthammar, C.G., in *Particles and Fields in the Magnetosphere*, edited by B.M. McCormac, p. 387, D. Reidel, Hingham, Mass., 1970.
12. Fälthammar, C.G., Walt, M., *J. Geophys. Res.*, 74, 4184, 1969.
13. Newkirk, L.L., and M. Walt, *J. Geophys. Res.*, 73, 7231, 1968b.
14. Kavanaugh, L.D., Jr., *J. Geophys. Res.*, 73, 2959, 1968.
15. Nakada, M.P., and G.D. Mead, *J. Geophys. Res.*, 70, 4777, 1965.
16. Tverskoy, B.A., *Geomagn. Aeron. Engl. Transl.*, 5, 617, 1965.
17. Birmingham, T.J., *J. Geophys. Res.*, 77, 2169, 1969.
18. Cornwall, J.M., *Radio Sci.*, 3, 740, 1968.
19. Holzworth, R.H., and F.S. Mozer, *J. Geophys. Res.*, 84, 2559, 1979.
20. Sibeck, D.G., R.W. McEntire, A.T.Y. Lui and R.E. Lopez, *J. Geophys. Res.*, 92, 13485, 1987.

# A NONLINEAR MODEL OF WAVE-PARTICLE INTERACTIONS IN THE TRAPPED RADIATION BELTS: AURORAL PULSATION SOLUTIONS

G. T. Davidson and Y. T. Chiu

Lockheed Palo Alto Research Laboratories, Palo Alto, CA 94304

**Abstract.** The interactions of waves and trapped electrons are described by a closed system of three nonlinear coupled equations. The model has applications to many aspects of wave-particle interactions in the magnetosphere. Nonlinear numerical solutions pertinent to auroral pulsations have been computed for realistic ranges of physical parameters. The results confirm that precipitation pulsations can be initiated by either an injection of energetic trapped particles or an increase in the plasma ionization density. Relaxation of the system results in cyclic phase trajectories about a (quasi equilibrium) point that is not located at the initial equilibrium point. That observation may explain the tendency of auroral pulsations to appear superimposed upon an increase in the general rate of electron precipitation. The results also imply that precipitation pulsations are most readily initiated by an encounter of drifting energetic electrons with a region of enhanced cold plasma density.

## 1. Introduction

The interaction between waves and trapped particles in the magnetosphere is a key problem in magnetospheric physics [Kennel and Petschek, 1966] whose basic elements are considered to be well understood. However, the complexity of a full treatment, based on first principles, of the diffusion of particles into the loss cone and the response of waves to particle diffusion has restricted quantitative studies to a handful of artificial situations [e.g., Inan et al., 1985]. Other modelling applications for which a full treatment is needed are: the dynamic response of the radiation belts to injections of cold plasma, kinetic modelling of the generator which supplies a steady stream of electrons to the loss cone opened up by a parallel potential drop in the eveningside aurora, and modelling of the morningside aurora. Among these, the morningside aurora problem is the best natural laboratory because it is generally believed to be a case of pristine wave-particle interactions, relatively unaffected by the complications of parallel electric fields. Given the difficulties of a first-principles treatment, an heuristic model, in which detailed processes are represented by simple empirical relations [e.g., Schulz, 1974], is appropriate because, once tested, it can then be packaged as a subsidiary unit to be incorporated into the more complex magnetospheric models mentioned above. This paper demonstrates that such an approach is feasible, for

it provides, for the first time, explanations to a number of nonlinear features of the morningside aurora.

Nonlinear processes are expected to govern the interactions of waves and particles in the outer regions of the magnetosphere. In the approach adopted here, the growth of VLF waves and the precipitation of trapped electrons is described by a system of nonlinear differential equations [Davidson and Chiu, 1986]. The system comprises three equations: an equation describing the evolution of the total electron flux  $I$  [Schulz, 1974],

$$\frac{dI}{dt} \approx -\frac{DI}{1+D\tau_s} + \frac{D_0 I_0}{1+D_0\tau_s}, \quad (1)$$

an equation describing the evolution of the wave intensity, as represented by the diffusion rate  $D$  [Schulz, 1974],

$$\frac{dD}{dt} \approx D \left( 2\gamma - \frac{1}{\tau_w} \right) + \frac{W}{\tau_s}, \quad (2)$$

and an equation describing the evolution of the pitch-angle anisotropy, as represented by the wave growth rate  $\gamma$  [Davidson and Chiu, 1986],

$$\frac{d\gamma}{dt} \approx \gamma \left[ \frac{\tau_s}{\tau_r} \frac{D_0 - D}{1 + D\tau_s} + \frac{1}{I} \frac{dI}{dt} \right]. \quad (3)$$

The subscript 0 denotes the values of the variable parameters at the equilibrium point, where the time derivatives vanish. The physical parameters are the strong diffusion lifetime,  $\tau_s$ , the wave loss or escape time,  $\tau_w$ , the wave source,  $W$ , and a response time,  $\tau_r$ , that is a measure of the time taken for pitch-angle diffusion to fill the loss cone. Since we are mainly interested in purely temporal behavior, the relative transverse motions of waves and particles are ignored.

The closure of the system through Equation (3) is of primary importance. For example, in the case of morningside aurora, the first two equations yield long period oscillatory solutions for large values of  $D$ ; but the third equation is critical to the formation of precipitation pulsations at the relatively short periods observed in pulsating aurorae [Davidson and Chiu, 1986]. While the existence of short-period pulsations was demonstrated by Davidson [1986] in the context of a two dimensional system, the two-dimensional model offers no clues to how the pulsations might be initiated. The characteristic periods resulting from a linear analysis have been discussed in a previous paper [Davidson and Chiu, 1986], the work described here is an extension of that study to obtain fully nonlinear solutions.

Copyright 1987 by the American Geophysical Union

Paper number 7L6638

0094-8276/87/0071-6638\$03.00

The U.S. Government is authorized to reproduce and sell this report. Permission for further reproduction by others must be obtained from the copyright owner.

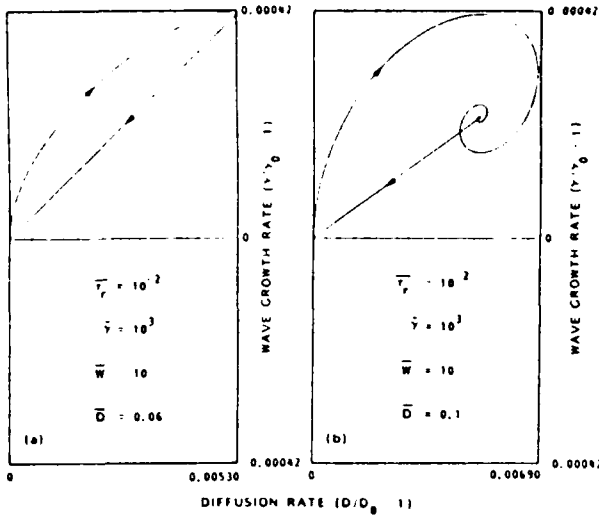


Fig. 1. Solutions of the nonlinear equations for equilibrium diffusion rates (dimensionless) of  $\bar{D} = 0.06$  and  $\bar{D} = 0.1$ , started with a displacement to  $D = 2D_0$ ;  $\gamma$ ,  $D$  projections.

In Section 2 we describe the results of numerical computations showing how the system responds to various assumed initial perturbations, and the assumptions upon which the computations were based. Our conclusions are discussed in Section 3.

## 2. Results Of Numerical Computations

It has been found useful to reduce the number of parameters by scaling the solutions to the strong diffusion lifetime [Davidson and Chiu, 1986]. The physical parameters are thus replaced by their dimensionless forms:

$$\bar{D} \equiv D_0 \tau_s / (1 + D_0 \tau_s), \quad (4a)$$

$$\bar{W} \equiv W \tau_s = D_0 \tau_s^2 (1/\tau_s - 2\gamma_0) \geq 0, \quad (4b)$$

$$\bar{\gamma} \equiv \gamma_0 \tau_s, \quad (4c)$$

$$\bar{\tau}_r \equiv \tau_r / \tau_s. \quad (4d)$$

The behavior of a system of differential equations depends strongly on the location of the phase-space attractors or critical points [Bender and Orszag, 1978]. The system of three first order equations (1–3) has three critical points. The nonlinear equations are similar to a well known set, the Lorenz system [Lorenz, 1963] that has a strange attractor. It is therefore worthwhile to inquire whether any of the critical points in the present system constitute a strange attractor.

There is a simple critical point at the equilibrium values of  $I^{(1)} = I_0$ ,  $D^{(1)} = D_0$ , and  $\gamma^{(1)} = \gamma_0$ . All the phase trajectories eventually spiral inward toward that point. The most interesting solutions in that region are those for which the linear analysis yields a characteristic frequency,  $\Omega$ , having a real part. Solutions for which  $|\Omega| \ll 1/\tau_s$  can be ignored because they will not lead to perceptible effects within realistic time scales. The linearized solutions for  $\Omega$  at small values of  $\bar{D}$  have two branches with purely imaginary  $\Omega$ . The upper branch gives for  $\bar{\Omega} = \Omega \tau_s$ ,

$$\bar{\Omega} = \text{Im} \bar{\Omega}_1 \sim \bar{W} / \bar{D}; \quad (5)$$

the lower branch gives

$$\bar{\Omega} = \text{Im} \bar{\Omega}_2 \sim 2\bar{\gamma} \bar{D}^2 / \bar{W} \bar{\tau}_r. \quad (6)$$

The numerical designation of the roots of  $\Omega$  is the same as in Davidson and Chiu [1986], in order of increasing  $|\bar{\Omega}|$ .

Cyclic solutions are found above some critical diffusion rate,  $\bar{D} = D^*$ . Above  $D^*$  complex roots appear in the characteristic equation, whose real and imaginary parts are

$$\bar{\Omega}_{2,3} \sim \pm \sqrt{2\bar{\gamma} \bar{D} / \bar{\tau}_r} + i \bar{W} / 2\bar{D}. \quad (7)$$

The transition between the two types of solutions occurs where the four roots meet, or, more precisely, at

$$D^* \approx \bar{W}^{2/3} \bar{\tau}_r^{1/3} / 2\bar{\gamma}^{1/3}. \quad (8)$$

We concentrate on parameter regimes appropriate to the outer trapping regions and the morningside auroral regions. In the vicinity of  $D^*$ , the behavior becomes more regular toward either higher or lower values of  $\bar{D}$ . For the values of the parameters adopted by Davidson and Chiu [1986],  $\tau_s \approx 240$  s,  $\bar{\tau}_r \approx 10^{-2}$ ,  $\bar{\gamma} \approx 10^3$ ,  $\bar{W} \approx 1-100$ , the resulting pulsation period at  $D^*$  is about 1.5–7 s, which agrees well with the observed periods of pulsating aurorae [Johnstone, 1979, 1983].

One of the other critical points is physically uninteresting, because it corresponds to a vanishing total flux,  $I = 0$ . The third critical point, at  $I^{(3)} = I_0$ ,  $D^{(3)} = D_0[2\bar{\gamma} \bar{D} + 1]$ ,  $\gamma^{(3)} = 0$  is not a simple attractor. Although there is a possibility that an interaction between the first and third critical points could result in a strange attractor, the phase space trajectories for realistic sim-

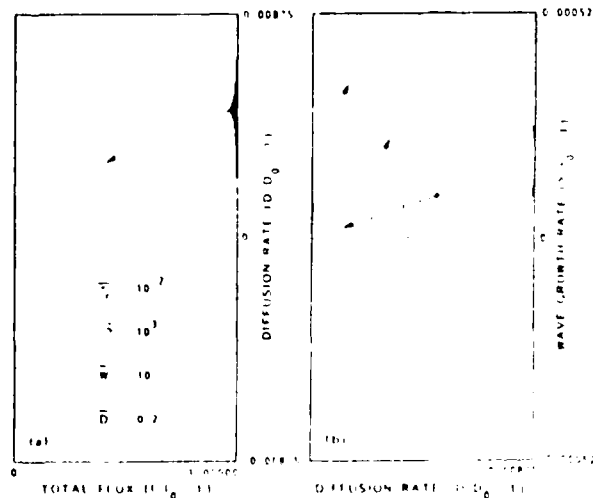


Fig. 2. Solution of the nonlinear equations for an equilibrium diffusion rate (dimensionless) of  $\bar{D} = 0.2$ , started with a displacement to  $D = 1D_0$ .

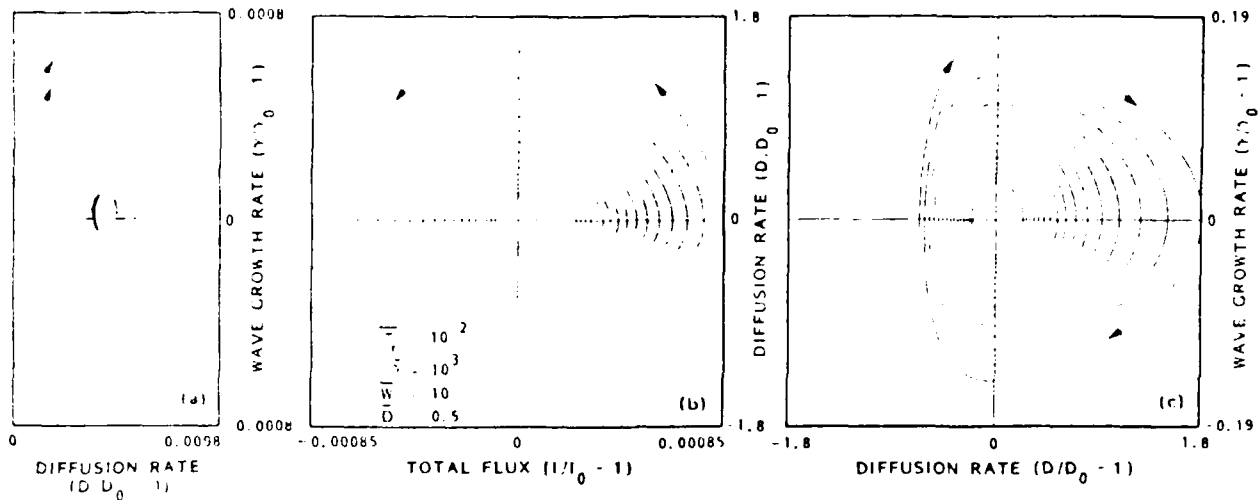


Fig. 3. Solution of the nonlinear equations for an equilibrium diffusion rate (dimensionless) of  $\bar{D} = 0.5$ , started with a displacement to  $\gamma = 1.01\gamma_0$  (panels b and c). Panel a shows a case with the same physical parameters, but starting conditions similar to Figure 2. The innermost loops of the spirals are omitted for clarity; the trajectories all eventually decay back to the origin.

ulations in the parameter regimes appropriate to morningside aurorae do not approach the third critical point closely enough that they could be significantly influenced by it.

Examples of the numerical results are presented in Figures 1 through 3. They show projections of the phase trajectories on the  $(I, D)$  and  $(D, \gamma)$  planes. (The figures are plotted to dimensionless scales to emphasize the universality of the solutions.) The figures were constructed for the parameters  $\tau_e = 10^{-2}$ ,  $\bar{\gamma} = 10^3$ ,  $\bar{W} = 10$ . Those values are physically realistic, and were chosen because they provide the most easily visualized trajectories. Figures 1, and 2 depict cases that start with a displacement along the  $I$  axis. An initial displacement of  $I$  is equivalent to a sudden increase in the total energetic trapped particle intensity. The  $(I, D)$  projections are not presented in Figure 1 because they are characterized by a rapid rise followed by a nearly monotonic decay, similar to the trajectory in Figure 2. Three cases are shown in order of increasing values of  $\bar{D}$ . The trajectories are qualitatively similar to Figure 2 for larger values of  $\bar{D}$ . At the approach to strong diffusion,  $\bar{D} \sim 1$ , the spirals become too tightly wrapped to reproduce on the scale of the figures.

Figure 3, panels b and c, begins with an initial displacement confined to the  $(D, \gamma)$  plane. Figure 3 is intended to represent a sudden increase in the plasma density. The wave growth rate is proportional to the total plasma density [Kennel and Petschek, 1966], so such a perturbation corresponds to a sudden change in  $\gamma$ , from an equilibrium state having a relatively low value of  $\gamma$  to a new state having an increased value of  $\gamma$ . Because the equilibrium solutions of (2) involve both  $D$  and  $\gamma$ , the initial displacement must be related to an initial value of  $D$  consistent with the earlier equilibrium state. Thus, for a constant  $W$ , the value of  $D_0$  in each state must be inversely proportional to  $(2\gamma_0 - 1/\tau_w)$ . For comparison with

the results of Figures 1 and 2, panel 3a shows the phase trajectory that would result from an initial displacement in  $I$  for the same physical parameters as panels b and c. Combinations of the two types of initial perturbation yield trajectories that resemble the  $(I, D)$  projection of Figure 2 and the  $(D, \gamma)$  projection of Figure 3.

### 3. Conclusions

The results of numerical solutions of the nonlinear differential equations, (1 — 3), indicate general classes of behavior of waves and trapped electrons expected in the auroral regions and outer trapping regions. They confirm that cyclic solutions exist, and that cyclic solutions may follow either an increase in the trapped electron density or an increase in the cold plasma density. Such solutions reproduce the gross features of auroral pulsations insofar as the electron precipitation rate is a reflection of the diffusion rate,  $D$ .

Several interesting aspects of the detailed solutions could not have been predicted from the linear analysis. For diffusion rates higher than  $D^*$  an initial perturbation in the total trapped flux is followed by spiral orbits about a point that is displaced from  $(I_0, D_0, \gamma_0)$ . The periods of those orbits are similar to the periods derived from the linear analysis; the periods do not strongly depend on the amplitude of the oscillations. The examples of Figure 1, with few or no complete pulsation cycles, are probably appropriate to the radiation belts, where isolated precipitation "bursts" are occasionally seen [Trefall and Williams, 1979]. As the diffusion rate is further increased, in Figure 2, the damping rate is diminished and the number of loops increases. The spiral phase trajectories do not enclose the stable critical point, but tend to approach a point that is located at larger values of  $D$  and  $\gamma$ . The effect of the displacement of the "center" of the spirals is to shift the average diffusion rate so that the instantaneous

diffusion rate remains greater than the equilibrium value. For morningside aurora that result is consistent with the observation by Davidson and Sears [1980] that auroral pulsations are superimposed upon a general elevation of the emission intensity resulting from electron precipitation; the "background" intensity tends to rise before the pulsations begin. Such a finding is important, because it confirms the need for a three-parameter system (Equations 1 — 3), explicitly including the total trapped flux as a variable.

A comparison of Figures 3a and 3c reveals that the amplitude of the pulsation amplitude, as measured by the precipitation rate or  $D$ , is most sensitive to the total plasma density. While it is difficult to speculate on what constitutes a "typical" initial perturbation, the simulations in which the initial total flux is increased by a factor of 2 seem reasonable. The initial perturbation of Figure 3, on the other hand, corresponds to a mere 1% increase in the plasma density or  $\gamma$ . The implication, applicable to a broad range of physical parameters, is that an abrupt increase in the plasma density experienced by drifting electrons is more effective in initiating precipitation pulsations than an increase in the total intensity of energetic electrons.

The sensitivity of the pulsation amplitude to a sudden increase in  $\gamma_0$  raises an interesting question: whether a compression of the magnetic field might initiate pulsations, as suggested by Coroniti and Kennel [1970]. While a detailed treatment of that issue is beyond the scope of the present work, the results discussed above indicate that such a mechanism might be very effective. Any perturbation in the initial value of  $\gamma_0$  would serve to initiate pulsations.

The picture implied by the above results for pulsating aurorae, is that they follow an injection of energetic trapped electrons in the outer trapping regions. Repetitive pulsations turn on when the drifting trapped electrons encounter a region of enhanced cold plasma density. These conclusions follow from a closed nonlinear model that does not depend on the specification of wave modes; predictions from the model are fully general and can be applied to the various cases mentioned in the introduction. The nature of the detailed wave modes enters only in the determination of the physical parameters (4).

A strange attractor was not found for simulations in the time domain alone. We leave open the question whether a strange attractor may occur for conditions appropriate to spatial-temporal structures. Although our model explains the semi-regular temporal structure of pulsating aurorae, the apparently random spatial structure remains a major unsolved problem.

**Acknowledgements.** This work was supported by NSF Grant ATM-8506843, AFGL/F19628-85-0073, and by the

Lockheed Independent Research Program. We are grateful to one of the referees for pointing out the possible effect of a compression of the magnetic field.

## References

- Bender, C. M., and S. A. Orszag, *Advanced Mathematical Methods for Scientists and Engineers*, McGraw-Hill, New York, pp185ff, 1978
- Coroniti, F. V., and C. F. Kennel, Auroral micropulsation instability, *J. Geophys. Res.* 75, 1863, 1970
- Davidson, G. T., Self-modulated VLF wave-electron interactions in the magnetosphere: A cause of auroral pulsations, *J. Geophys. Res.* 84, 6517, 1979b.
- Davidson, G. T., Pitch-angle diffusion in morningside aurora: 2. The formation of repetitive auroral pulsations, *J. Geophys. Res.* 91, 4429, 1986
- Davidson, G. T., and Y. T. Chiu, A closed nonlinear model of wave-particle interactions in the outer trapping and morningside auroral regions, *J. Geophys. Res.* 91, 13 705, 1986
- Davidson, G. T., and R. D. Sears, Pulsating aurora: Evidence for flux limiting, *Geophys. Res. Lett.* 7, 185, 1980
- Davis, H. T., *Introduction to Nonlinear Differential and Integral Equations*, Dover, New York, 1962
- Inan, U. S., H. C. Chang, R. A. Helliwell, W. L. Imhof, J. B. Reagan, and M. Walt, Precipitation of radiation belt electrons by man-made waves: a comparison between theory and measurement, *J. Geophys. Res.* 90, 359, 1985
- Johnstone, A. D., Pulsating aurora, *Nature*, 274, 119, 1978
- Johnstone, A. D., The mechanism of pulsating aurora, *Annales Geophysicae*, 1, 397, 1983
- Kennel, C. F. and H. E. Petschek, Limit on stably trapped particle fluxes, *J. Geophys. Res.* 71, 1, 1966
- Lorenz, E. N., Deterministic nonperiodic flow, *J. Atmospheric Sciences*, 20, 134, 1963
- Schulz, M., Particle saturation of the outer zone: A nonlinear model, *Astrophys. Space. Sci.* 29, 233, 1974
- Trefall, H. and D. J. Williams, Time structure of post-midnight energetic electron precipitation and the limit of stable trapping, *J. Geophys. Res.* 84, 2723, 1979
- G. T. Davidson and Y. T. Chiu, Lockheed Palo Alto Research Laboratories, Space Sciences Laboratory, D91-20, B255, Palo Alto, CA 94304

(Received August 3, 1987;  
Revised September 14, 1987;  
Accepted September 15, 1987.)



## **Towards Dynamic Modeling of the Outer Electron Radiation Belt**

Y. T. Chiu, M. A. Rinaldi, W. E. Francis and R. W. Nightingale

Lockheed Palo Alto Research Laboratory, California

### **Abstract**

We show that the general solution of a simple form of the simultaneous bimodal (radial and pitch-angle) diffusion equation can represent the SCATHA outer belt electron distribution to a high degree of accuracy for periods up to more than 10 hours. The data representation requires diffusion parameters that are in agreement with all previous experimental and theoretical determinations of such diffusion coefficients. Such a representation satisfies the basic requirements towards the dynamic modeling of the outer electron radiation belts for  $L < 7$  at quiet and moderate geomagnetic conditions. For  $L \sim 7$  the representation has difficulties with "butterfly" distributions that may signify energetic electron encounters with the magnetopause. It is demonstrated with a typical example of computer simulation of electron encounters with the magnetopause that the effects of the encounter may be highly anisotropic in configuration or in invariant space.

### **1. Introduction**

The variability of the electron fluxes in the outer radiation belt ( $L \geq 5$ ) is not only a matter of concern for space activities in the region but is also a major challenge to understanding the macroscopic consequences of wave-particle interactions in the magnetosphere. Theories on the generation of plasma wave disturbances and on the scattering of individual electrons by such waves exist; however, a systematic test of the integration of such microscopic effects into a diffusion description of the global dynamics of the outer electron radiation belt has yet to be attempted. To be sure, episodic work [e.g., Reagan et al., 1981; West et al., 1981; Sibeck et al., 1987] have established the plausibility of various aspects of the diffusion description in some regions of space. On the global scale, even a description of the observational data organized according to the generic concepts of diffusion theory does not presently exist. In anticipation to the upcoming Air Force-NASA Combined Release and Radiation Effects Satellite (CRRES), we have initiated an attempt to determine if diffusion theory can provide an adequately quantitative and computationally efficient description of the behavior of the outer electron belt as observed by the SCATHA satellite [Chiu et al., 1988; hereafter referred to as Paper I]. This attempt was not directed towards the microphysics of wave-particle interaction theory; rather, it addressed a much more primitive question: Were the observational data organizable in terms of simultaneous

pitch-angle and radial diffusion theory, even in the restrictive context of piece-wise slices of space-time as in satellite observations?

This work and the preceeding effort in Paper I are focused upon this central issue of whether a computationally efficient dynamic model of the outer electron belt can be constructed in principle, or not. The results of Paper I were encouraging in that solutions of simultaneous bimodal (pitch-angle and radial) diffusion theory were shown to have the potential to provide an efficient description of a SCATHA outer-belt electron data set over the phase space volume:  $(5.3 \leq L \leq 6.7; \Delta t = 5 \text{ hrs.}; 200 \text{ keV} \leq E \leq 2000 \text{ keV}; \alpha_c \leq \alpha \leq 90^\circ)$ , where  $\alpha$  is the pitch-angle,  $\alpha_c$  is the edge of the loss cone and  $E$  is the energy. The description was achieved in essentially the initial pass without a systematic fitting procedure. The diffusion parameters required happened to cluster around values in agreement with those obtained by other workers. These initial results established plausibility for the approach. However, to go beyond plausibility towards dynamic modeling of the outer electron belt, a number of deficiencies of Paper I need to be addressed. Among these, at least three major issues require attention if the bimodal diffusion approach to dynamic modeling is to be pursued.

First, we must establish a systematic iterative procedure to achieve a fit of the data consistent with all the constraints of the solution. This requirement involves not only specification of the accuracy of the fit in four-dimensional phase space but also satisfaction of diffusion parameter constraints imposed by bimodal theory. Second, the form of the bimodal diffusion theory used was computationally efficient but its validity was recognized to be restricted to a sufficiently thin slice of  $L$ -space [Walt, 1970]. Such a property is not incompatible with dynamic modeling with a satellite data base since satellite data are necessarily restricted in  $(L, t)$  space. Nevertheless, it is crucial to determine the observational extent of  $L$ -space over which the version of bimodal diffusion theory is valid. Third and most important, the degree of uniqueness of the data representation must be established since dynamic modeling implies the projection of electron fluxes from measurements on a satellite trajectory to other regions of phase space where direct measurements are not available. Note that the solution representation of the theory is necessarily unique everywhere if the on-trajectory specification is unique. However, the data fit to the solution is over a trajectory on which  $L$  and  $t$  are mixed; therefore, the on-trajectory specification is not necessarily unique insofar as the separation of  $L$  and  $t$  effects are concerned. In order to insure that our iterative procedure for untangling  $L$  and  $t$  effects does not alias

the projection to other regions of space-time, we must at least demonstrate that our data representation yields flux projections independent of the projection path.

In this paper, we shall address the above three issues. We shall demonstrate that simultaneous bimodal diffusion theory is an efficient representation of SCATHA outer-belt electron data in the configuration space range ( $5 \leq L \leq 7$ ;  $\Delta t \leq 10$  hrs.) for Day 165, 1980 and Day 110, 1979. Iterative procedures have been devised to improve the fit and to satisfy diffusion parameter constraints that were not enforced in Paper I. The result is a reduction of parameters (by  $\sim 15\%$ ) to achieve better fits over a much larger data base (by  $\sim 100\%$ ). We are also able to demonstrate that fit errors do not impact the uniqueness of off-trajectory flux projections based on the solution representation.

## 2. Constraints on Bimodal Diffusion Representation

In order to organize the discussion in this paper, we briefly summarize the salient features of simultaneous bimodal diffusion theory [Walt, 1970; Fälthammar and Walt, 1969; Roederer and Schulz, 1969] and its specific form developed for efficient data representation in Paper I.

By introducing an approximate invariant valid over a sufficiently thin slice of  $L$ -space, Walt [1970] showed that the bimodal diffusion equation can be formulated in configuration and pitch-angle coordinates  $(L, x, t)$  where  $x \equiv \cos \alpha$ . Such a formulation is particularly convenient for data applications because the coordinates are simple, although it needs to be emphasized that its validity is restricted to slices in  $L$ -space, over which energy gained or lost from radial diffusion does not impact Walt's invariant. In Paper I, we showed that if the pitch-angle and radial diffusion coefficients,  $D_{xx}$  and  $D_{LL}$ , respectively, take on certain generic forms

$$\begin{aligned} D_{xx} &\equiv D_{xx}(E) \\ D_{LL} &\equiv \xi(E)L^\mu \end{aligned} \tag{1}$$

where  $\mu$  is a given constant, then the general solution to the bimodal diffusion equation can be expanded in terms of eigenfunctions of various Bessel forms. This convenient property forms our basic principle to characterize the state of the outer electron belt in a piecewise-continuous fashion in terms of a data base measured along a satellite trajectory  $L(t)$ .

The general solution consists of the linear sum of three modal expansions: (1) single-mode pitch-angle diffusion, (2) single-mode radial diffusion and (3) simultaneous bi-modal

diffusion. Using the device of the Kronecker delta  $\delta_{n0}$ , the three modal expansions can be written in terms of a single eigenfunction expansion

$$f = \sum_{n=0}^{\infty} \left[ \delta_{n0} + (1 - \delta_{n0}) \frac{\sqrt{2}}{x_c} \cdot \frac{J_0(k_n x/x_c)}{J_1(k_n)} \right] \left( c_n(1 - \delta_{n0}) e^{t/\tau_n} + e^{t/t_n} [a_n Y_n(L) + b_n Z_n(L)] \right) \quad (2)$$

where  $k_n$  is the  $n^{th}$  zero of the Bessel function  $J_0$  and  $x_c = \cos \alpha_c$ . The parameters and functions are defined as follows:

$$\epsilon \equiv 3(1 - \frac{\nu}{2})/(\mu - 2)$$

$$\sigma \equiv -\frac{\mu}{2} - \frac{1}{2} + \frac{3}{4}\nu \quad (3)$$

$$\lambda \equiv \frac{\mu}{2} - 1$$

$$Y_n(L) = L^\sigma \cdot [J_{1+\epsilon}(|\beta_n|/L^\lambda)]_> \cdot [I_{1+\epsilon}(|\beta_n|/L^\lambda)]_< \quad (4)$$

$$Z_n(L) = L^\sigma \cdot [N_{1+\epsilon}(|\beta_n|/L^\lambda)]_> \cdot [K_{1+\epsilon}(|\beta_n|/L^\lambda)]_< \quad (5)$$

$J$  is the regular Bessel function,  $I$  and  $K$  are the modified Bessel functions, and  $N$  is the Neumann function. The usual notation  $[g]_>$  is defined in this case by

$$[g]_> = g \quad \text{if} \quad t_n > 0 \quad (6)$$

$$[g]_> = 1 \quad \text{if} \quad t_n < 0$$

and analogously for  $[g]_<$ . The separation constants  $(t_n, \beta_n)$  and parameters of the solution are related by the algebraic relations

$$t_n^{-1} = (1 - \delta_{n0})\tau_n^{-1} - \xi\beta_n^2\lambda^2 \quad (7)$$

$$\tau_n^{-1} \equiv -D_{zz} k_n^2/x_c^2 \quad (8)$$

The parameter value  $\lambda = 4$  (i.e.,  $\mu = 10$ ) is chosen to conform with the consensual  $L$ -dependence of the radial diffusion coefficient [Schulz and Lanzerotti, 1974]. From Paper I the parameter  $\nu$  is set to 2 (i.e.,  $\epsilon = 0$ ) for ease of computing the Bessel functions. Other values of  $\nu$  are easily accommodated at the expense of computational speed. Our work so far has demonstrated the economy of using  $\nu = 2$ , but further refinements can be readily

accommodated in our procedure. Equation (7) will be referred to as the separation equation because the entire separable diffusion differential equation is reduced by the eigenfunction expansion into this constraint on the diffusion parameters. It is seen from (8) that the single pitch-angle mode time constants are negative as expected, since single-mode pitch-angle diffusion always leads to decay. For radial diffusion, however, the time constants  $t_n$  can be either positive or negative over a finite time interval. This is due to the fact that the phase space density in the finite  $L$  domain can rise or fall in time in response to particle transport into and out of the adjacent volumes. With the sign of each  $t_n$  not predetermined, the separation constant  $\beta_n^2$  can be positive or negative. This is the origin of the  $(J, I)$  and  $(N, K)$  options of (4) and (5).

When a data set is fitted to the general solution expansion exclusive of the separation equation (7), the electron distribution function is characterized by the set of parameters  $(a_n, b_n, c_n, t_n, \tau_n, \beta_n)$ . In Paper I it was found that five orders of eigenfunctions ( $n = 0-4$ ) per energy channel, i.e., 30 parameters per energy channel, are sufficient to characterize a data base of 5040 data points. For this paper, we include the effects of the separation equation (7) in constraining the diffusion parameters  $(\tau_n, \beta_n, \xi)$ . Note that the diffusion parameter  $\xi$  is independent of order  $n$ , whereas the others are order dependent. In Paper I,  $\tau_n$  and  $\beta_n$  were independently derived from the fit and (7) was not imposed. No iterations were made and a value of  $\xi$  was determined for each order from (7), i.e. a set of  $\xi_n$ . It was found that these order-dependent values of  $\xi$  clustered closely around those determined by other workers, an indication that the representation is reasonable. Here we use the constraint (7) as the focus for an iterative fitting scheme in determining the best order-independent value of  $\xi$ . Since (7) is imposed,  $(\tau_n, \xi)$  and  $\beta_n$  are no longer independent, thus the number of required parameters per energy channel is reduced by 4 in this work. The iteration also improves the fit to the data set.

### 3. Iterative Fit of Data Sets

The process of fitting a data set to the representation begins with decomposing the electron distribution functions into pitch-angle eigenfunctions and their amplitudes. We have demonstrated in Paper I that this procedure is highly accurate. We shall focus our discussion upon the decomposition of the pitch-angle amplitudes into eigenfunction expansions in  $L$ .

We have devised a nonlinear fitting procedure keyed to the iterative determination of

the order-independent radial diffusion parameter  $\xi$  in the separation equation (7). In the first pass, the procedure described in Paper I is applied and the separation equation (7) is solved for each order, resulting in a set of order-dependent parameters  $\xi_n$ . Iterations begin with the choice of an interim mean value  $\xi = \langle \xi_n \rangle$  where the averaging is weighed by the eigenfunction amplitudes  $(a_n, b_n)$ . The interim value  $\xi$  is enforced in (7) to determine new values of the parameters  $(\tau_n, \beta_n)$  in a new fit. With the new parameters, a new set of  $\xi_n$  is determined by solving (7) exactly and another iteration cycle begins. The iterative procedure continues until the residual error in the equality between the left and right hand side of (7) can no longer be improved upon. The final value of  $\xi$  is taken to be the fit value of the diffusion parameter. This is a nonlinear iterative procedure; therefore, there is no a priori guarantee that it is convergent. In practice, it converges because the set of  $\xi_n$  in the first pass is closely clustered to begin with. Figure 1 shows an example of the degree to which the constraint (7) is obeyed by the initial and final iterations of the procedure.

The iterative scheme has been applied to  $\sim 4$  hours of SCATHA electron belt data for Day 165, 1980 and to  $\sim 9$  hours of data for Day 110, 1979. Figures 2 and 3 show three-dimensional plots of the data and the fit reconstructions for these two days, respectively. It should be noted that reconstruction errors for both days are primarily concentrated in the high- $L$  and  $\alpha \sim 90^\circ$  region. We found that this region is rich in "butterfly" distributions [Sibeck et al., 1987]. These will be discussed in more detail in Section 5 below. Figures 4 and 5 show the distributions of the fit errors for each data point in the initial and final passes of the iterations for the two days, respectively. The data points associated with the large-error tail of the error distributions, less than 1000 data points in each data set, are again related to "butterfly" distributions, although a substantial portion of the large fit errors are also contributed to by some noisy data in the data base. Unsmoothed raw data is used to tally the percentage error in these figures. Figure 6 shows the comparison of radial diffusion coefficients determined in this work with all other known observational and theoretical determinations. The mottled band of  $D_{LL}$  values in the figure corresponds to this work. The spread of the band is due to energy dependence of the diffusion coefficient. The larger cross-hatched band of  $D_{LL}$  values was determined in Paper I and is due not only to the spread of energy channels but also primarily to the dependence of  $\xi$  on order. It is seen that our enforcement of (7) allows for a much more precise determination of the radial diffusion coefficient. Energy dependence is not always addressed in other work.

#### 4. Off-Trajectory Projection of Electron Distributions

For a data representation scheme to qualify as a dynamic modeling scheme, it must demonstrate the ability to uniquely predict (or obtain by projection), the off-trajectory electron distributions, from a set of on-trajectory electron distributions. The use of the general solution to bimodal diffusion theory yields a naturally unique off-trajectory projection within the limitations of the assumed physics. Whether the assumed physics correctly describe the actual processes prevailing in the particular region of the outer electron belt is a separate issue to be discussed in Section 5. Within the scope of diffusion theory, if the on-trajectory representation is exact, the projection to any off-trajectory point is also independent of path because the solution is uniquely specified everywhere that it is valid. Since the on-trajectory representation is not given a priori (but given as a fit based on a data set that mixes  $L$  and  $t$ ), an important question arises: Can the fit errors due to aliasing  $L$  and  $t$  destroy the uniqueness of the projection by making it path dependent?

We have investigated this problem of projection consistency (or path dependence) for our representation by projecting to an off-trajectory point from two well-separated on-trajectory points: one having the same  $L$  and the other having the same  $t$  as the off-trajectory point. The projection paths are thus along the  $t$  and the  $L$  axes, respectively. Figure 7 shows the results of such a uniqueness test for Day 110, 1979. The projection in our representation is indeed path independent. This test clears a hurdle for using the bimodal diffusion solution for outer-belt dynamic modeling, since it demonstrates that uniqueness is not destroyed by the fit errors. It must be noted that this is only an internal consistency test, not a validity test that diffusion theory correctly describes the prevailing physics of the outer belt. A validity test requires data sets from more than one satellite. A valid dynamic model should be able to "predict" one satellite data set from the solution fit to the other satellite's data set, and vice versa.

## 5. Effects of Drastic Violations of the Third Invariant

We have repeatedly stated from the outset that the validity of the form of simultaneous bimodal diffusion theory chosen for this study is very severely limited, particularly in regions of the outer electron belt at  $L \geq 7$ . The first limitation is that Walt's invariant [1970] remains so only within a limited slice of  $L$ . This property of piecewise invariance is exploited as much as possible in our application in the region  $5 \leq L < 7$ , but there must be constraints to the exploitation. In the stable regions of the outer belt at  $L < 5$ , we do not see any reason why the application of the representation will be different from that shown here, although it is necessary to test it with another satellite data set because SCATHA

does not cover that region. For  $L > 6$ , we sometimes encounter difficulties with "butterfly" pitch-angle distributions. We recognized at the outset that an important factor limiting the validity of the representation is the effects of third invariant violations that may or may not be describable in terms of diffusion. Such effects can be due to severe magnetic or electric shell splitting or to encounters with the magnetopause. In such encounters, the electron distribution on a given  $L$ -shell can be changed catastrophically. Since such third-invariant violating effects are deemed to be most effective at the equatorial region, it is usually assumed that their signature is a loss to the drift shell of equatorially mirroring particles (those with  $\sim 90^\circ$  pitch angle) leading to the so-called "butterfly" distributions [West, 1979; Sibeck et al., 1987]. Such an expectation seems reasonable as far as the pitch-angle distribution is concerned; however, the transport in the configuration part of phase space is a matter that has not been investigated beyond the expectation that the third invariant is drastically violated.

Since our representation is not expected to be valid for describing such drastic violations of the third invariant, the inclusion of such distribution functions in our data base incurs large errors in the representation. These constitute a part of the large-error tail of the error distributions shown in Figures 4 and 5. The successful treatment of the "butterfly" events constitutes the remaining hurdle towards dynamic outer electron belt modeling. The solution to this important problem is beyond the scope of this brief report but we shall address some salient points here. An initial reaction to the failure of the simple form of radial diffusion used is to assume that another form of radial diffusion, perhaps in third invariant coordinates, may be a better description of the physics involved in "butterflies". Such may indeed be the case, but a more primitive question needs to be considered first: Are encounters involving drastic violations of the third invariant necessarily diffusive in the configuration part of phase space?

In order to answer this and related questions, we have initiated computer simulations of energetic electron encounters with magnetopauses in realistic geomagnetic field models. Figure 8 shows the encounter of a 10 MeV electron with a non-turbulent paraboloidal magnetopause [Stern, 1985] in the configuration of a Tsyganenko [1987] field model. The magnetic field magnitude drops by 30 nT across the magnetopause at the sub-solar point. The field configuration outside merges smoothly into a uniform southward interplanetary configuration. Figure 8 shows the projection of the three-dimensional electron trajectory onto the equatorial plane. The important feature of this magnetopause encounter is that



the electron executes trapped bounce motion occasionally on inward field lines and, in between bounces, it skips along the equatorial regions sometimes inward and sometimes outward of the magnetopause boundary; i.e., there is little evidence of scatter perpendicular to the boundary. The electron trajectory shown on Figure 8 is one example in a Monte Carlo simulation of encounters with a smooth magnetopause in which all scatterings seem to be directed along the boundary, even though individual trajectories differ in the amount of residence time inside or outside of the boundary surface, depending on their pitch angle and gyration phases as they encounter the boundary. Such anisotropic scatterings in encounters with the magnetopause can hardly be described in simple terms of isotropic diffusion, in invariant coordinates or otherwise. The encounter effects are somewhat more isotropic in configuration space if the magnetopause is not smooth, but the anisotropy will remain since the average magnetic field is non-zero both inside and outside. Clearly the equatorial skippings are likely to lead to enhanced pitch-angle diffusion; however, pitch-angle diffusion cannot produce a "butterfly" population. On the other hand, skippings along the equatorial magnetopause, which cuts through many  $L$ -shells, clearly constitute transport in  $L$  and, consequently, violation of the third invariant, as expected. The loss to a given  $L$ -shell of electrons, which skip to a different  $L$ -shell along the equatorial magnetopause, will clearly produce a "butterfly" distribution. The surprising feature of the simulation is that this transport in  $L$  is anisotropic in configuration space and can hardly be considered diffusive. Based on computer simulations of magnetopause encounters, the "butterfly" distribution is but a superficial signature peculiar to the process in which violations of invariants occur with drastic anisotropy in configuration space. Further, the channeling of electron motion provided by the sharp magnetic field gradient at the magnetopause boundary surface indicates that it acts macroscopically as a scattering boundary to outer-belt electrons, having simultaneously the properties of a sink to electrons approaching the boundary on given initial  $L$ -shells intercepting the magnetopause and of a highly anisotropic source of electrons to  $L$ -shells intercepting the magnetopause inward of the initial  $L$ -shell. In the non-turbulent magnetopause case, virtually no electrons were lost to interplanetary space. It appears that diffusion in invariant space is not the panacea that cursory considerations make it out to be. Detailed results of the computer simulation study will be published elsewhere.

## 6. Conclusions

By testing against a SCATHA electron data base, we have found a computationally

practicable representation for the outer-belt electron distribution from the general solution of a simple version of the simultaneous bimodal diffusion theory that satisfies the basic requirements for outer-belt dynamic modeling inwards of  $L \sim 7$ . The representation fails to characterize the small portion of outer-belt electron populations known as "butterfly" distributions. The nature of outer-radiation-belt electron encounters with the magnetopause needs to be investigated beyond the superficial formation of "butterfly" pitch-angle distributions. In particular, the distribution of "butterflies" in configuration space can shed light on the scattering processes in encounters with the magnetopause.

*Acknowledgments.* This work is supported by the Air Force Geophysics Laboratory under contract F19628-85-C-0073 and by the Lockheed Independent Research Program. It is a pleasure to thank G. Mullen, S. Gussenhoven and M. Schulz for discussions on various aspects of this work. The SCATHA SC-3 payload and initial data analysis were sponsored by the Office of Naval Research under contract N00014-76-C-0444. The SCATHA spacecraft is sponsored and operated by the USAF Space Test Program.

## References

- Birmingham, T.J., Convection electric fields and the diffusion of trapped magnetospheric radiation, *J. Geophys. Res.*, 77, 2169, 1969.
- Chiu, Y.T., R. W. Nightingale and M. A. Rinaldi, Simultaneous radial and pitch angle diffusion in the outer electron radiation belt, *J. Geophys. Res.*, 93, 2619, 1988.
- Cornwall, J.M., Diffusion processes influenced by conjugate point wave phenomena, *Radio Sci.*, 3, 740, 1968.
- Fälthammar, C.G., Introductory survey of radiation belt diffusion, in *Particles and Fields in the Magnetosphere*, edited by B.M. McCormac, p. 387, D. Reidel, Hingham, Mass., 1970.
- Fälthammar, C.G., Walt, M., Radial motion resulting from pitch-angle scattering of trapped electrons in the distorted geomagnetic field, *J. Geophys. Res.*, 74, 4184, 1969.
- Farley, T. A., Radial diffusion of starfish electrons, *J. Geophys. Res.*, 74, 3591, 1969.
- Frankenthal, S., F.R. Paolini, and G.C. Theodoridis, Bimodal diffusion in the earth's magnetosphere II. on the electron belts, *Ann. Geophys.*, 24, 1015, 1968.
- Haerendel, G., *Earth's Particles and Fields*, edited by B.M. McCormac, pp. 171-191, Reinhold Book Corp., New York, 1968.
- Holzworth, R.H., and F.S. Mozer, Direct evaluation of the radial diffusion coefficient near  $L = 6$  due to electric field fluctuations, *J. Geophys. Res.*, 84, 2559, 1979.
- Kavanaugh, L.D., Jr., An empirical evaluation of the radial diffusion coefficients for electrons of 50-100 keV from  $L = 4$  to  $L = 7$ , *J. Geophys. Res.*, 73, 2959, 1968.
- Lanzerotti, L. J., C. G. MacLennan, and M. Schulz, Radial diffusion of outer zone electrons: An empirical approach to third invariant violation, *J. Geophys. Res.*, 75, 5351, 1970.
- Nakada, M.P., and G.D. Mead, Diffusion of protons in the outer radiation belt, *J. Geophys. Res.*, 70, 4777, 1965.
- Newkirk, L.L., and M. Walt, Radial diffusion coefficients for electrons at low  $L$  values, *J. Geophys. Res.*, 73, 1013, 1968a.

- Newkirk, L.L., and M. Walt, Radial diffusion coefficients for electrons at  $1.76 < L < 5$ , *J. Geophys. Res.*, 73, 7231, 1968b.
- Reagan, J.B., R.W. Nightingale, E.E. Gaines, W.L. Imhof, and E.G. Stassinopoulos, Outer-zone energetic electron spectral measurements, *J. Spacecraft Rockets*, 18, 83, 1981.
- Roederer, J.G., and M. Schulz, Effect of shell splitting on radial diffusion in the magnetosphere, *J. Geophys. Res.*, 74, 4117, 1969.
- Schulz, M., and L. J. Lanzerotti, *Physics and Chemistry in Space*, vol. 7, *Particle Diffusion in the Radiation Belts*, 215 pp., Springer, New York, 1974.
- Sibeck, D.G., R.W. McEntire, A.T.Y. Lui and R.E. Lopez, Magnetic drift-shell splitting: Cause of unusual dayside particle pitch angle distributions during storms and substorms, *J. Geophys. Res.*, 92, 13,485, 1987.
- Stern, D. P., Parabolic harmonics in magnetospheric modeling: The main dipole and the ring current, *J. Geophys. Res.*, 90, 10851, 1985.
- Tomassian, A.D., T.A. Farley, and A.L. Vampola, Inner-zone energetic electron repopulation by radial diffusion, *J. Geophys. Res.*, 77, 3441, 1972.
- Tsyganenko, N. A., Global quantitative models of the geomagnetic field in the cislunar magnetosphere for different disturbance levels, *Planet. Space Sci.*, 35, 1347, 1987.
- Tverskoy, B. A., Transport and acceleration of charged particles in the earth's magnetosphere, *Geomagn. Aeron. Engl. Transl.*, 5, 617, 1965.
- Walt, M., Radial diffusion of trapped particles, in *Particles and Fields in the Magnetosphere*, edited by B.M. McCormac, p. 410, D. Reidel Hingham, Mass., 1970.
- West, H. I., The signatures of the various regions of the outer magnetosphere in the pitch angle distributions of energetic particles, in *Quantitative Modeling of Magnetospheric Processes*, edited by W.P. Olson, p. 150, American Geophysical Union, Washington, D.C., 1979.
- West, H. I., Jr., R. M. Buck, and G. T. Davidson, The dynamics of energetic electrons in the Earth's outer radiation belt during 1973 as observed by the Lawrence Livermore National Laboratory's spectrometer on OGO 5, *J. Geophys. Res.*, 86, 2111, 1981.

## Figure Captions

- Figure 1. Values of the right hand side (RHS) and left hand side (LHS) of the separation equation (7) are plotted as functions of order  $n$  for (a) the initial iteration and (b) the final iteration. The equality is enforced as a fit constraint in this paper. Note the large divergence at order 2 in the initial iteration.
- Figure 2. Three-dimensional presentation of the phase space density of (a) the data base and (b) its reconstitutions for the 288.5 keV channel of Day 165, 1980 in pitch angle and  $L$ . Large errors are found primarily in the corner of (b) pertaining to large  $L$  and large pitch angles. Noisy data near  $L \sim 5.7$  also resulted in some error.
- Figure 3. Three-dimensional presentation of the phase space density of (a) the data base and (b) its reconstitutions for the 448 keV channel of Day 110, 1979 in pitch angle and  $L$ . As in Figure 2, the large errors are mainly confined to the corner of (b) pertaining to large  $L$  and large pitch angles.
- Figure 4. The distribution of fit percentage errors in the reconstitution of all the data points in the Day 165, 1980 data base. The error distributions of the initial and final iterations are shown as dots and asterisks, respectively.
- Figure 5. Same as Figure 4 except the distribution is for the Day 110, 1979 data base.
- Figure 6. Comparison of the radial diffusion coefficients determined in this paper for the energy range 0.2-2.0 keV (mottled area) with Paper I (cross-hatched area), and with the compilation of West et al. [1981], whose individual analysis yields curve 1. Curves 2-8 are experimental: 2. Tomassian et al. [1972]; 3. Farley [1969]; 4. Newkirk and Walt [1968b]; 5. Lanzerotti et al. [1970]; 6. Newkirk and Walt [1968b]; Fälthammar [1970]; 7. Newkirk and Walt [1968a]; 8. Kavanaugh [1968]. Curves 9-14 are theoretical or semi-theoretical: 9. Nakada and Mead [1965]; 10. Iverskoy [1965]; 11. Birmingham [1969]; 12, 13. Cornwall [1968]; 14. Holzworth and Mozer [1979].
- Figure 7. Demonstration of path independence in projecting the electron distributions from on-trajectory to off-trajectory points. Panels A and B are measured and fitted phase space distributions at the trajectory locations shown on the

SCATHA trajectory panel. Using the eigenfunction representation, the distributions are projected along the  $t$  and  $L$  axes respectively to the off-trajectory point C. The comparison of the two projected distributions is shown on Panel C.

Figure 8. Projection on the equatorial plane of the trajectory of a 10 MeV electron as it makes encounters with the non-turbulent magnetopause indicated by the parabola. The electron is initially bouncing and drifting towards the magnetopause on an  $L$ -shell inside the magnetosphere. Upon encounter, the electron leaves the initial  $L$ -shell skips along the equatorial magnetopause partially inside and partially outside of the magnetosphere until it finds itself on a new magnetospheric  $L$ -shell on which it executes its regular bounce-drift motion.

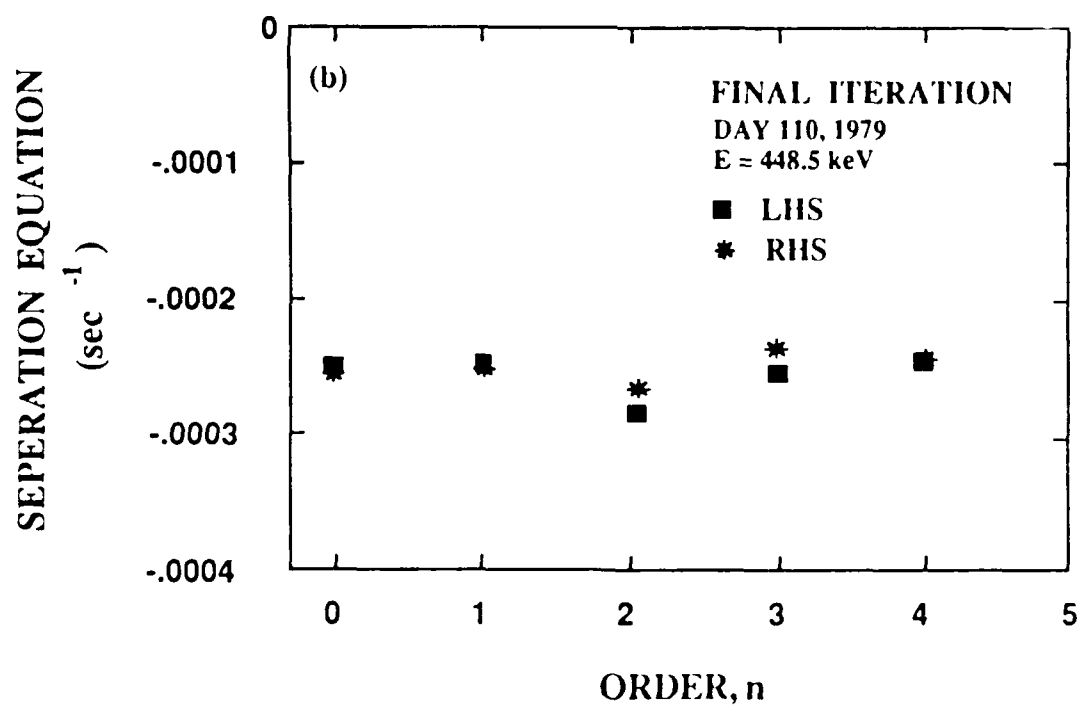
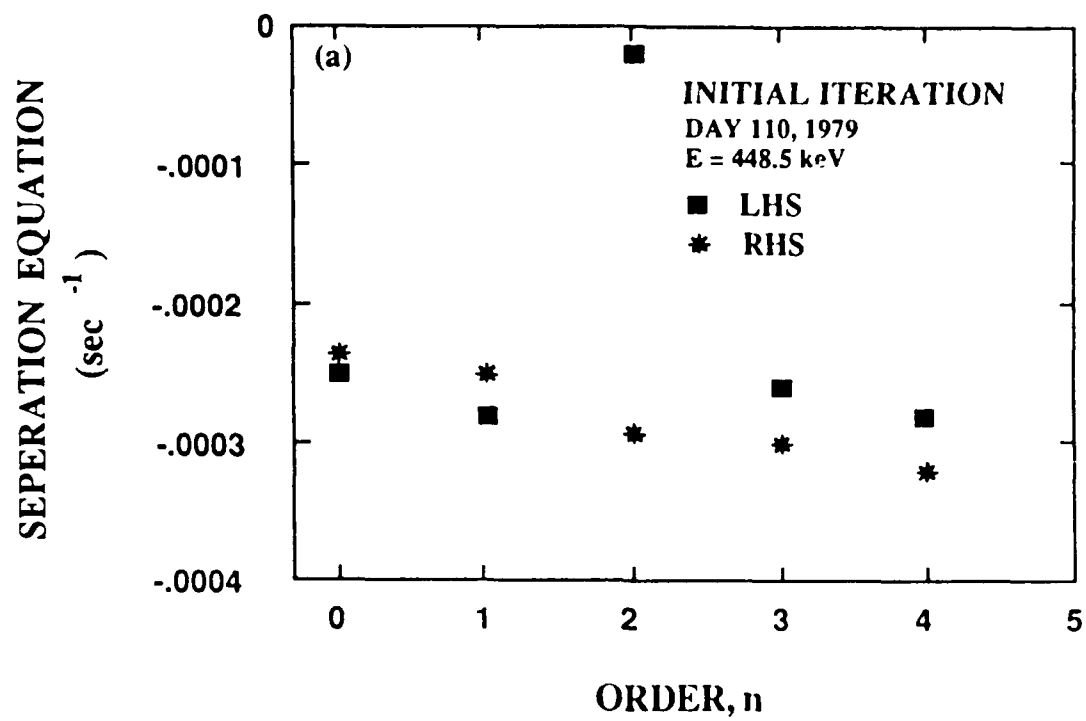


Figure 1

DAY 165, 1980

$E = 288.5 \text{ keV}$

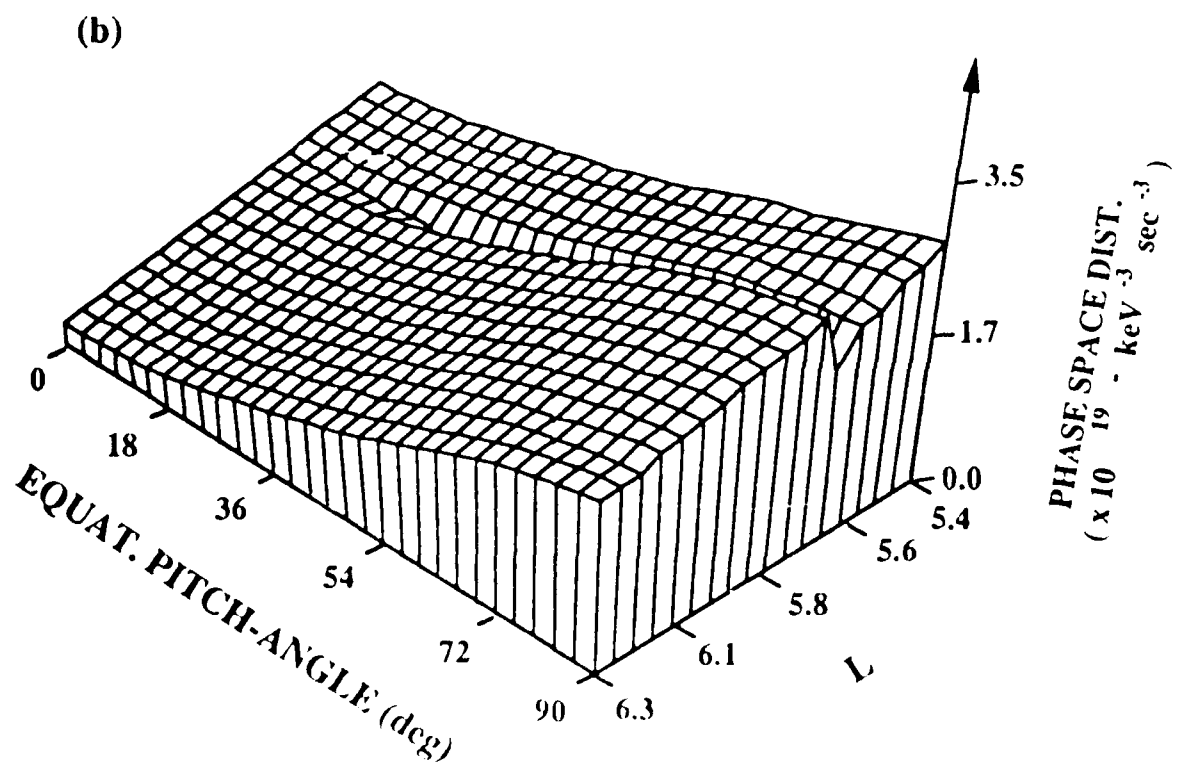
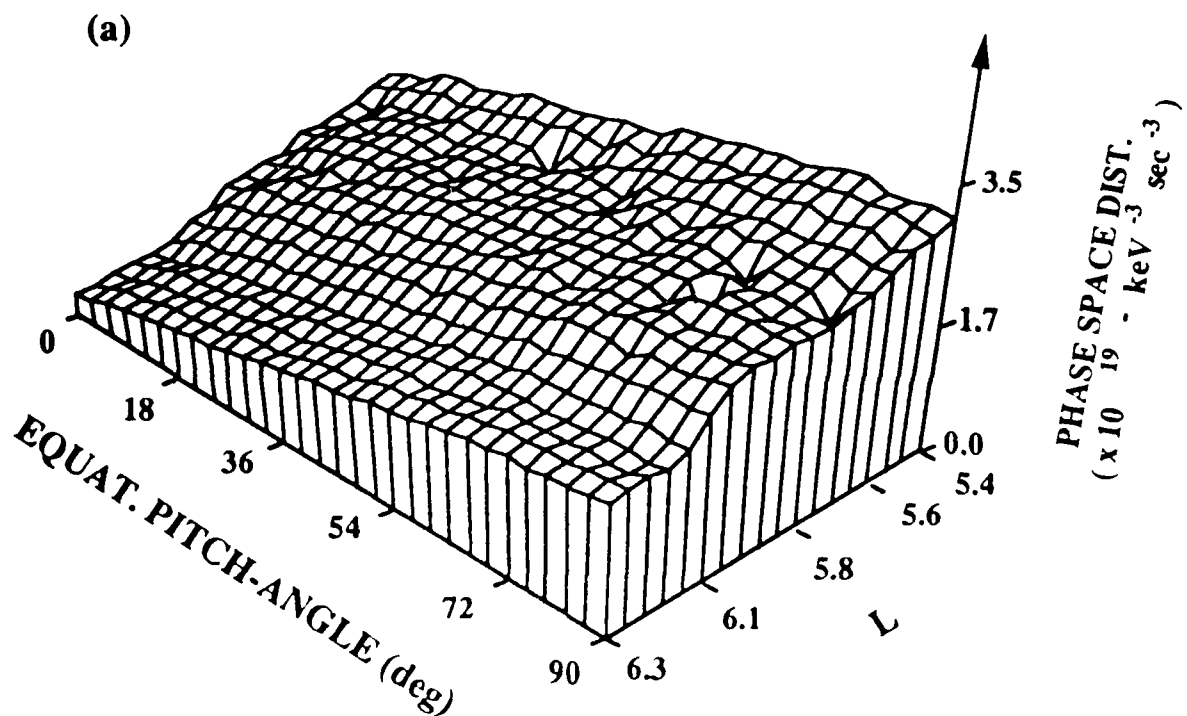
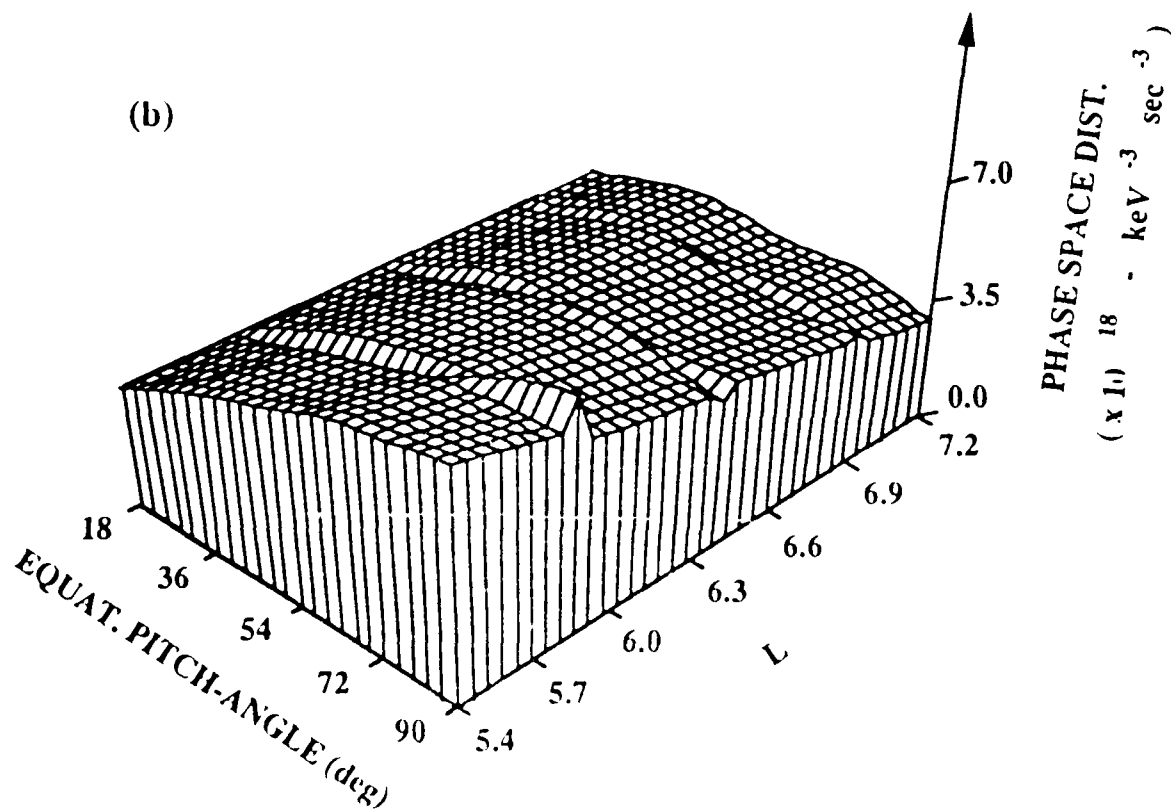
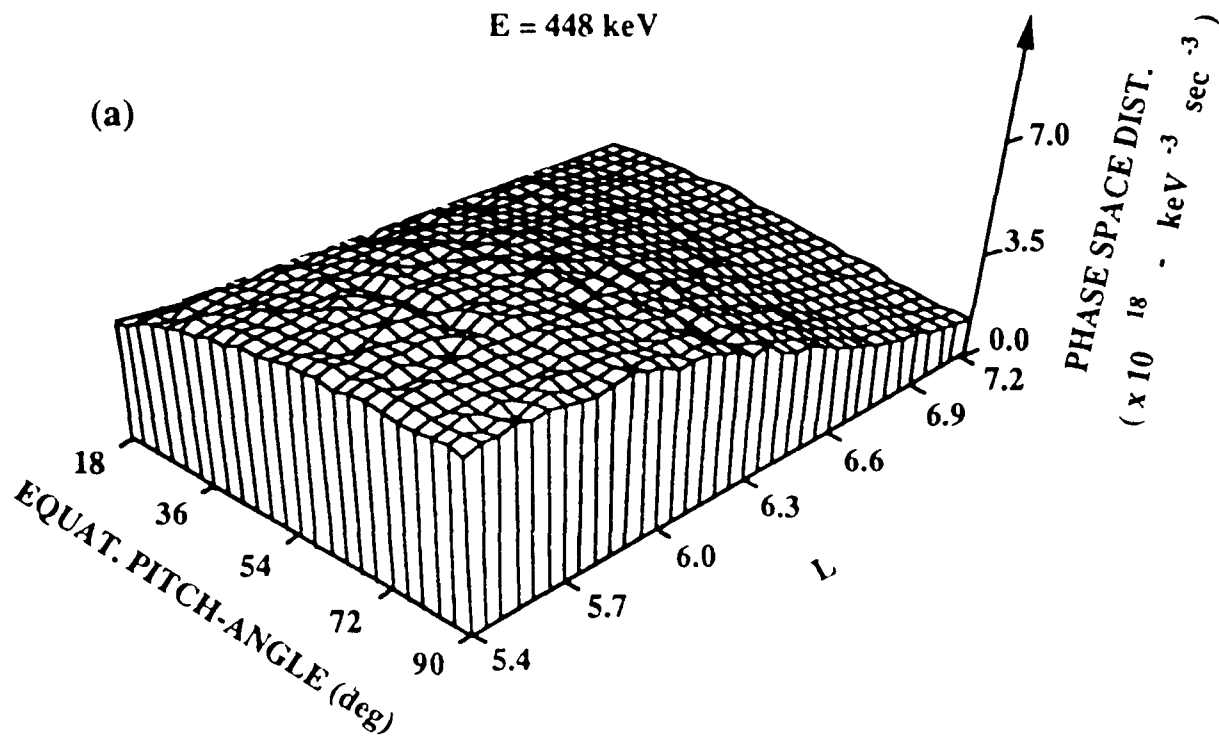


Figure 2



DAY 110, 1979

E = 448 keV



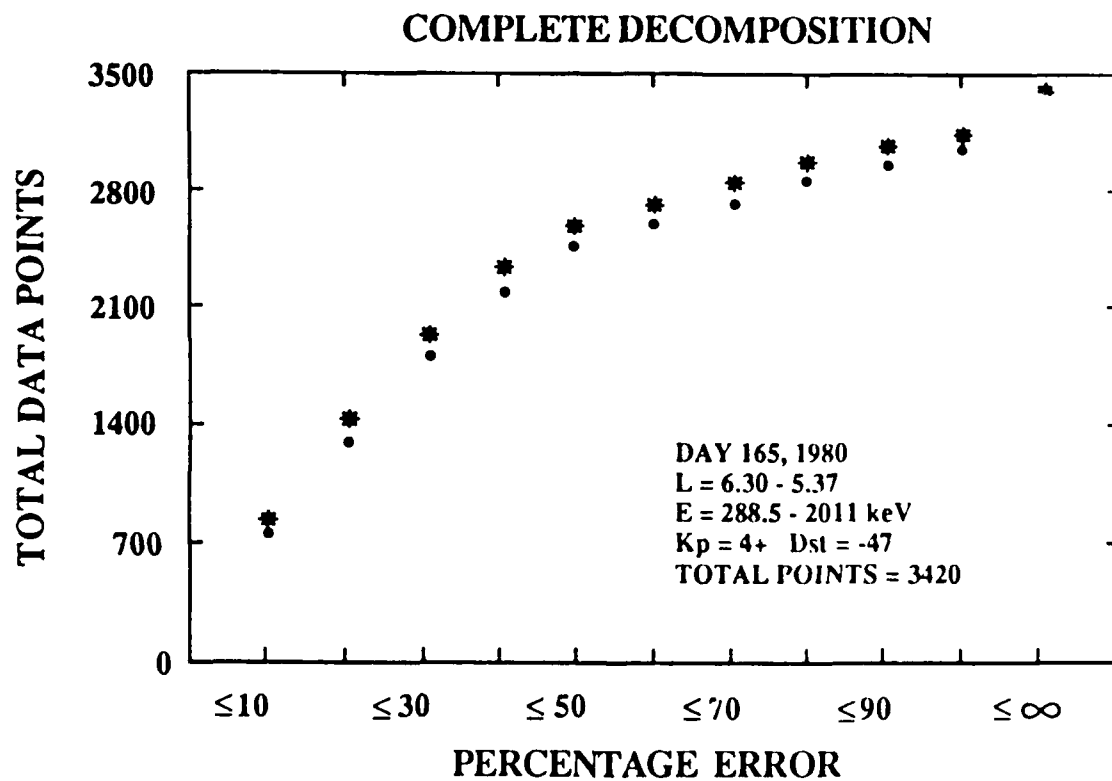


Figure 4

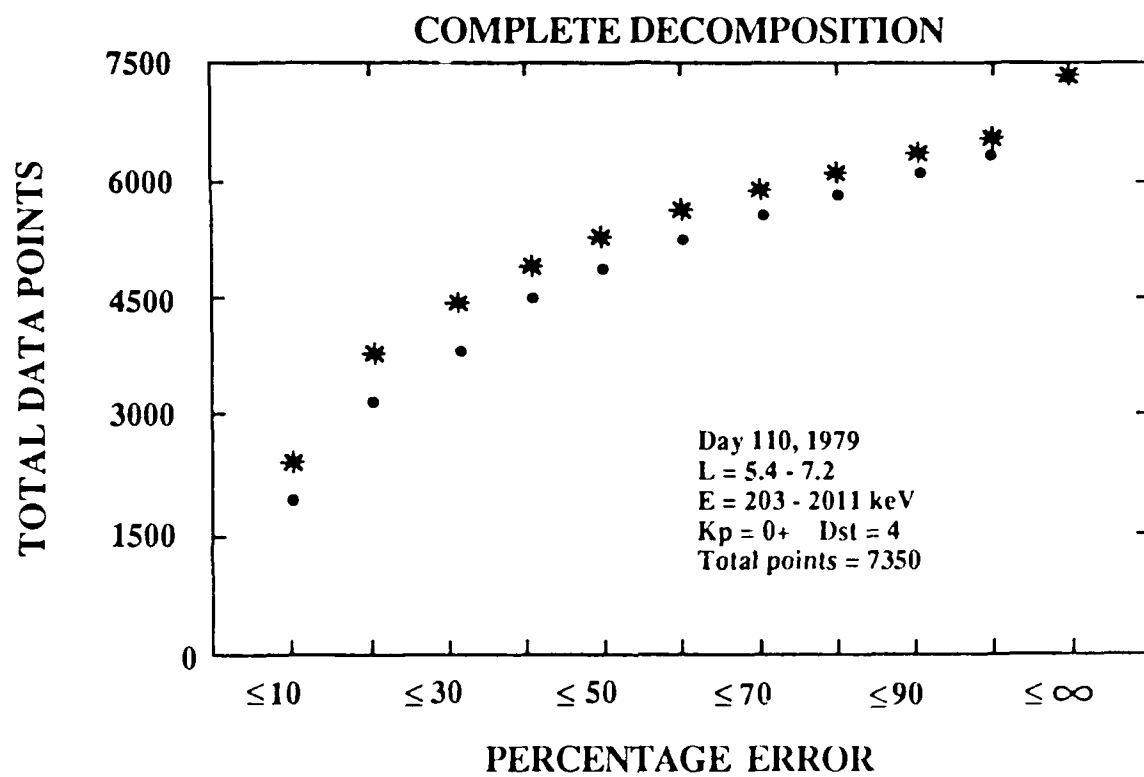


Figure 5

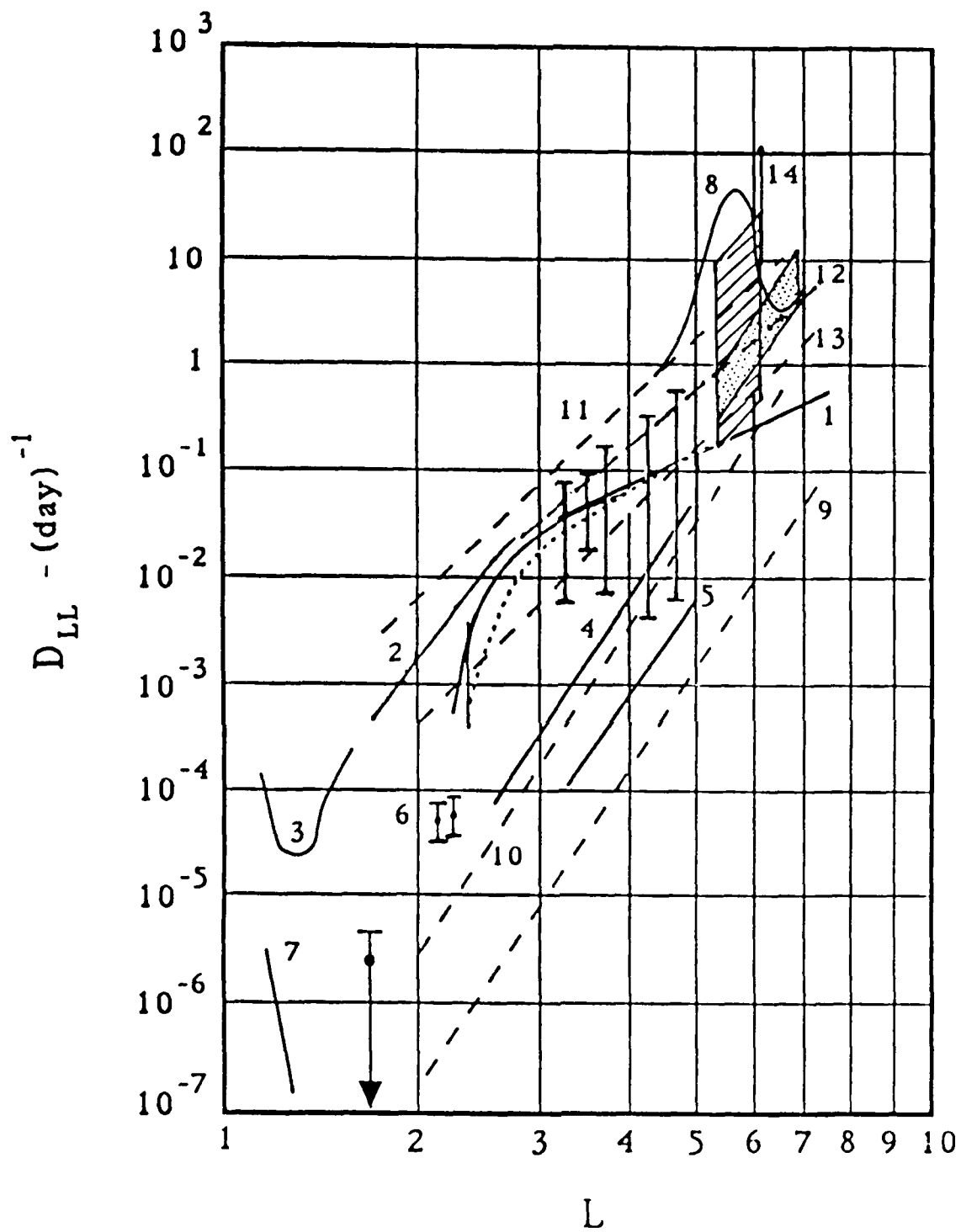


Figure 6

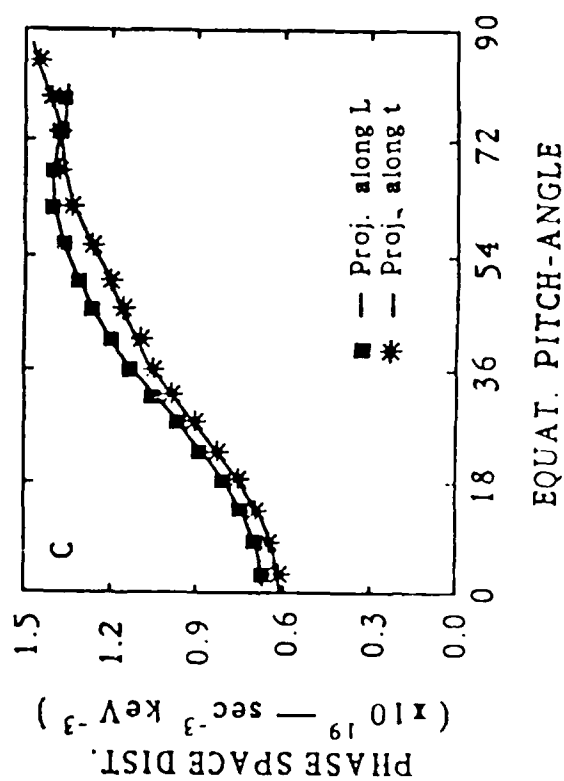
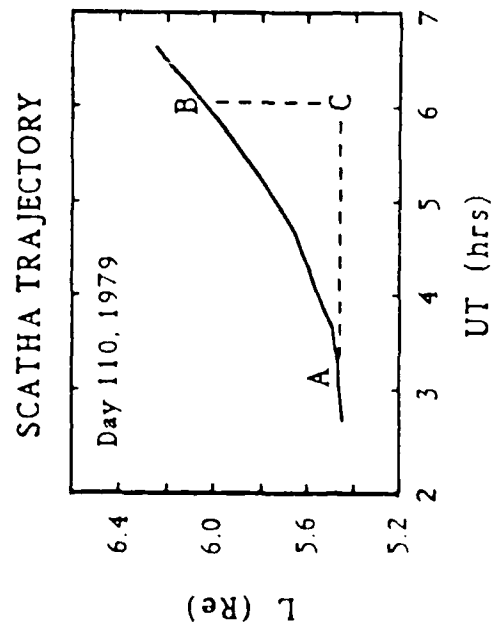
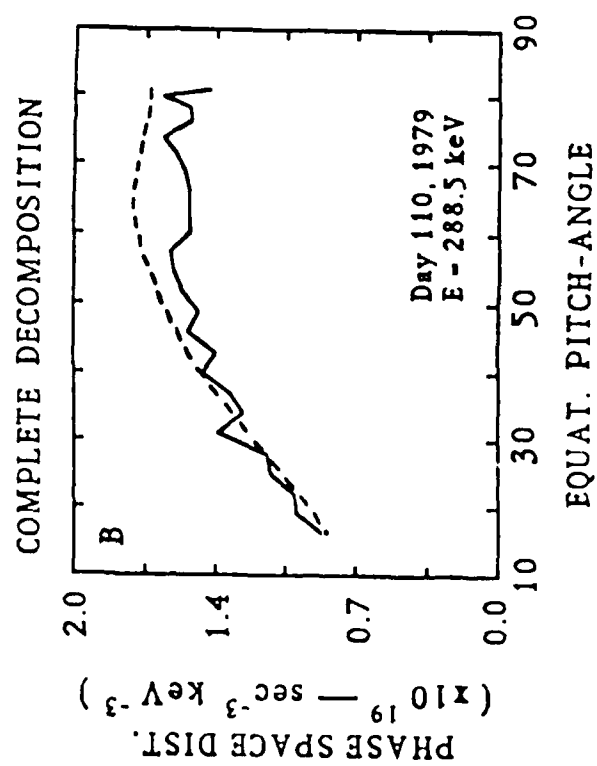
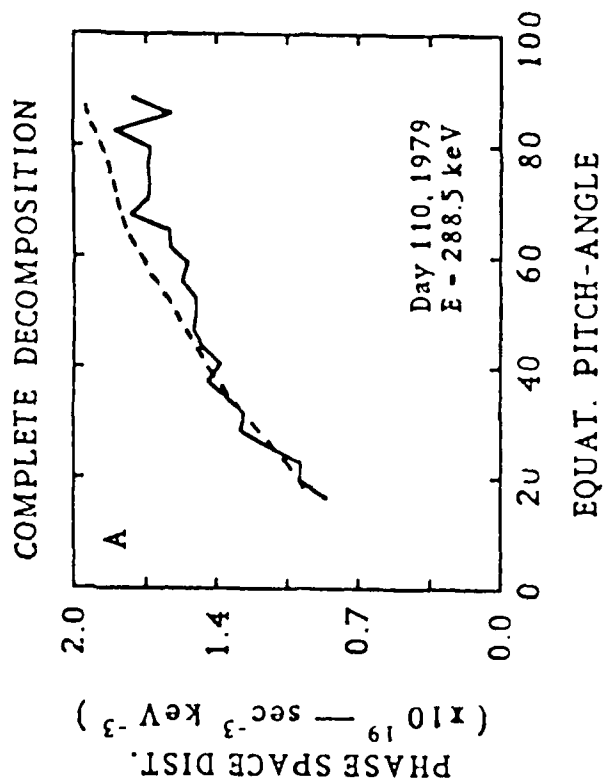


Figure 7

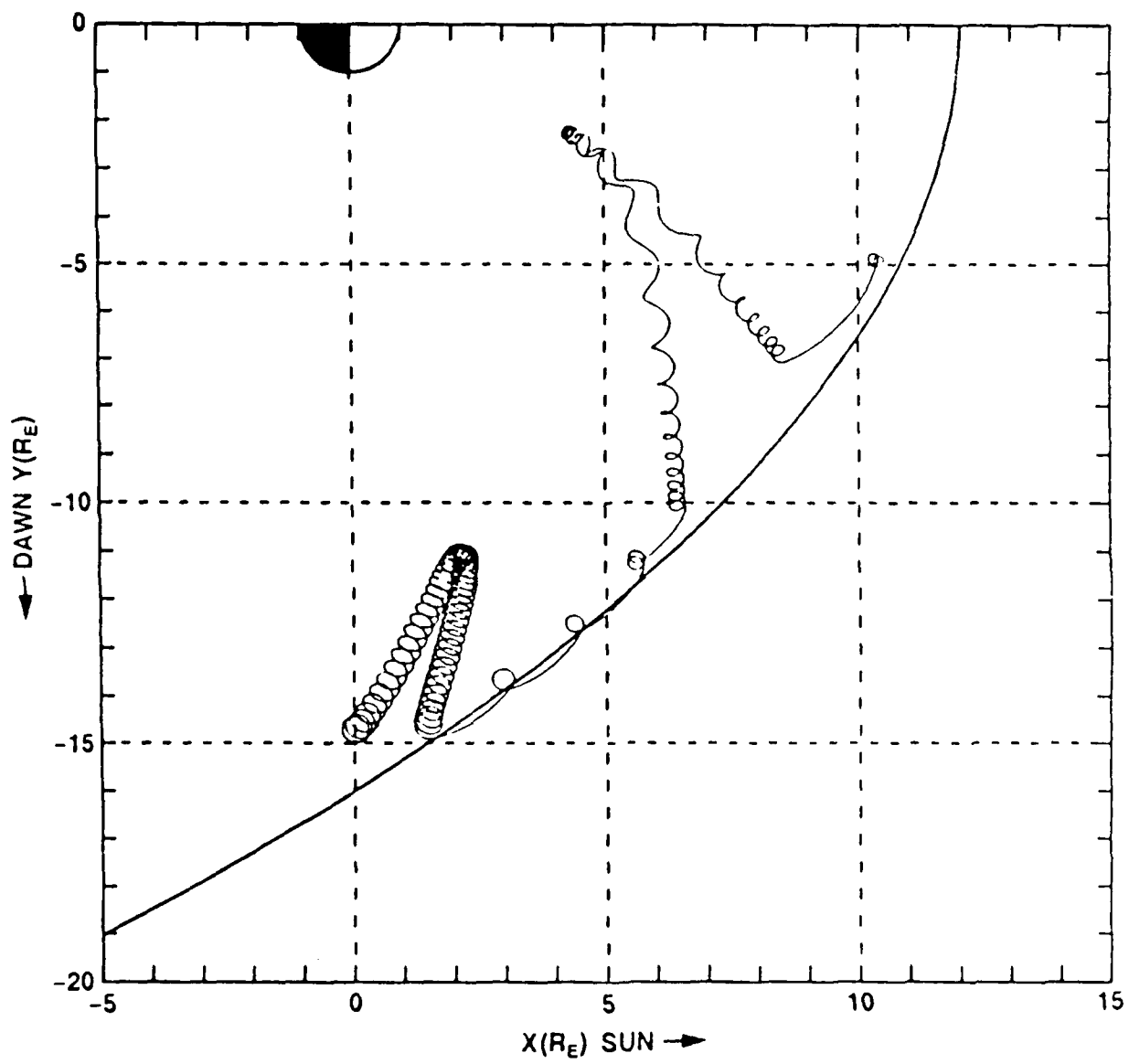


Figure 8